

A specific circuit in the midbrain detects stress and induces restorative sleep

**Xiao Yu^{a, e, f}, Guangchao Zhao^c, Dan Wang^c, Sa Wang^c, Rui Li^c, Ao Li^c, Huan Wang^{h, i},
Mathieu Nollet^{a, b}, You Young Chun^a, Tianyuan Zhao^a, Raquel Yustos^a, Huiming Li^c,
Jianshuai Zhao^c, Jiannan Li^c, Min Cai^d, Alexei L. Vyssotski^g, Yulong Li^{h, i}, Hailong Dong^c,
Nicholas P. Franks^{a, b}, William Wisden^{a, b}**

^aDepartment of Life Sciences and ^bUK Dementia Research Institute, Imperial College, London SW7 2AZ, United Kingdom

^cDepartment of Anesthesiology & Perioperative Medicine and ^dDepartment of Psychiatry, Xijing Hospital, Fourth Military Medical University, Xi'an, China

^ePresent address: Maurice Wohl Clinical Neuroscience Institute, Department of Basic and Clinical Neuroscience, Institute of Psychiatry, Psychology and Neuroscience and ^fUK Dementia Research Institute, King's College, London SE5 9RT, United Kingdom

^gInstitute of Neuroinformatics, University of Zürich/ETH Zürich, Zürich, Switzerland

^hState Key Laboratory of Membrane Biology, Peking University School of Life Sciences and

ⁱPKU-IDG/McGovern Institute for Brain Research, Beijing, 100871, China

X.Y. and G.Z. contributed equally.

Corresponding author. E-mail: xiao.1.yu@kcl.ac.uk, hldong6@hotmail.com, n.franks@imperial.ac.uk, w.wisden@imperial.ac.uk

Abstract

In mice, social defeat stress (SDS), an ethological model for psychosocial stress, induces sleep. Such sleep could enable resilience, but how stress promotes sleep is unclear. Activity-dependent tagging revealed a subset of ventral tegmental area GABA-somatostatin ($VTA^{Vgat-Sst}$) cells that sense stress and drive NREM and REM sleep via the lateral hypothalamus, and also inhibit corticotropin-releasing factor (CRF) release in the paraventricular hypothalamus. Transient stress enhances the activity of $VTA^{Vgat-Sst}$ cells for several hours, allowing them to exert their sleep effects persistently. Lesioning of $VTA^{Vgat-Sst}$ cells abolished SDS-induced sleep; without it, anxiety and corticosterone levels remained elevated after stress. Thus, a specific circuit allows animals to restore mental and body functions via sleeping, potentially providing a refined route for treating anxiety disorders.

Introduction

Acute stress activates the hypothalamic-pituitary-adrenal axis, and the resulting fast increase in blood glucocorticoid levels aids immediate survival (1-3). But chronically elevated levels of glucocorticoids are harmful (1, 2), as can be memories of stressful experiences (4). Although stress can cause insomnia and raise stress hormones (3, 5-8), the opposite is also true: chronic stress elevates REM sleep (9); and sleep in rodents is induced by specific types of stress, such as social defeat stress (SDS). Although the function and benefits of sleep remain unclear, sleep is certainly restorative (10). Thus, sleep has been suggested to be one of the mechanisms for alleviating the malign effects of stress (4, 9, 11, 12). Whether a specific circuit links stress and sleep is, however, unknown. We reasoned that the ventral tegmental area (VTA) in the midbrain could provide a link.

The VTA regulates reward, aversion, goal-directed behaviors and social contact (13-15). It also influences responses to stress and threats (16, 17), and strongly affects sleep and wake: VTA^{Vglut2} and VTATH neurons promote wakefulness (18, 19); whereas VTA^{Vgat or Gad67} neurons induce sleep (18, 20, 21). Because some GABAergic VTA neurons are activated by stressful and aversive stimuli (16, 22-24), we hypothesized that this route allows stress to induce sleep.

Social defeat stress induces sleep

We first assessed the sleep-wake architecture of mice after they had experienced either SDS from aggressors with consecutive episodes of SDS for one hour, or a control procedure, in which the experimental mouse (intruder) was separated from the resident aggressor by a clear partition (Fig. S1A). As a further control, instead of an aggressor mouse, we introduced a juvenile male mouse as the resident for 1 hour (Fig. S1B). During this non-stress procedure, the experimental mice

experienced social interaction. As a control for whether physical activity induces sleep, the mice experienced voluntary wheel running or forced treadmill running continuously for 1 hour (Fig. S1C, D); or, alternatively, as another control, the mice were placed in a novel environment with a novel object (Fig. S1E). Corticosterone (CORT) levels in mice increased after the SDS sessions (Fig. 1A), but not following exposures to juvenile mice, physical exercise, or novel environment/objects (Fig. S2A, C, E, G). After SDS, NREM sleep latency was shortened, and both NREM and REM sleep were continuously elevated for 5 hours (Fig. 1B, C and Fig. S2I), consistent with previous observations (11, 25). Mice that experienced a non-stressful procedure, voluntary wheel running, forced treadmill running or that were deprived of one hour of sleep by placing them in a novel environment, however, did not have induced sleep above baseline (Fig. S2A-H, J-M), suggesting social interaction or physical exercise did not induce sleep and SDS procedures did not cause a sleep rebound while the mice were awake.

Sleep relieves SDS-induced anxiety and CORT levels independently

We explored potential functions of sleep after SDS. For mice allowed sufficient sleep (home cage sleep) after SDS, anxiety-like behaviors caused by SDS were rapidly reduced, as seen in the elevated-plus maze and open-field assays (Fig. 1D-F). If mild sleep deprivation over 4 hours took place immediately after SDS, the mice remained in an anxious state (Fig. 1D-F). For mice allowed sufficient home cage sleep after SDS, raised CORT levels returned to baseline over 60 mins (Fig. 1G). If mild sleep deprivation occurred immediately after stress, however, CORT levels remained elevated (Fig. 1G). But pharmacologically reducing the CORT levels induced by SDS during sleep deprivation, using a corticosterone synthesis inhibitor metyrapone (Fig. S3A), did not reduce anxiety after sleep deprivation (Fig. S3B, C).

Identification of neurons activated by stress

To identify the circuitry that induces restorative sleep, we mapped cFOS expression throughout the brain. Following the SDS protocol (Fig. S1A), cFOS was elevated strongly in brain areas involved in stress responses (Fig. S4A, B), including the VTA (Fig. 1H and Fig. S4). In the VTA, cells activated (cFOS-positive) by stress predominantly expressed the GABAergic marker *Vgat* (60%) or GABA (57%) (Fig. 1I and Fig. S5A, B), whereas relatively fewer cells expressed the glutamatergic marker *Vglut2* (20%) or the dopaminergic marker tyrosine hydroxylase (10%) (Fig. S5C, D). However, physical exercise did not induce cFOS in the VTA as a whole, and particularly not in VTA^{Vgat} cells, but forced treadmill running slightly increased cFOS expression in TH-positive cells (Fig. S5E, F, G). For the subsequent studies, we focused on the VTA^{Vgat} neurons, as only these induce sleep (18).

VTA^{Vgat} neurons have persistently increased activity in response to SDS

VTA^{Vgat} neurons rapidly and strongly responded when mice experienced an attack during SDS (Fig. 1J, K), as assessed by GCaMP6 fiber photometry. The cells did not respond when the mice were presented with novel objects or placed in a novel environment (Fig. S6A, B). During SDS, the calcium signal in VTA^{Vgat} neurons increased, and stayed enhanced for about 5 hours (Fig. 1L), correlating with the behavioral result of prolonged sleep after SDS (Fig. 1B, C). In contrast, voluntary wheel running, forced treadmill running or a novel environment did not affect baseline activity of VTA^{Vgat} neurons (Fig. S6C, D).

Subsets of VTA^{Vgat} neurons mediate SDS-induced sleep

Because only a subset of VTA^{Vgat} neurons (20%) were excited by SDS (Fig. 1I), we undertook cFOS-dependent activity-tagging linked to expression of DREADD hM3Dq-mCherry to test if this VTA subset could induce sleep (Fig. 2A). Mice experienced either SDS, or a non-stressful procedure, **voluntary wheel running or forced treadmill running**, while the VTA^{Vgat} neurons were selectively activity-tagged using Cre-recombinase-dependent tagging vectors (*AAV-cFOS-tTA* and *AAV-TRE-DIO-hM3Dq-mCherry*, Fig. 2A and Fig. S7A, **D, G**). Compared with pan-VTA^{Vgat} neurons expressing mCherry, only 15% of the VTA^{Vgat} neurons were captured by activity-tagging during SDS (Fig. 2B). We then reactivated these SDS-tagged VTA^{Vgat} neurons with CNO. Chemogenetic reactivation decreased sleep latencies, and increased sleep times (Fig. 2C, D). Thus, reactivation of SDS-activated VTA^{Vgat} neurons recapitulated sleep architectures induced by SDS (Fig. 2E). Of note, a few cells (2.6%) were tagged during the non-stressed procedures (Fig. 2B). However, chemogenetic reactivation of these particular tagged VTA^{Vgat} cells did not elicit sleep (Fig. S7B, C). **Moreover, only rare cells were tagged when mice experienced physical exercise (Fig. 2B), and therefore chemogenetic reactivation did not induce sleep (Fig. S7D-I).**

To examine the necessity of VTA^{Vgat} subsets for SDS-induced sleep, we chemogenetically inhibited SDS-tagged VTA^{Vgat} neurons using cFOS-dependent expression of DREADD hM4Di-mCherry. *AAV-cFOS-tTA* and *AAV-TRE-DIO-hM4Di-mCherry* were injected into the VTA of *Vgat-IRES-Cre* mice (Fig. 2F). Mice were subjected to SDS (1st stress episode) to allow VTA^{Vgat} neurons to become tagged with hM4Di-mCherry, then given CNO to inhibit the tagged neurons, and mice were subsequently challenged with a second bout of SDS (2nd stress episode), followed by measurement of their sleep profile (Fig. 2F). SDS-induced sleep was diminished after chemogenetically-inhibiting tagged VTA^{Vgat} neurons (Fig. 2G, H).

Circuits linking stress and sleep

We next investigated the circuitry linking SDS and VTA^{Vgat}-induced sleep. We expressed GCaMP6 selectively in VTA^{Vgat} cells and used fiber photometry to measure how the VTA^{Vgat} terminals in different locations responded to stress. Only the terminals of the VTA^{Vgat} cells projecting to the LH had increased Ca²⁺ signals following SDS (Fig. 3A, B), whereas the VTA^{Vgat} projections in the CeA, LHb, and hippocampal dentate granule cells (DG) showed no responses (Fig. S8). To determine the function of the VTA^{Vgat}→LH pathway activated by stress on sleep, we injected *retro-AAV-TRE-DIO-Flpo* into the LH, together with the injection of *AAV-cFOS-tTA* and *AAV-fDIO-hM3Dq-mCherry* into the VTA of *Vgat-IRES-Cre* mice (Fig. 3C). Following intersectional activity-tagging during SDS and chemogenetic reactivation, VTA→LH pathway promoted sleep (Fig. 3D, E). The hM3Dq-mCherry labeling produced in the VTA^{Vgat} neurons of this experiment mainly traced out axons to the LH (Fig. S9).

We used optogenetics to confirm the above result. The behavioral experiments were repeated using cFOS-based activity-tagging with ChR2 delivered into the VTA of *Vgat-IRES-Cre* mice (Fig. S10A). VTA^{Vgat} neurons became selectively ChR2-tagged during SDS (Fig. S10A). Mapping of VTA^{Vgat} projections by injecting *AAV-DIO-ChR2-EYFP* into *Vgat-IRES-Cre* mice showed broad projections (Fig. S10B) (18). However, those SDS-tagged VTA^{Vgat} cells detected with ChR2 activity-mapping primarily innervated the LH (Fig. S10C). When SDS-ChR2-tagged terminals in the LH of the VTA^{Vgat}→LH pathway were reactivated by optogenetic-stimulation, this elicited NREM sleep from waking (Fig. S10D, E).

Stress-driven input-output organizations

We investigated the identity and activity of VTA^{Vgat} afferents relevant for stress using a rabies system, combined with activity mapping. VTA^{Vgat} neurons were seeded with rabies coat protein and its receptor by injecting *AAV-DIO-N2cG* and *AAV-DIO-TVA-nGFP*, followed by injection of *RABV-N2cΔG-EnvAmCherry* into the VTA (Fig. 3F). The animals were then given control experiences or SDS, respectively. Then we conducted brain-wide mapping of rabies-labeled presynaptic inputs and stress-activated cFOS expression (Fig. 3F). cFOS was induced by stress in many brain regions (Fig. S4), and from the rabies tracing, VTA^{Vgat} inputs originated in many locations (Fig. S11) (26). However, only the LPO, PVH and PAG areas had overlap with cFOS-positive cells and rabies-labeled VTA^{Vgat} inputs (Fig. 3G, H, L and Fig. S12A-C, S13A).

We determined the inputs of VTA^{Vgat} neurons that project to the LH. *AAV-DIO-N2cG* and *AAV-DIO-TVA-nGFP* were seeded as before in VTA^{Vgat} neurons, and *RABV-N2cΔG-EnvAmCherry* was injected into the terminal fields of the VTA^{Vgat} neurons in the LH. As before, the mice were given control experiences or SDS. Then we mapped cFOS expression (Fig. 3I). We obtained an identical result as above: LH-projecting VTA^{Vgat} neurons received stress-activated inputs from LPO, PVH and PAG (Fig. 3J, K, L and Fig. S12D-F, S13B).

We further determined if these stress-activated inputs were specific to the stress-activated VTA^{Vgat} subset. The SDS-activated VTA^{Vgat} cells were specifically ablated with Casp3 using activity-tagging (*AAV-cFOS-tTA* and *AAV-TRE-DIO-Casp3*). Then we conducted rabies tracing and activity mapping (Fig. S14A). Ablation of SDS-activated VTA^{Vgat} cells largely reduced the stress-driven inputs (cFOS/rabies) (Fig. S14B, C and Fig. 3L).

VTA somatostatin neurons are necessary for SDS-induced sleep

Given that GABAergic VTA cells are heterogeneous (13, 27, 28), and only a subset of VTA^{Vgat} cells responded to SDS (Fig. 2B), we looked for subtypes of VTA^{GABA} cells responsible for SDS-induced sleep. First, we examined by single-cell qPCR the molecular identities of SDS-tagged cells (Fig. S15A): a large proportion (42%) expressed *vgat/somatostatin (sst)*, and others were characterized by *vgat/parvalbumin (pv)* (10%) or *vgat expression* alone (32%), the remaining cells being 2% *vgat/vglut2*, 2% *vgat/vglut2/sst* and 2% *vgat/vip* (Fig. S15B).

We further characterized the SDS-activated cells using reporter mice (Fig. 4A, B and Fig. S15C, D). Nearly 40% of the VTA^{Sst} neurons expressed cFOS following SDS (Fig. 4A and Fig. S15E, F), whereas there was no induction of cFOS following SDS in VTA^{Pv} cells (Fig. 4B). We next determined the activity of individual subtypes responding to stress using fiber photometry (Fig. 4C, D). Both the VTA^{Sst} and VTA^{Pv} populations responded transiently to SDS, but the collective calcium signal for VTA^{Sst} cells was larger (Fig. 4C, D), and only VTA^{Sst} neurons had persistent activation following SDS, with enhanced activity for a few hours (Fig. 4E). In contrast, the transient activity of VTA^{Pv} neurons after SDS was not sustained (Fig. 4F).

We next used activity-tagging with hM3Dq to capture SDS-tagged VTA^{Sst} neurons (Fig. S16A, B). Because VTA^{Sst} cells are heterogeneous (28), we examined the molecular identities of SDS-tagged cells (Fig. S16C). These tagged cells predominantly expressed *vgat/gad1* (90%) (Fig. S16D).

We tested whether VTA^{Sst} cells could respond to two types of insomnia-inducing stress, restraint and cage-change (7, 29). However, these procedures did not affect the acute or long-term calcium activity in VTA^{Sst} neurons (Fig. S17A-D). In addition, we did not observe any VTA^{Sst} neurons becoming tagged by restraint stress or cage-change stress (Fig. S17E).

Next, we measured spontaneous activities of VTA^{Sst} neurons across brain states. From calcium photometry, VTA^{Sst} neurons were primarily active during spontaneous NREM and REM sleep (Fig. 4G, H), whereas VTA^{Pv} neurons were wake-active (Fig. 4I, J). Chemogenetic stimulation of VTA^{Sst} neurons directly increased sleep (Fig. S18). We further defined how VTA^{Sst} neurons link stress and sleep. We recorded the spontaneous activity of stress-tagged VTA^{Sst} populations across brain states (Fig. S19A). The tagged cells were also primarily active during NREM and REM sleep (Fig. S19B). Chemogenetic reactivation of SDS-tagged VTA^{Sst} cells was sufficient to promote NREM and REM sleep (Fig. S19C-E).

To explore if the VTA^{Sst}→LH pathway links stress and sleep, we conducted fiber photometry to measure terminal activity in the LH responding to stress by expressing GCaMP6 in VTA^{Sst} neurons (Fig. S20A). The VTA^{Sst}→LH projection responded to SDS (Fig. S20B). Following intersectional activity-tagging during SDS (Fig. S20C), chemogenetic reactivation of VTA^{Sst}→LH pathway promoted sleep (Fig. S20D, E).

Finally, we examined directly whether VTA^{Sst} neurons are necessary for SDS-induced sleep. Genetic ablation specifically depleted VTA^{Sst} neurons (Fig. S21). Lesioning of VTA^{Sst} neurons decreased baseline sleep (Fig. 5A-C). When VTA^{Sst}-caspase mice were challenged with SDS, SDS-induced sleep was abolished (Fig. 5B, C). This was also confirmed by chemogenetic manipulation, inhibition of VTA^{Sst} neurons also decreased SDS-induced sleep (Fig. S22). In contrast, ablation of VTA^{Pv} neurons decreased baseline NREM sleep, but SDS-induced sleep could still be elicited (Fig. 5D-F).

SDS-induced sleep by VTA^{Sst} neurons reduces stress-induced anxiety

Given the proposed restorative function of sleep after SDS (Fig. 1D-G), we explored if this function was linked to VTA^{Vgat-Sst} neurons. Ablation of VTA^{Sst} neurons or chemogenetic inhibition of SDS-tagged VTA^{Vgat} neurons had no effect on baseline anxiety-like behaviors (Fig. S23). However, after SDS, mice lacking SDS-induced sleep (because of selective lesioning/inhibition of VTA^{Sst} neurons or inhibition of SDS-tagged VTA^{Vgat} neurons (Fig. 5A-C, Fig. S22 and Fig. 2F-H)) remained in an anxious state (Fig. 6A-C and Fig. S24), similar to the effects of sleep deprivation after SDS (Fig. 1E, F and Fig. S25). When VTA^{Vgat-Sst} neurons were unimpeded, while the mice had sufficient SDS-induced sleep, the SDS-induced anxiety-like behaviors were reduced to baseline (Fig. 6B, C and Fig. S24). We found that sleep deprivation after SDS suppressed activity in VTA^{Sst} neurons induced by SDS (Fig. S26). However, during the sleep deprivation procedure after SDS while mice were awake, VTA^{Sst} cell stimulation did not reduce anxiety even if VTA^{Sst} neurons were activated (Fig. S27), suggesting the anxiolytic effects require SDS-induced sleep.

Activation of VTA^{Sst} neurons suppresses corticotrophin releasing factor levels induced by SDS

How do VTA^{Sst} neurons regulate CORT production? VTA^{Sst} neurons expressing hM3Dq-mCherry sent numerous mCherry-positive axons into the PVN area (Fig. S28A, B), a major site of corticotrophin releasing factor (CRF) production. Following SDS, cells in the PVH are excited, as inferred from their strong expression of cFOS; but stimulation of VTA^{Sst} neurons inhibited SDS-activated cells in the PVN (Fig. S28C).

We next employed a novel genetically-encoded CRF sensor (*AAV-hSyn-GRAB_{CRF1.0}*)(30) to determine the dynamics of CRF release around the PVN (Fig. S28D and Fig. 6D). CRF sensor signals were indistinguishable between control and chemogenetic activation of VTA^{Sst} neurons (Fig. S28E), consistent with CORT levels also not changing with VTA^{Sst} stimulation (Fig. S28F). But following SDS, there were large increases in CRF (Fig. S28G). However, chemogenetic activation of VTA^{Sst} neurons prevented this increase (Fig. 6E), consistent with correspondingly decreased CORT levels (Fig. 6F). On the other hand, chemogenetic inhibition of VTA^{Sst} neurons further elevated SDS-induced CRF levels (Fig. 6G), thereby increasing CORT levels after SDS (Fig. 6H).

SDS-induced sleep by VTA^{Sst} neurons reduces CORT levels

For mice unable to have SDS-induced sleep, either because their VTA^{Sst} neurons had been ablated or were inhibited (Fig. 6I and Fig. S29A), CORT levels remained higher during their home cage sleep after SDS (Fig. 6J and Fig. S29B), similar to the effects of sleep deprivation after SDS (Fig. 1G). However, when VTA^{Vgat-Sst} neurons were unimpeded, the SDS-induced sleep correlated with CORT levels returning to baseline (Fig. 6J and Fig. S29B). In addition, activation of VTA^{Sst} cells during sleep deprivation after SDS, (i.e. activation of these cells while mice were awake), partially reduced CORT levels (Fig. S29C, D), but the overall CORT levels still remained elevated (Fig. S29D), suggesting that sleep after SDS is also needed to reduce CORT levels.

Discussion

Our proposed circuit model for how SDS translates to sleep and reduction of anxiety, with VTA^{Vgat-Sst} cells playing a central role, is shown in Fig. 6K. Once activated by SDS, VTA^{Vgat-Sst} cells drive

sleep through the lateral hypothalamus, a brain region containing a diverse population of cells implicated in regulating stress, anxiety and sleep/wake behaviours (31, 32). $VTA^{Vgat-Sst}$ cell activity is maintained for some hours beyond the stress episode, suggesting a form of plasticity which enables them to keep promoting NREM and REM sleep episodes for a sustained period. In parallel to their sleep-inducing and anxiety-reducing effects, $VTA^{Vgat-Sst}$ cells inhibit CRF-producing neurons in the PVN hypothalamus, thereby reducing CORT levels after SDS. We found that SDS-induced anxiety persisted even in the presence of CORT inhibitors. These results suggest that physiological activation of VTA^{Sst} neurons during and after SDS represses CRF and therefore CORT production, guarding against overproduction of CORT. Persistently elevated CORT levels have deleterious effects on body organs (1). We propose the reduced anxiety comes from the sleep component. After SDS, the restorative sleep by $VTA^{Vgat-Sst}$ cells also aids CORT levels returning to baseline, so there seem to be parallel routes to reducing CORT levels, but with VTA^{Sst} cells coordinating both mechanisms.

The output pathways regulated by $VTA^{Vgat-Sst}$ cells in the LH to induce sleep and reduce anxiety are unclear. VTA^{Gad67} neurons inhibit orexin/Hcrt neurons in the LH (20). However, chemogenetic inhibition of LH^{Hcrt} cells did not reduce anxiety after SDS (Fig. S30), and orexin receptor antagonists did not restore the anxiolytic effects that were missing in VTA^{Sst} -lesioned mice that had undergone SDS (Fig. S31), suggesting that orexin/Hcrt cell inhibition is not required for the anxiolytic actions of $VTA^{Vgat-Sst}$ cells. Thus, identifying the targets of $VTA^{Vgat-Sst}$ cells requires further study. Local action within the VTA of the VTA^{Sst} neurons is also possible.

In summary, GABA^{Sst} neurons in the VTA respond to SDS, an ethological model for psychosocial stress, by inducing restorative sleep and decreasing CRF production. Targeting these neurons could potentially provide a new route for treating anxiety disorders.

1. G. Russell, S. Lightman, *Nat Rev Endocrinol* **15**, 525-534 (2019).
2. B. S. McEwen, H. Akil, *J Neurosci* **40**, 12-21 (2020).
3. M. Nollet *et al.*, *Interface Focus* **10**, 20190092 (2020).
4. A. N. Goldstein, M. P. Walker, *Annu Rev Clin Psychol* **10**, 679-708 (2014).
5. D. A. Kalmbach *et al.*, *J Sleep Res* **27**, e12710 (2018).
6. E. J. W. Van Someren, *Physiol Rev* **101**, 995-1046 (2021).
7. S. B. Li *et al.*, *Sci Adv* **6**, (2020).
8. R. G. Foster, *Interface Focus* **10**, 20190098 (2020).
9. M. Nollet *et al.*, *Proc Natl Acad Sci U S A* **116**, 2733-2742 (2019).
10. N. P. Franks, W. Wisden, *Science* **374**, 556-559 (2021).
11. X. Feng *et al.*, *Neurosci Bull* **36**, 1137-1146 (2020).
12. N. Gujar *et al.*, *Cereb Cortex* **21**, 115-123 (2011).
13. M. Morales, E. B. Margolis, *Nat Rev Neurosci* **18**, 73-85 (2017).
14. V. Krishnan *et al.*, *Nature* **543**, 507-512 (2017).
15. L. A. Gunaydin *et al.*, *Cell* **157**, 1535-1551 (2014).
16. C. Bouarab *et al.*, *Front Neural Circuits* **13**, 78 (2019).
17. J. H. Jennings *et al.*, *Nature* **496**, 224-228 (2013).
18. X. Yu *et al.*, *Nat Neurosci* **22**, 106-119 (2019).
19. A. Eban-Rothschild *et al.*, *Nat Neurosci* **19**, 1356-1366 (2016).
20. S. Chowdhury *et al.*, *eLife* **8**, e44928 (2019).
21. Y. Takata *et al.*, *J Neurosci* **38**, 10080-10092 (2018).

22. Z. Zhou *et al.*, *Neuron* **103**, 473-488.e476 (2019).
23. A. Eban-Rothschild *et al.*, *eNeuro* **7**, (2020).
24. K. R. Tan *et al.*, *Neuron* **73**, 1173-1183 (2012).
25. S. Fujii *et al.*, *Front Neurosci* **13**, 322 (2019).
26. L. Faget *et al.*, *Cell Reports* **15**, 2796-2808 (2016).
27. E. J. Paul *et al.*, *Eur J Neurosci* **50**, 3732-3749 (2019).
28. E. Nagaeva *et al.*, *Elife* **9**, (2020).
29. M. K. Kaushik *et al.*, *Scientific Reports* **7**, 8892 (2017).
30. H. Wang *et al.*, *bioRxiv* <https://doi.org/10.1101/2022.03.26.485911>, (2022).
31. E. Arrigoni *et al.*, *Neuropharmacology* **154**, 34-49 (2019).
32. S. B. Li *et al.*, *Science* **375**, eabh3021 (2022).
33. L. Vong *et al.*, *Neuron* **71**, 142-154 (2011).
34. H. Taniguchi *et al.*, *Neuron* **71**, 995-1013 (2011).
35. S. Hippenmeyer *et al.*, *PLoS Biol* **3**, e159 (2005).
36. L. Madisen *et al.*, *Nat Neurosci* **13**, 133-140 (2010).
37. W. J. Giardino *et al.*, *Nature Neuroscience* **21**, 1084-1095 (2018).
38. S. Ren *et al.*, *Science* **362**, 429-434 (2018).
39. Z. Zhang *et al.*, *Nature Neuroscience* **18**, 553-561 (2015).
40. E. C. Harding *et al.*, *Current Biology* **28**, 2263-2273.e2264 (2018).
41. M. J. Krashes *et al.*, *J Clin Invest* **121**, 1424-1428 (2011).
42. X. Yu *et al.*, *Nat Neurosci* **22**, 106-119 (2019).
43. T. W. Chen *et al.*, *Nature* **499**, 295-300 (2013).
44. K. T. Beier *et al.*, *Nature* **549**, 345-350 (2017).
45. C. F. Yang *et al.*, *Cell* **153**, 896-909 (2013).
46. A. J. Murray *et al.*, *Nat Neurosci* **14**, 297-299 (2011).
47. D. G. Tervo *et al.*, *Neuron* **92**, 372-382 (2016).

48. R. Lin *et al.*, *Nat Methods* **15**, 1033-1036 (2018).
49. T. R. Reardon *et al.*, *Neuron* **89**, 711-724 (2016).
50. S. Fujii, M. K. Kaushik, X. Zhou, M. Korkutata, M. Lazarus, *Front Neurosci* **13**, 322 (2019).
51. S. A. Golden, H. E. Covington III, O. Berton, S. J. Russo, *Nat Protoc* **6**, 1183-1191 (2011).
52. M. K. Kaushik, K. Aritake, A. Takeuchi, M. Yanagisawa, Y. Urade, *Scientific Reports* **7**, 8892 (2017).
53. N. Charoenphandhu *et al.*, *Scientific Reports* **12**, 5959 (2022).
54. G.-W. Zhang *et al.*, *Nature Neuroscience* **24**, 516-528 (2021).
55. X. Yu *et al.*, *Molecular Psychiatry* **26**, 5213-5228 (2021).
56. K. Tossell *et al.*, *bioRxiv*, 2020.2007.2001.179671 (2020).
57. L. A. Gunaydin *et al.*, *Cell* **157**, 1535-1551 (2014).
58. G. M. Alexander *et al.*, *Neuron* **63**, 27-39 (2009).
59. E. S. Boyden, F. Zhang, E. Bamberg, G. Nagel, K. Deisseroth, *Nat Neurosci* **8**, 1263-1268 (2005).
60. V. N. Anisimov *et al.*, *Nature Methods* **11**, 1135-1137 (2014).
61. P. Mitra, H. Bokil, Oxford University Press, New York. (2008).
62. C. Tronche *et al.*, *Neurobiology of Learning and Memory* **93**, 343-351 (2010).
63. R. M. Sears *et al.*, *Proc Natl Acad Sci U S A* **110**, 20260-20265 (2013).

Acknowledgements

We thank K. Beier, L.Q. Luo, R.C. Malenka for sharing plasmids; A. Murray for providing rabies virus; Z.A. Hu for providing *Hcrt-IRES-Cre* mice and J. Hu for providing *Sst-IRES-Cre* mice.

Funding: Our work was supported by the Wellcome Trust (107839/Z/15/Z, 107841/Z/15/Z and 220759/Z/20/Z, N.P.F. and W.W.); the UK Dementia Research Institute (UK DRI-5004, W.W. and N.P.F.); and the National Natural Science Foundation of China (Grant No. 82030038, 81620108012 and 81901080 H.D. and N.P.F.). **Author contributions:** X.Y., N.P.F. and W.W. conceived, and with X.Y., G.Z. and H.D. designed the experiments; X.Y., G.Z., D.W., S.W., A.L., R.L., H.L., J.Z., J.L., M.N., Y.C., T.Z., M.C., R.Y. performed the experiments and/or data analysis; A.L.V. provided the Neurologgers; H.W. and Y.L. engineered the CRF sensor; N.P.F. and W.W. contributed to the data analysis and with H.D. supervised the project; X.Y., N.P.F., and W.W. wrote the paper. **Competing interests:** The authors declare no competing interests. **Data and materials availability:** All data necessary to understand and assess the conclusions of this study are available in the manuscript or the supplementary materials. Constructs generated in this study have been deposited at Addgene with accession numbers provided in the Supplementary Material.

Figure legends

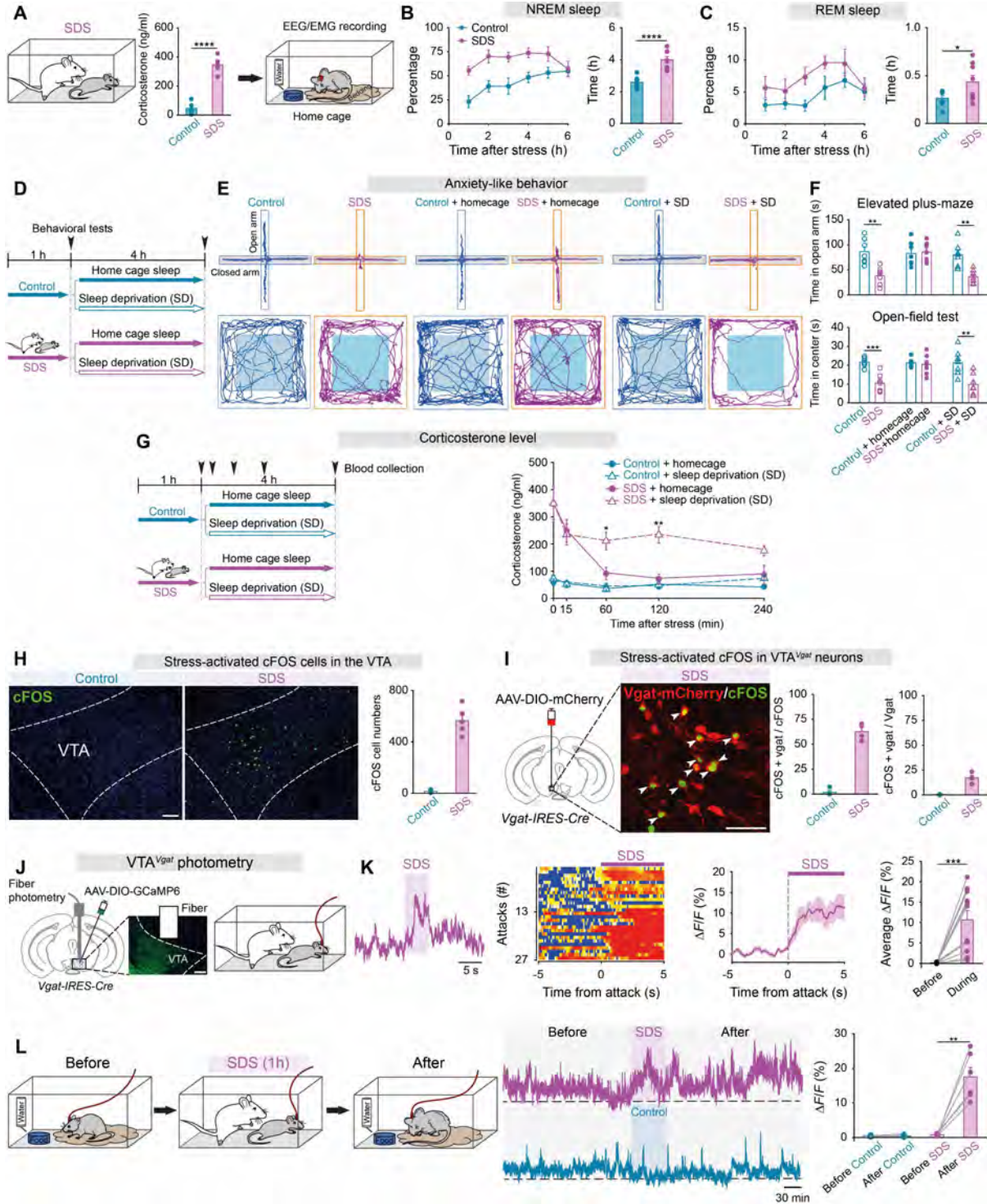


Fig. 1 Stress increases sleep while sleep reduces SDS-induced anxiety and stress activates VTA^{Vgat} neurons.

(A) The experimental procedure and corticosterone levels (n=6 mice per group).

(B, C) Percentage and time of NREM (B) and REM (C) sleep after control or SDS (n=8 mice per group).

(D-F) Plan of the experimental procedure (D), tracing of locomotion for representative animals (E), time spent in the open arms of the elevated plus-maze and in the center zone during the open-field test (F) (n=7 mice per group).

(G) Plan of the experimental procedure and corticosterone levels (n=6 mice per group).

(H, I) cFOS expression and quantification in the VTA after control or SDS (n=5 mice per group) (H); or in genetically labeled VTA^{Vgat} neurons (n=4 mice per group) (I). Arrowheads indicate double-labeled cells. Scale bar, 100 μ m.

(J, K) Fiber photometry setup and GCaMP6 expression in VTA^{Vgat} neurons (J). Fiber photometry measuring calcium signals responding to SDS (n=11 mice, 27 trials). Raw calcium signal traces, color matrix of signals for all trials, $\Delta F/F$ ratios across the experimental period and average $\Delta F/F$ ratios before and during the procedure (K). Scale bar, 100 μ m.

(L) Fiber photometry measuring long-term calcium signals in VTA^{Vgat} neurons. Traces across the experimental procedure and average $\Delta F/F$ ratios before and after the procedures (n=6 mice per group).

(A, B, C) Unpaired *t*-test, * $p < 0.05$, **** $p < 0.0001$; (F, G) Two-way ANOVA with bonferroni *post hoc* test, * $p < 0.05$, ** $p < 0.01$, *** $p < 0.001$; (K, L) Paired *t*-test, ** $p < 0.01$, *** $p < 0.001$.

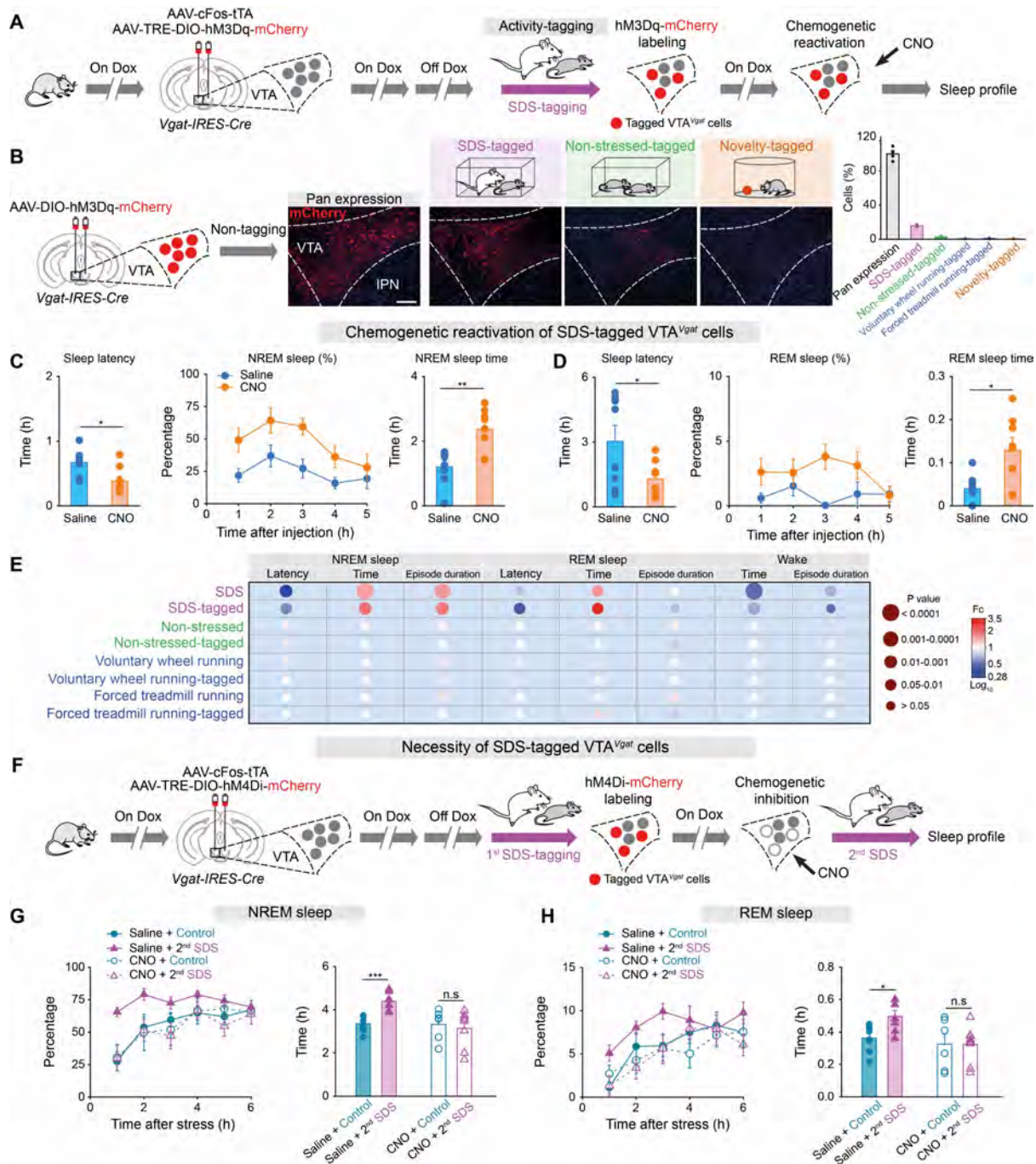


Fig. 2 Sufficiency and necessity of the stress-activated VTA^{Vgat} neurons for SDS-induced sleep

(A) The activity-tagging protocol for testing the sufficiency of SDS-activated VTA^{Vgat} cells for sleep.

(B) Expression and quantification of pan or activity-tagged hM3Dq-mCherry transgene in VTA^{Vgat} neurons (n=4 mice per group). Scale bar, 100 μm.

(C, D) Chemogenetic reactivation of tagged VTA^{Vgat} neurons for sleep (n=8 mice per group). Graphs show sleep latency, percentage and time of NREM (C) or REM (D) sleep. Unpaired *t*-test, **p*<0.05, ***p*<0.01.

(E) Matrix bubble summary shows fold of changes (Fc) of sleep parameters after SDS, non-stressed, **voluntary wheel running**, **forced treadmill running** or the chemogenetic reactivation of tagged VTA^{Vgat} neurons.

(F) Activity-tagging protocol for testing the necessity of SDS-activated VTA^{Vgat} cells for sleep.

(G, H) Percentage and time of NREM (G) or REM sleep (H) in mice given 2nd SDS after chemogenetic inhibition of 1st SDS-tagged VTA^{Vgat} cells (n=6-8 mice per group). Two-way ANOVA with bonferroni *post hoc* test. **p*<0.05, ****p*<0.001, n.s: not significant.

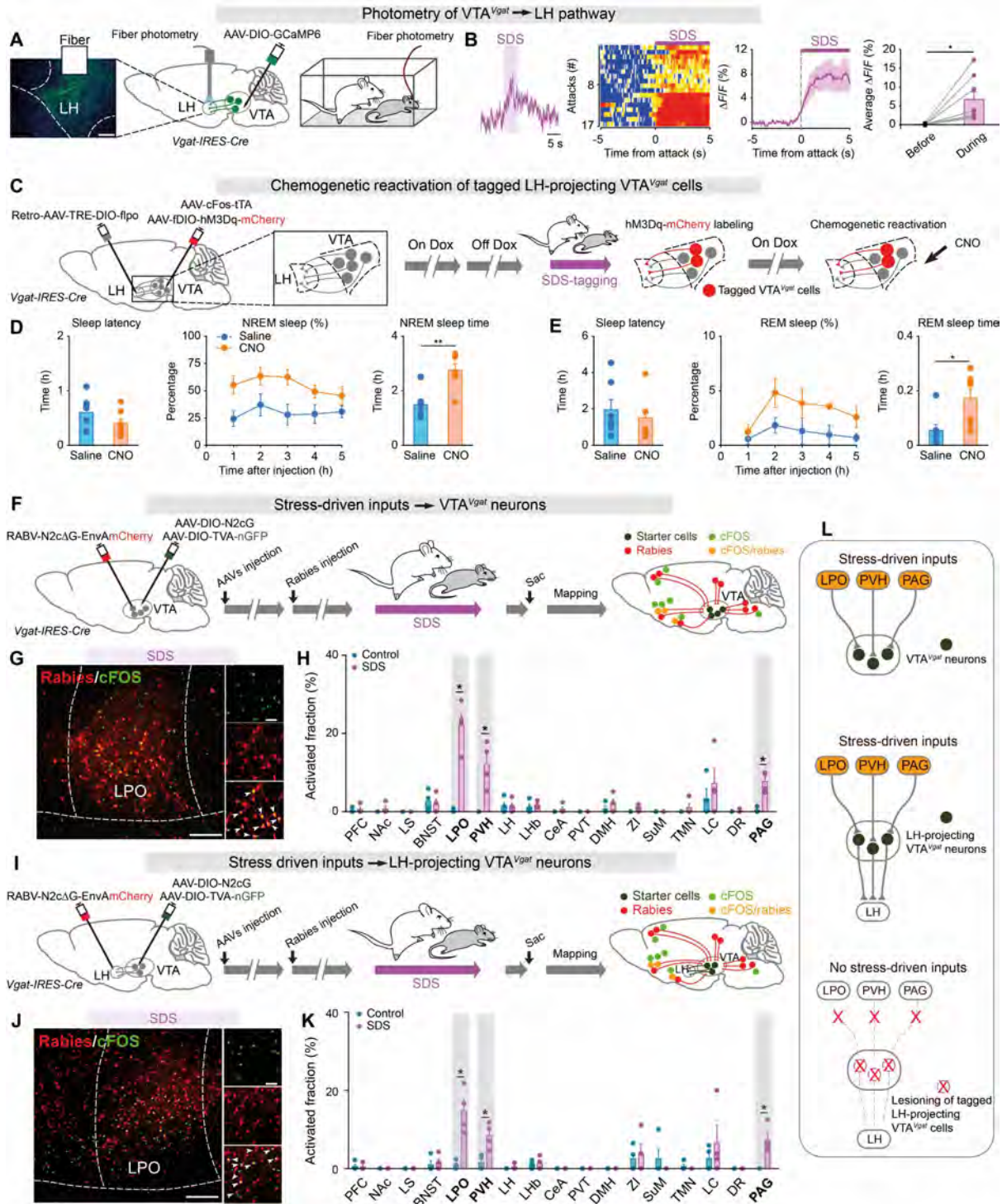


Fig. 3 Input-output circuitry linking stress and sleep

(A, B) Fiber photometry measuring terminal calcium signals of the VTA^{Vgat}→LH pathway responding to SDS (A). Raw traces, color matrix of GCaMP6 signals of VTA^{Vgat}→LH for all trials,

$\Delta F/F$ ratios across the experimental period and average $\Delta F/F$ before and during SDS (n=8 mice, 17 trials) **(B)**. Paired *t*-test, **p*<0.05. Scale bar, 100 μ m.

(C) Activity-tagging protocol for reactivating the SDS-tagged LH-projecting VTA^{Vgat} cells.

(D, E) Sleep latency, percentage and time of NREM **(D)** and REM **(E)** sleep after reactivation of SDS-tagged LH-projecting VTA^{Vgat} cells (n=7 mice per group). Unpaired *t*-test, **p*<0.05, ***p*<0.01.

(F) Rabies virus-based retrograde tracing for identification of stress-driven inputs to VTA^{Vgat} neurons.

(G) Immunostaining images showing presynaptic inputs to VTA^{Vgat} neurons from LPO, and cFOS-positive cells activated by SDS. Scale bar, 200 μ m and 50 μ m (inset).

(H) Summary statistics of activated fractions (cFOS/rabies double-labeled cells/total rabies-positive cells) (n=4 mice per group). For abbreviations, see Fig. S4. Mann-Whitney test, **p*<0.05.

(I) Protocol for identification of stress-driven inputs to VTA^{Vgat} neurons that output to LH.

(J) Immunostaining shows presynaptic inputs to LH-projecting VTA^{Vgat} neurons from LPO, and cFOS-positive cells activated by stress. Scale bar, 200 μ m and 50 μ m (inset).

(K) Summary statistics of activated fractions to LH-projecting VTA^{Vgat} neurons (n=4 mice per group). Mann-Whitney test, **p*<0.05.

(L) Schematic diagram summarizing the stress-driven input-output relations.

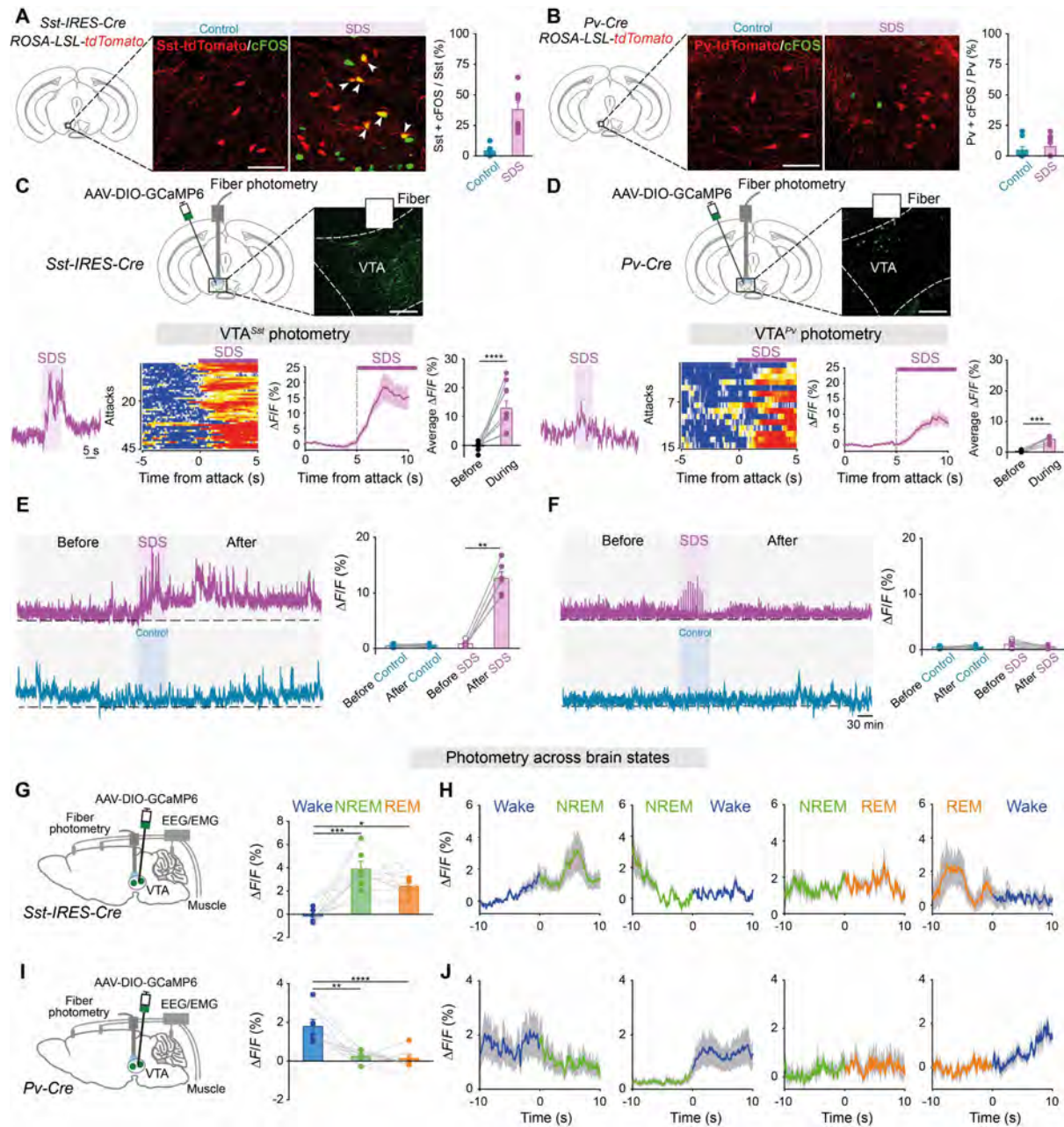


Fig. 4 Activity of VTA^{Sst} or Pv neurons responding to stress and across brain states

(A, B) cFOS expression and quantification in genetically labeled VTA^{Sst} (A) or VTA^{Pv} (B) neurons after control experience or SDS (n=8 mice per group). Scale bar, 100 μ m.

(C, D) Fiber photometry measuring calcium signals in VTA^{Sst} (n=10 mice per group, 45 trials) (C) or VTA^{Pv} (n=6 mice per group, 15 trials) (D) neurons responding to SDS. Raw calcium signal

traces, color matrix of signals for all trials, $\Delta F/F$ ratios across the experimental period and average $\Delta F/F$ ratios before and during SDS. Paired t -test, *** $p < 0.001$, **** $p < 0.0001$. Scale bar, 200 μm .

(E, F) Fiber photometry measuring long-term calcium signals in VTA^{Sst} **(E)** or VTA^{Pv} **(F)** neurons. Raw traces and average $\Delta F/F$ ratios before and after the procedures (n=6 mice per group). Paired t -test, ** $p < 0.01$.

(G-J) Fiber photometry with EEG/EMG measuring spontaneous activity across brain states. $\Delta F/F$ ratios in VTA^{Sst} **(G)** or VTA^{Pv} **(I)** neurons during wakefulness, NREM and REM sleep, and at transitions of vigilance states (n=6 mice per group) **(H, J)**. One-way Repeated ANOVA, * $p < 0.05$, ** $p < 0.01$, *** $p < 0.001$, **** $p < 0.0001$.

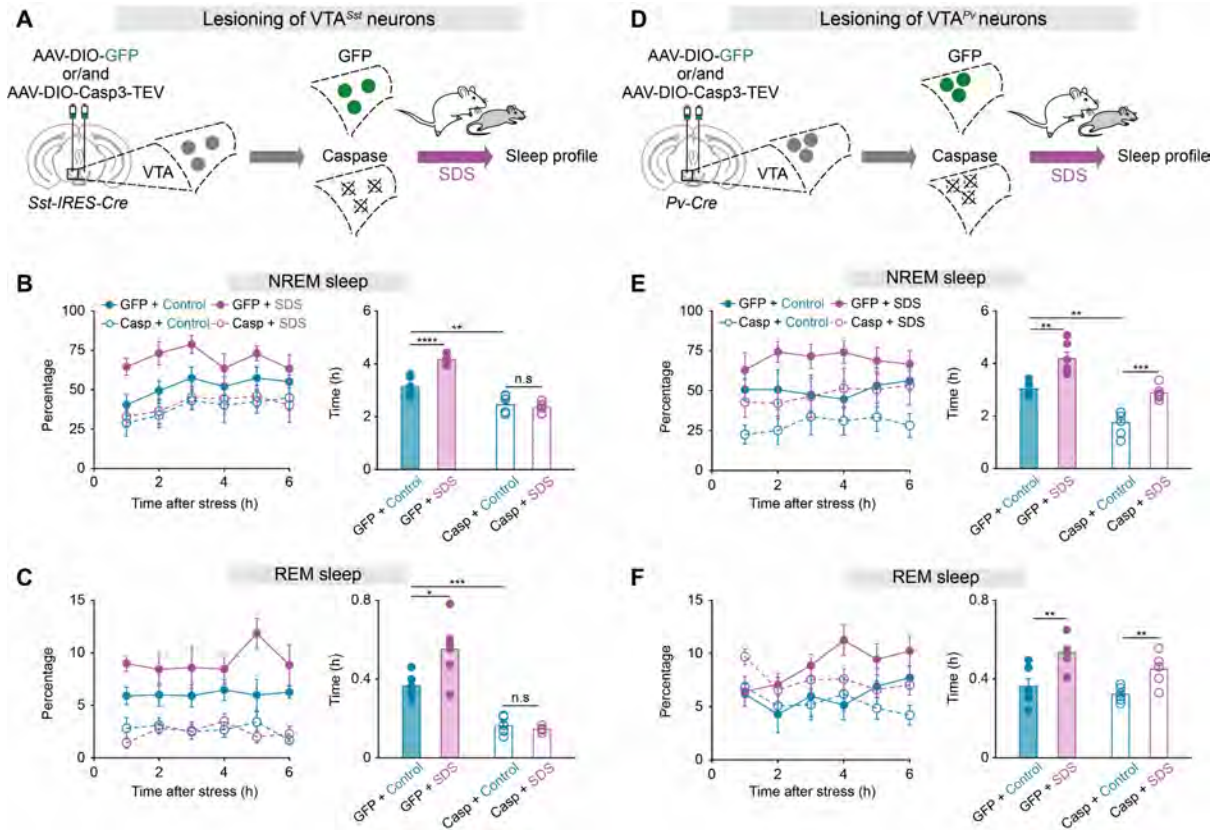


Fig. 5 VTA^{Sst} neurons are necessary for SDS-induced sleep

(A, D) Genetic ablation of VTA^{Sst} (A) or VTA^{Pv} (D) neurons.

(B, C, E, F) Percentage and time of NREM or REM sleep in VTA^{Sst} (B, C) or VTA^{Pv} (E, F) ablated mice or control mice given control or SDS. Two-way ANOVA with bonferroni *post hoc* test.

*p<0.05, **p<0.01, ***p<0.001, ****p<0.0001, n.s: not significant.

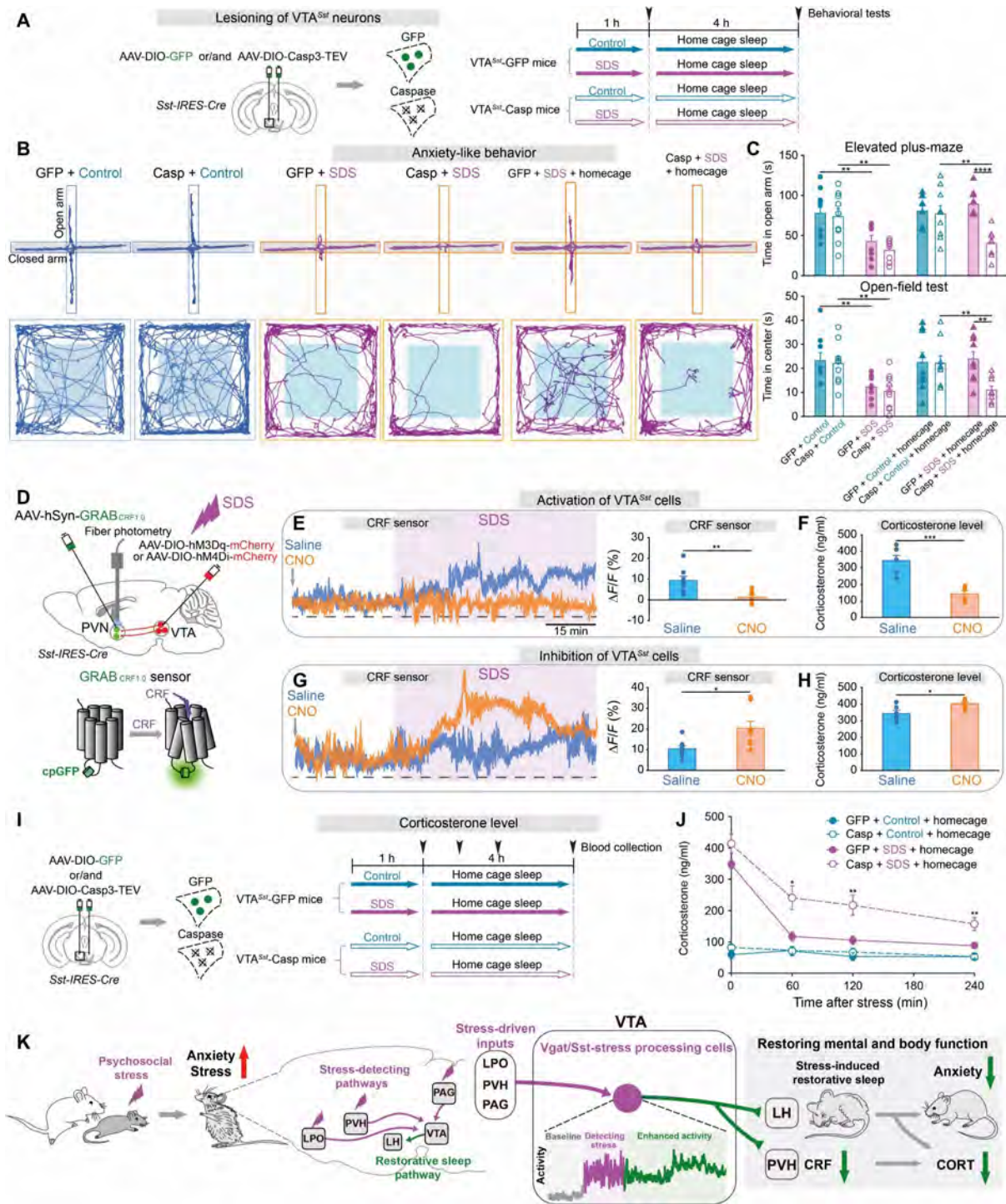


Fig. 6 Activity and SDS-induced sleep by VTA^{Sst} neurons reduces anxiety and corticosterone levels

(A-C) Plan of the experimental procedure (A), tracing of locomotion for representative animals (B), time spent in the open arms of the elevated plus-maze and in the center zone during the open-field test (n=9 mice per group) (C).

(D) Delivering genetically-encoded CRF sensor in the PVN hypothalamus alongside chemogenetic manipulation of VTA^{Sst} neurons.

(E, G) Raw PVN CRF sensor traces and $\Delta F/F$ ratios during SDS after chemogenetic activation (E) or inhibition (G) of VTA^{Sst} neurons (n=8 mice per group).

(F, H) Corticosterone levels following SDS after chemogenetic activation (F) or inhibition (H) of VTA^{Sst} neurons (n=6 mice per group).

(I, J) Plan of the procedure (I) and corticosterone levels (n=4-9 mice per group) (J).

(K) Conceptual summary diagram.

(C, J) Two-way ANOVA with bonferroni *post hoc* test, *p<0.05, **p<0.01, ****p<0.0001.

(E-H) Unpaired *t*-test, *p<0.05, **p<0.01, ***p<0.001.

List of Supplementary Content

Materials and Methods

Figs. S1 to S33

References

Supplementary Materials for

A specific circuit in the midbrain detects stress and induces restorative sleep

**Xiao Yu, Guangchao Zhao, Dan Wang, Sa Wang, Rui Li, Ao Li, Huan Wang, Mathieu Nollet,
You Young Chun, Tianyuan Zhao, Raquel Yustos, Huiming Li, Jianshuai Zhao, Jiannan Li,
Min Cai, Alexei L. Vyssotski, Yulong Li, Hailong Dong, Nicholas P. Franks, William Wisden**

Correspondence to: xiao.1.yu@kcl.ac.uk, hldong6@hotmail.com, n.franks@imperial.ac.uk,
w.wisden@imperial.ac.uk

This PDF file includes:

Materials and Methods
Figs. S1 to S33
References

Other Supplementary Materials for this manuscript include the following:

MDAR Reproducibility Checklist

Materials and Methods

Animals

All experiments were performed in accordance with the UK Home Office Animal Procedures Act (1986); all procedures were approved by the Imperial College Ethical Review Committee and the Ethics Committee for Animal Experimentation of the Fourth Military Medical University, Xijing Hospital, Xi'an, and were conducted according to the Guidelines for Animal Experimentation of the Chinese Council institutes. The following strains of mice were used: *Vgat-IRES-Cre: Slc32a1^{tm2(cre)Lowl/J}*, JAX stock 016962 and *Vglut2-IRES-Cre: Slc17a6^{tm2(cre)Lowl/J}*, JAX stock 016963, both generated by B.B. Lowell (33); *Sst-IRES-Cre: Sst^{tm2.1(cre)Zjh/J}*, JAX stock 013044, generated by Z. J. Huang (34); *Pv-Cre: B6.129P2-Pvalb^{tm1(cre)Arbr/J}*, JAX stock 008069, generated by S. Arber (35), and Ai9 (*Rosa-LSL-tdTomato*), JAX stock 007909, generated by H. Zeng (36); *Hcrt-IRES-Cre; Hcrt^{tm1.1(cre)Ldl}*, Stanford_006_mHcrt_1B1, generated by Luis de Lecea (37) and kindly provided by Zhian Hu (Third Military Medical University, Chongqing, China) (38). CD-1 mice, 6–8 months old and C57BL/6j mice were purchased from Charles River Laboratories, Inc., and Beijing Vital River Laboratory Animal Technology, Beijing, China. Mice were maintained on a 12 h:12 h light:dark cycle at constant temperature and humidity with *ad libitum* food and water.

AAV vectors, AAV production, and rabies system

Plasmid *pAAV-cFOS-tTA* (Addgene plasmid#66794) was generated in our lab as previously described (39). *pAAV-TRE-DIO-hM3Dq-mCherry* (Addgene plasmid#115161) (39, 40) and *pAAV-TRE-DIO-hM4Di-mCherry* (Addgene plasmid#182532) were constructed in our lab, where the *hM3Dq-mCherry* or *hM4Di-mCherry* reading frame is inverted between

heterologous pairs of lox sites (double inverted orientation, DIO) downstream of the *TRE* (Tet-Response-Element) promoter (Clontech). To make this plasmid, we did the following: the promoter *TRE* fragment was cut out and isolated from *pAAV-TRE-hM3Dq-mCherry* plasmid that we made before (Addgene plasmid #66795) using *MluI* and *Sall* restriction enzymes. The plasmid *pAAV-hSyn-DIO-hM3Dq-mCherry* or *pAAV-hSyn-DIO-hM4Di-mCherry* (gift from Bryan L. Roth, Addgene plasmid #44361 (41) or #50475) was double-digested with *MluI* and *Sall* to remove the *hSynapsin* promoter. The *TRE* promoter was ligated into the backbone between *MluI* and *Sall* sites to give *pAAV-TRE-DIO-hM3Dq-mCherry* or *pAAV-TRE-DIO-hM4Di-mCherry*, respectively. To make *pAAV-TRE-DIO-ChR2-EYFP* (Addgene plasmid#183765), the backbone, *AAV-TRE-DIO-*, was purified from *pAAV-TRE-DIO-hM3Dq-mCherry-*, after double digestion with *Ascl* + *NheI* and gel purification. The insert, *ChR2-EYFP*, was taken from Addgene plasmid #20298 (humanized *ChR2* with H134R mutation fused to *EYFP*, gift from Karl Deisseroth), after double digestion with *Ascl* + *NheI* and gel purification. Both fragments were ligated to produce the final construct *pAAV-TRE-DIO-ChR2-EYFP*. The plasmid *pAAV-hSyn-DIO-GCaMP6s* was created as we previously described (18); we used the *GCaMP6s* reading frame from *pGP-CMV-GCaMP6s* (gift of Douglas Kim, Addgene plasmid #40753) (42). Then, to make *pAAV-TRE-DIO-GCaMP6s* (Addgene plasmid#183809), *pAAV-hSyn-DIO-GCaMP6s* and *pAAV-TRE-hM3Dq-mCherry* were digested with *MluI* and *Sall*. After double digestion, the 6.2 kb band corresponding to the backbone (*AAV-MluI-...-Sall-DIO-GCaMP6s*) was gel purified, leaving behind the *hSyn* promoter; similarly, the *MluI-TRE-Sall* promoter was gel purified (band around 344bp). The two fragments were ligated to produce *pAAV-TRE-DIO-GCaMP6s*. Plasmid *pAAV-fDIO(FLP-Cre-dependent)-hM3Dq-mCherry* was a gift from Kevin T. Beier generated in Robert C. Malenka's lab (43). *pAAV-TRE-DIO-Casp3-TEV* was generated in our lab. To make *pAAV-TRE-DIO-Casp3-TEV* (Addgene plasmid#183766), the backbone *AAV-DIO-*

Casp3-TEV was gel purified from *pAAV-hSyn-DIO-Casp3-TEV* (Addgene plasmid #45580) (44) after double digestion with *MluI* and *Sall* to remove the *hSynapsin* promoter. At the same time, TRE was also gel purified from *AAV-TRE-hM3Dq-mCherry* after double digestion with *MluI* and *Sall*. The two fragments were ligated to give *pAAV-TRE-DIO-Casp3-TEV*.

We packaged the transgenes (*AAV-DIO-ChR2-EYFP*, *AAV-DIO-GCaMP6s*, *AAV-cFOS-tTA*, *AAV-TRE-DIO-hM3Dq-mCherry*, *AAV-TRE-DIO-hM4Di-mCherry*, *AAV-TRE-DIO-ChR2-EYFP*, *AAV-TRE-DIO-GCaMP6s*, *AAV-TRE-DIO-FLPo*, *AAV-TRE-DIO-Casp3-TEV* and *AAV-fDIO-hM3Dq-mCherry*) into AAV capsids (capsid serotype 1/2) in house as described previously (45). To produce retro-*AAV-TRE-DIO-FLPo*, we used the AAVpro Purification Kit (all Serotypes) (Takara-Clontech, Cat#6666) and the rAAV2 packaging plasmid, a gift from Alla Karpova and David Schaffer (Addgene plasmid #81070) (46), and the helper plasmid *pFΔ6*, together with *AAV-TRE-DIO-FLPo* from Minmin Luo (Addgene plasmid #118027) (47).

For the rabies system, *pAAV-DIO-N2cG*, *pAAV-DIO-TVA-nGFP* and *RABV-N2cΔG-EnvAmCherry* were kindly provided by Andrew Murray (Sainsbury Wellcome Center, UCL, UK) (48). *AAV-DIO-GFP* was purchased from Addgene (#50457-AAV2). *AAV-DIO-hM3Dq-mCherry*, *AAV-DIO-hM4Di-mCherry*, *AAV-DIO-taCasp3-TEVp* and *AAV-DIO-mCherry* were provided by BrainVTA Technology Co., Ltd. (Wuhan, China).

Surgery

The surgical procedure was conducted as previously described (18). 10-14-week-old male mice were anesthetized with 2% isoflurane in oxygen by inhalation and received buprenorphine (0.1 mg/kg) and carprofen (5 mg/kg) injections, and then placed on a stereotaxic frame (Angle Two, Leica Microsystems, Milton Keynes, Buckinghamshire, UK).

The AAVs were injected through a stainless steel 33-gauge/15mm/PST3 internal cannula (Hamilton) attached to a 10 μl Hamilton syringe at a rate of 0.1 $\mu\text{l min}^{-1}$. For the AAV injections, the virus was bilaterally or unilaterally injected into the VTA, LH, LHb, DG or CeA.

The injection coordinates and volumes were:

VTA: ML = ± 0.35 mm, AP = - 3.52 mm, DV = - 4.25 mm; 50 nl + 50 nl

LH: ML = ± 1.00 mm, AP = - 1.56 mm, DV = - 5.20 mm; 100 nl + 100 nl

After injection, the cannula was left at the injection site for 5 min and then slowly pulled out.

After injections, mice that were to undergo the sleep experiments were implanted with three gold-plated miniature screw electrodes (-1.5 mm Bregma, $+1.5$ mm midline; $+1.5$ mm Bregma, -1.5 mm midline; -1 mm Lambda, 0 mm midline – reference electrode) with two EMG wire (AS634, Cooner Wire, CA). The EMG electrodes were inserted between the neck musculatures. EEG-EMG connector for the Neurologger 2A was affixed to the skull with Orthodontic Resin power and Orthodontic Resin liquid (Tocdental, UK).

For the telemetry EEG and EMG surgery, the mice were anesthetized with isoflurane as above and implanted in the abdominal subcutaneous with wireless TL11M2-F20-EET device (Data Sciences International) biotelemetry transmitters. Four of the wires were attached subcutaneously to the neck of the mice through a guide cannula. Then, mice were placed into a stereotaxic instrument in a prone position. Next, two surface EEG electrodes (biopotential leads tethered to miniature stainless-steel screws) were implanted over the left frontal lobe (AP 0.2 mm, ML 1.5 mm, DV -0.1 mm) and the contralateral parietal lobe (AP -1.7 mm, ML -0.2 mm, DV -0.1 mm) and lowered until they contacted the dura of the skull, with dental cement to secure in place. Two biopotential EMG electrodes were embedded through the small incision, which was made at the oblique cervical muscle with a 21G needle and fixed

with insoluble silk sutures. The incision site was sutured and treated with local anesthetic (2% lidocaine) and topical antibiotic. For EEG/EMG recording, mice were individually housed following surgery in standard Plexiglas home cages placed on RPC-1 PhysioTel receivers, which receive signals from the transmitters. RPC-1 PhysioTel receivers are concatenated to a data exchange matrix, which transmits continuous and synchronized EEG, EMG and motor activity.

For the fiber photometry or optogenetic experiments, after virus injection, mice received unilateral surgical implantations above the VTA, LH, LHb, DG or CeA of a monofiberoptic cannula (200 μ m; Doric Lenses, Inc., Quebec, Canada). The fiber placement coordinates were:

VTA: ML = 0.35 mm, AP = - 3.52 mm, DV = - 3.9 mm

LH: ML = 1.00 mm, AP = -1.56 mm, DV = -5.10 mm

LHb: ML = 0.5 mm, AP = - 1.6 mm, DV = - 2.3 mm

DG: ML = 1.3 mm, AP = - 2.2 mm, DV = - 1.6 mm

CeA: ML = 2.7 mm, AP = - 1.4 mm, DV = - 4.15 mm

Cannula Implantation and administration of orexin receptor antagonists

Mice were placed in an induction chamber with 1.2-1.4% isoflurane (Baxter Healthcare, Puerto Rico) vaporized by oxygen flowing at 1.0 L/min and then transferred and fixed to a stereotaxic frame while keeping the mice anesthetized by 0.8% isoflurane via a mask. After cleaning and exposure of the skull, *AAV-DIO-taCasp3-TEV* was injected into the VTA of *Sst-IRES-Cre* mice as described above. Three weeks after virus injection, a guide cannula (Stoelting, Co., US) was stereotaxically directed into the lateral cerebral ventricle (ML = -1.00

mm, AP = 0.50 mm, DV = -2.00 mm). The mice were allowed to recover for at least 7 days after the surgery.

Behavioral protocols

Social defeat stress, the non-stressful procedure, restraint stress, exposure to novel environments, voluntary wheel running, forced treadmill running and activity-tagging all took place one hour before the start of “lights on”. The cage-change mild stress procedure was conducted at the beginning of “lights on”. Mice were habituated for 10 min in the experimental room for a continuous period of 3 days before the experiments. Open-field tests (OFT) and elevated plus-maze (EPM) were performed at specific time points below: 1, before control or SDS (1-h before the start of “lights on”); 2, straight after control or SDS (at the beginning of “lights on”); 3, after control or SDS followed by 4-h home cage sleep or 4-h sleep deprivation (4-h after “lights on”).

Social defeat stress was performed as reported with small modifications (Fig. S1A) (25, 49). Before performing social defeat experiments, male CD-1 retired breeder mice at 4–6 months of age, were singly housed, allowing habituation for a minimum of 7 d prior to screening. The appropriate CD-1 aggressive mice were selected from the 3-d screening process to meet the social defeat criterion (49). For screening the aggressors, C57BL/6j mice between 8 and 20 weeks of age were used. The CD-1 mice that showed extreme aggressive behavior or no aggression were excluded from experiments. Only mice showing aggression within 1 min and persistent aggressive intention were used in social defeat sessions (49).

For social defeat stress, an intruder mouse (experimental mouse) was introduced into the home cage of the CD1 resident mouse for 5 min. During these 5 min, there was usually 5-8

conflicts. Then a transparent partition was used to separate the intruder and resident mice, but the intruder remained in olfactory, visual and auditory contact with the resident for 10 min. During the social defeat sessions, the procedure was repeated four times at 15 min intervals, for a total of 60 min (Fig. S1A). At the end of the stress procedure, the intruder exhibited an apparent freezing behavior or a submissive posture. Normally, no wound was found on intruders following this stress procedure; however, when the intruder mouse had visible wounds, the intruder and corresponding CD-1 mouse were excluded. For the controls, the intruder mouse was placed into the home cage of the aggressive resident mouse without contact for 60 min using a transparent partition to separate the intruder and resident mice, but remained in olfactory, visual and auditory contact with the resident (Fig. S1A). Video recording was performed with recordings of fiber photometry signals.

Non-stressful procedure. This protocol was used as the control for the physical movements during the social defeat stress. In detail, an intruder mouse (experimental mouse) was introduced into the home cage of the juvenile (younger) mouse for 5 min. During these 5 min, the mice experienced movements, physical activity and social interaction but typically had no conflicts. If the mice had any conflicts, the intruder and corresponding juvenile mouse were excluded. Then a transparent partition was used to separate the intruder and resident mice, but the intruder remained in olfactory, visual and auditory contact with the resident for 10 min. During the non-stressful sessions, the procedure was repeated four times at 15 min intervals, for a total of 60 min (Fig. S1B). At the end of the non-stressful procedure, the intruders exhibited normal behaviors without having freezing behavior or a submissive posture. For the controls, the intruder mouse was placed into the home cage of the juvenile resident mouse without contact for 60 min using a transparent partition to separate the

intruder and resident mice, but remained in olfactory, visual and auditory contact with the resident (Fig. S1B).

Restraint stress. The restraint paradigm was performed as previously described (7). Mice were individually placed into a well-ventilated 50 ml Falcon conical tube with a narrow open window on top to allow for movement and sliding of the fiber patch cord. During the entire restraint procedure, mice were in a natural body position without physical harm. For the control experiment of long-term fiber photometry, mice were placed into a 5L cylinder for 60 min without any restraint.

Cage-change - mild stress. At the beginning of “lights on”, animals’ home cages were exchanged with new cages with fresh bedding and food in the holding room. For the control experiment of long-term fiber photometry, mice were in the home cages for 60 min.

Novel environments. Mice were placed in a novel cage with a novel object in the experimental room for 60 min (Fig. S1C). For the controls, the mice were in their home cages in the holding room (Fig. S1C).

Novel objects. An object was placed in the resident mouse’s home cage in the experimental room. Video recording was performed with recordings of fiber photometry signals.

Mild sleep deprivation. This was performed as we previously reported (39). Mice were sleep deprived at the start of “lights on” for 4-h using novel cages and novel objects. When mice showed signs of drowsiness, a soft brush was used to touch the mouse for 1-2 s.

Voluntary wheel running. Wheel running exercise experiments were performed using activity cages (37 (h) x 26 (w) x 35 (d) cm) with a running wheel installed (diameter 25 cm) (Shanghai Yuyan Instruments Co., Ltd.). Animals were acclimatized to the activity cage for 10 min on three consecutive days before the experiments. Mice were allowed voluntary wheel running for 60 min. For the control group, animals remained sedentary in their home cages in the

behavioral room. For fiber photometry experiments, we used a cage-free running wheel on the table. The mice run freely on the wheel for 60 min with fiber photometry recorded.

Forced treadmill running. The treadmill exercise regimen was adapted from a previous study (50). To reduce the amount of stress to the animals, prior to the running experiment, mice were acclimatized to the stationary treadmill apparatus (Shanghai Yuyan Instruments Co., Ltd.) for 10 min, increasing to a speed of 4-10 m/min on three consecutive days. After this adaption period, mice experienced exercise training for 60 min, with the treadmill set at a speed of 4-6 m/min. The protocol corresponded to approximately 50% of maximal oxygen consumption.

Open-field tests

The Open Field Test (OFT) was used to test the anxiety-like behaviors of mice (51). The mice were gently placed in a 40 cm × 40 cm × 40 cm open-field, which was invisibly divided into 25 small squares. During the experiment, mice were placed in the central square and then allowed free movement in the open field with real-time position tracking and video recording for 10 minutes. The average speed and time in the center area within the last 5 min were captured and analyzed using an ANY-maze 7.0 (Stoelting, USA).

Elevated plus-maze

The Elevated Plus-Maze test (EPM) was used to test the anxiety-like behaviors of the mice, as we previously performed (52). Following the Open Field Test, the experimental mice were taken out and placed in the central area of the elevated plus-maze. The head and upper limbs of mice were randomly placed in the open arm, and then mice moved freely on the elevated platform for 5 min. At the end of the test, we cleaned each arm of the elevated plus-maze

and eliminated the odor with 20% alcohol. The position track and real-time performance of mice during the EPM test were recorded. Time in the Open Arm was analyzed using the ANY-maze 7.0 (Stoelting, USA).

Activity-tagging

The activity-tagging procedure was performed as we previously reported (39, 40, 53). *Vgat-IRES-Cre* or *Sst-IRES-Cre* mice were placed on doxycycline (200 mg/kg) (Envigo TD.09265) for at least one week prior to the virus injection. Mice were injected with the activity-tagging transgenes. 3-4 weeks after injection, mice were taken off doxycycline 24-h before activity-tagging (mice were kept undisturbed during this period). VTA^{Vgat} or VTA^{Sst} neurons were allowed to become tagged while mice experienced 1-h social defeat (SDS), or the non-stressful procedure (NS), or voluntary wheel running, or forced treadmill running, or restraint stress (RS), or cage-change or novel environments (novelty). For the control tagging, mice experienced 1-h control for social defeat or non-stressful procedure (using a transparent partition to separate the intruder and resident mice) (**Behavioral protocols – social defeat stress and non-stressful procedure**). To shut down the activity-tagging system, mice were put back on doxycycline for 5 to 7 days (without any disturbance in the first 2 days) before anatomical or behavioral assessments.

Assessment of the activity-tagging system

We assessed the efficacy and specificity of the activity-tagging by delivering transgenes into the VTA (**Fig. S32A**) or intersectionally into the VTA → LH pathway (**Fig. S32B**).

The efficacy of Dox: activity-tagging AAVs were injected into the VTA (**Fig. S32A**) or intersectionally into the VTA → LH pathway (**Fig. S32B**) of *Vgat-IRES-Cre* mice. After injection,

mice were constantly on Dox while tagged by SDS. Mice were put back on doxycycline for 5 to 7 days (without any disturbance in the first 2 days) before anatomical study (On Dox → On Dox → SDS-tagging → On Dox).

The specificity of tagging for SDS: activity-tagging AAVs were injected into the VTA (**Fig. S32A**) or intersectionally into the VTA → LH pathway (**Fig. S32B**) of *Vgat-IRES-Cre* mice. 24-h before activity-tagging, Dox was removed, and mice underwent SDS, control or home cage procedure. After activity-tagging, mice were put back on dox for 5 to 7 days (without any disturbance in the first 2 days) (On Dox → Off Dox → SDS-, control- or home cage-tagging → On Dox).

Fiber photometry

Fiber photometry was performed as described (15, 18). In detail, a Grass SD9 stimulator was used to control a 473-nm Diode-pumped solid-state (DPSS) blue laser with a fiber coupler (Shanghai Laser & Optics Century Co., Shanghai, China). The laser light was passed through a single source fluorescence cube (FMC_GFP_FC, Doric Lenses, Quebec, Canada) through an optical fiber patch cord (\emptyset 200 μ m, 0.22 NA, Doric Lenses). From the filter cube, a multimodal optical patch cord (\emptyset 200 μ m, 0.37 NA, Doric Lenses) was connected to the mouse chronically implanted fiber (\emptyset 200 μ m, 0.37 NA) with a ceramic split mating sleeves ferrules (Thorlabs, Newton, New Jersey). The GCaMP6 output was then filtered at 500-550 nm using a second dichroic in the fluorescence cube and converted to a voltage by an amplified photodiode (APD-FC, Doric Lenses). The photodiode output was amplified by a lock-in amplifier (SR810, Stanford Research Systems, California, USA), also used to drive the laser at 125 Hz with an average power of 80 μ W at the fiber tip. The signal was then digitized using a CED 1401 Micro

box (Cambridge Electronic Design, Cambridge, UK) and recorded at 1 kHz using Spike2 software (Cambridge Electronic Design, Cambridge, UK).

The photometry signals during the stress experiences were matched with video recordings. For each experiment, the photometry signal F was converted to $\Delta F/F$ by $\Delta F/F(t) = (F(t) - \text{median}(F)) / \text{median}(F)$ (18). Mice with an implanted optical fiber were connected to a patch cord for recording of the Ca^{2+} signal. After connection, the mice were habituated in their home cages, novel cages or other experimental cages for 30 min. In some recordings, we observed decay of the photometry signal at the beginning of the recordings. All the trials were conducted after the photometry signal became stable. For photometry recordings across brain states (vigilance states), the photometry signals were matched with EEG/EMG signals. The photometry signals were not due to movement, as the GFP signal originating from control *AAV-DIO-GFP* expression in VTA^{Vgat} neurons did not change during the stress (**Fig. S33**).

Fiber photometry of the CRF sensor

The GRAB_{CRF1.0} sensor was developed by Yulong Li's lab (Peking University, China).

rAAV-hSyn-CRF1.0-WPRE-hGHpA was packaged by WZ Biosciences Inc (Shandong, China). *Sst-IRES-Cre* mice were anesthetized and fixed to the stereotaxic apparatus. The CRF sensor were injected into the PVH (AP = -0.80 mm, ML = 0.20 mm, DV = -4.15 mm). Meanwhile, *rAAV-DIO-hM3Dq/hM4Di-mCherry* was injected into the VTA using a Nanoject II apparatus (Drummond Scientific, Broomall, PA) at a rate of 23 nL/min. After virus injection, an optical fiber (diameter: 200 μm) was implanted into the PVH (AP = -0.80 mm, ML = 0.20 mm, DV = -4.1 mm). Three weeks after implantation of the optical fiber in the PVH, fiber photometry recordings were performed for social defeat stress experiments (detected by QAXK-FPS-DC-LED, ThinkerTech Nanjing Bioscience Inc).

Chemogenetic protocols

We used the clozapine-N-oxide (CNO) chemogenetic method (54). CNO (C0832, Sigma-Aldrich, dissolved in saline, 1 mg/kg) or saline was injected *i.p.* Mice were split into random groups that received either saline or CNO injection. To test the sleep-promoting effects, we injected saline or CNO during the “lights off” period when the mice were in the active phase. In detail, for the activity-tagged VTA^{Vgat} neurons or activity-tagged VTA^{Sst} neurons with hM3Dq-mCherry, saline or CNO was given during the “lights off” period. For non-tagged VTA^{Sst} neurons expressing hM3Dq-mCherry, saline or CNO was given during the “lights off” period. To chemogenetically reactivate activity-tagged LH-projecting VTA^{Vgat} neurons or VTA^{Sst} neurons, saline or CNO was given during the “lights off” period. For the activity-tagged VTA^{Vgat} neurons with hM4Di-mCherry, saline or CNO was given 30 min before stress producers. Mice experienced SDS 1-h before the “lights on” period. Therefore, saline or CNO was given to these mice 90 min before the “lights on” period.

Optogenetic protocols

We used ChR2-based optogenetics (55). For optogenetic experiments, after the fiber patch cord was connected to the laser generator, the optical power meter (SANWA Electric Instrument, Tokyo, Japan) was used to measure laser intensity, to which the optic fiber was attached to obtain laser intensity at 10-15 mW. Then, the optic fibers on the head of mice were concatenated to the fiber patch via the rotary joint (ThinkerTech, Nanjing, China). During the experiments, the mice were stimulated optically (ChR2, 473 nm, 20 Hz, 30ms duration) every 60 s with 30 s interval. To test the sleep-promoting effects, opto-stimulation was conducted when the mice were awake.

Sleep-wake behavior and EEG analysis

Mice were attached with mock Neurologgers before experiments. EEG and EMG signals were recorded using Neurologger 2A devices (56). Wake, NREM or REM sleep was automatically classified at 5-s epoch using sleep analysis software Spike2 (Cambridge Electronic Design) and then manually re-scored. Episode duration was analyzed using MATLAB (R2020b) as we previously described (18).

For telemetry EEG and EMG, EEG data were analyzed using the NeuroScore Software (DSI, Harvard Bioscience, Inc). Vigilance states, including NREM sleep, REM sleep, and wake states, were first automatically assigned to each 5-s epoch using an automated scoring algorithm and then manually scored. The duration and bouts of vigilance state were calculated. Meanwhile, spectral power was quantified from the raw EEG data through a multitaper method for each vigilance state. Analysis was performed using a custom MATLAB script via the Chronux toolbox (<http://chronux.org>) (57).

Immunohistochemistry

Mice were transcardially perfused with 4% paraformaldehyde (Thermo scientific) in phosphate-buffered saline (Sigma). Brains were post-perfused with 4% paraformaldehyde in PBS for 24-h, and subsequently transferred in 30% sucrose/PBS. 40- μ m-thick coronal sections were cut using a cryostat microtome (Leica CM1900, Germany) or a sliding microtome (HM 450, Cambridge Scientific). Free-floating sections were washed in PBS three times for 5 min, permeabilized in PBS plus 0.4% Triton X-100 for 30 min, blocked by incubation in PBS plus 5% normal goat serum (NGS) (Vector), 0.2% Triton X-100 for 1-h. Sections were incubated with primary antibody diluted in PBS plus 2% NGS overnight at 4°C in a shaker. Incubated brain sections were washed three times in PBS for 10 min and incubated for 2 hours with secondary

antibody in PBS and subsequently washed 4 times in PBS for 10 min (all at room temperature). For the cFOS staining, the mice were perfused 90 min after SDS or control procedure. To examine the activation of VTA^{Sst} neurons (cFOS) by CNO during sleep deprivation, the mice were perfused 3 hours after saline or CNO injection.

Primary antibodies: Rabbit polyclonal cFOS (1:3000, ABE457, Millipore, UK); Rat monoclonal mCherry (1:1000, M11217, ThermoFisher); Rabbit polyclonal GFP (1:1000, A-11122, ThermoFisher); and Mouse monoclonal TH (1:2000, T2928, Sigma); Rabbit polyclonal GABA (1:200, GeneTex); Rat monoclonal somatostatin (1:1000, Merck); Mouse monoclonal orexin-A (OA) (1:200, MAB763, R&D Systems); Rabbit polyclonal cFOS (1:1000, Sigma-Aldrich); Mouse cFOS (1:1000, Sigma-Aldrich).

Secondary antibodies were Alexa Fluor 488 goat anti-rabbit, Alexa Fluor 488 goat anti-mouse, Alexa Fluor 594 goat anti-rabbit, Alexa Fluor 594 goat anti-mouse and Alexa Fluor 594 goat anti-rat (1:1000, Invitrogen Molecular Probes, UK). Alexa Fluor 488 donkey anti-rabbit, Alexa Fluor 488 donkey anti-mouse, Alexa Fluor 594 donkey anti-rabbit, Alexa Fluor 594 donkey anti-mouse, and Alexa Fluor 594 donkey anti-rat (1:1000, Jackson ImmunoResearch Laboratories). For the Ai9 reporter mouse, tdTomato was detected with primary fluorescence without antibody staining.

Slices were mounted on slides, embedded in Mowiol (with DAPI) (Vector Labs, H-1200), coverslipped (BIOTIUM), and analyzed using an upright fluorescent microscope (Nikon Eclipse 80i or 90i Nikon Corporation, JAPAN) or a Zeiss LSM 510 inverted confocal microscope or a Leica SP5 MP confocal microscope (Facility for Imaging by Light Microscopy, FILM, Imperial College London).

Enzyme immunoassay of serum corticosterone

Mice were decapitated immediately at each time point after the non-stressful procedure, SDS, restraint stress or novel environments, and their control protocols, respectively. Blood was rapidly collected in 1.5-ml plastic tubes placed in ice and centrifuged at $1,500 \times g$ for 20 min, and serum was collected and stored at -80°C until use. Serum samples were tested for corticosterone concentration using the Enzo ELISA kit (ADI-900-097; Enzo Life Sciences, Exeter, Devon, UK) according to the manufacturer's instructions.

Metyrapone

Metyrapone (Merck) was administrated (*i.p.*) as reported (58). Metyrapone was dissolved in 5% ethanol saline solution and injected *i.p.* (50 mg/kg) into the mice 30 min before the SDS.

Orexin/Hcrt receptor antagonists

Infusion of orexin receptor antagonists (*i.c.v.*) was performed as previously described (59). Before the experiments, SB-334867 (Tocris Bioscience, USA), Orexin1 receptor antagonist, and TCS-OX2-29 (Tocris Bioscience, USA), Orexin2 receptor antagonist, were dissolved in 5% DMSO at $33.3 \mu\text{g}/\mu\text{L}$. SB-334867 or TCS-OX2-29 was infused via *i.c.v.* at $0.1 \mu\text{L}/\text{min}$. Injector cannula were connected with micro-syringe with Polyethylene pipe filled with mineral oil. 500 nL of SB-334867 or TCS-OX2-29 was infused into the lateral cerebral ventricle through the injector cannula, respectively. Mice were allowed to move freely in their home cage during infusions. Afterwards, cannulas were left in place for an additional 2–3 min to allow drug diffusion. 20 min after drug infusion, SDS or behavioral tests were conducted.

The double Orexin/Hcrt receptor antagonist MK6096 (filorexant, Cambridge Bioscience) was dissolved in 50% saline/50% PEG-400 administered *i.p.* at a dose of 5.0 mg/kg 30 min before the behavioral study, as previously reported (37).

Single-cell RT-qPCR from acute brain slice of the VTA

Single-cell RT-qPCR was performed as we previously described (18, 53). SDS-tagged VTA^{Vgat} or VTA^{Sst} mice were killed by cervical dislocation. The brains were quickly removed and placed into cold oxygenated N-Methyl-D-glucamine (NMDG) solution (NMDG 93 mM, HCl 93 mM, KCl 2.5 mM, NaH₂PO₄ 1.2 mM, NaHCO₃ 30 mM, HEPES 20 mM, glucose 25 mM, sodium ascorbate 5 mM, Thiourea 2 mM, sodium pyruvate 3 mM, MgSO₄ 10 mM, CaCl₂ 0.5 mM). Coronal brain slices (200- μ m thickness) encompassing the VTA were obtained using a vibratome (VT1200S, Leica). Slices were kept in NMDG solution at 33°C for 15min with constant oxygenation and transferred to fully oxygenated standard ACSF (NaCl 120 mM, KCl 3.5 mM, NaH₂PO₄ 1.25 mM, NaHCO₃ 25 mM, glucose 10 mM, MgCl₂ 1 mM, CaCl₂ 2 mM) and were maintained in a chamber that was gently and continuously aerated with carbogen gas for at least 45 min at room temperature (20–22 °C). Slices were transferred to a submersion recording chamber and were continuously perfused at a rate of 3-4 ml/ min with fully oxygenated ACSF at room temperature.

The brain slices were visualized with a fixed upright microscope (BX51WI, Olympus) equipped with a water immersion lens (40 \times /0.8 W) and a digital camera (C13440, Hamamatsu). Patch pipettes were pulled from borosilicate glass capillary tubes using a pipette puller (P97, Sutter). The resistance of pipettes varied between 3 and 5 M Ω . The patch pipettes were filled with RNase-free intracellular solution containing (in mM): 140 K-gluconate, 5 NaCl, 10 HEPES, 0.1 EGTA, 2 MgCl₂, 2 Mg-ATP, and 0.3 Na-GTP (pH 7.35, osmolality 285 mOsm). The hM3Dq-mCherry-positive neurons were visually identified and randomly selected. The internal solution in the patch pipette was limited up to 1 μ l.

The single-cell RT-PCR assays were performed using the Single Cell-to-CT Kit (Thermo Fisher Scientific). The cytoplasm was aspirated into the patch pipette and expelled into a PCR tube containing lysate buffer. The content of the tagged neuron was aspirated into the recording pipette and expelled into cell lysis/DNase I solution. Reverse transcription and cDNA pre-amplification were performed according to the kit protocol. qPCR was performed using the QuantStudio Real-Time PCR system (Thermo Fisher Scientific). The mouse TaqMan assay probes were designed by TaqMan® Gene Expression Assays (Thermo Fisher Scientific) and purchased from Thermo Fisher Scientific. *18srRNA*, Mm03928990_g1; *Slc17a6 (Vglut2)*, Mm00499876_m1; *Slc6a3 (dat)*, Mm00438388_m1; *Gad1*, Mm04207432_g1; *Slc32a1 (Vgat)*, Mm00494138_m1; *Sst*, Mm00436671_m1; *Pv*, Mm00443100_m1; *Vip*, Mm00660234_m1. The single-cell gene expression matrix was made in Origin.

Quantification and statistics: We excluded mice in which it was subsequently found that the optical fibers were misplaced or that there was no AAV transgene expression, or when this expression was in the wrong place. Mice were assigned randomly to the experimental and control groups. For chemogenetic experiments, saline or CNO injections were blinded. For optogenetic experiments, control-tagged or stress-tagged groups were blinded. The analysis of EEG data and measurement of ELISA were done blinded. Animal behavior data that was scored from videos with fiber photometry was not blinded. The individual tests and the number (n) of mice for each experimental group are shown in the figure legends. A normality test was performed on each dataset using the Shapiro-Wilk test. The parametric tests (paired, unpaired *t*-tests, one-way or two-way ANOVA and *post hoc* test) were used if the datasets were normally distributed. The Mann–Whitney U-test was used for non-parametric tests. All data are given as mean \pm SEM. Statistical tests were run in “Origin 2021” (Origin Lab).

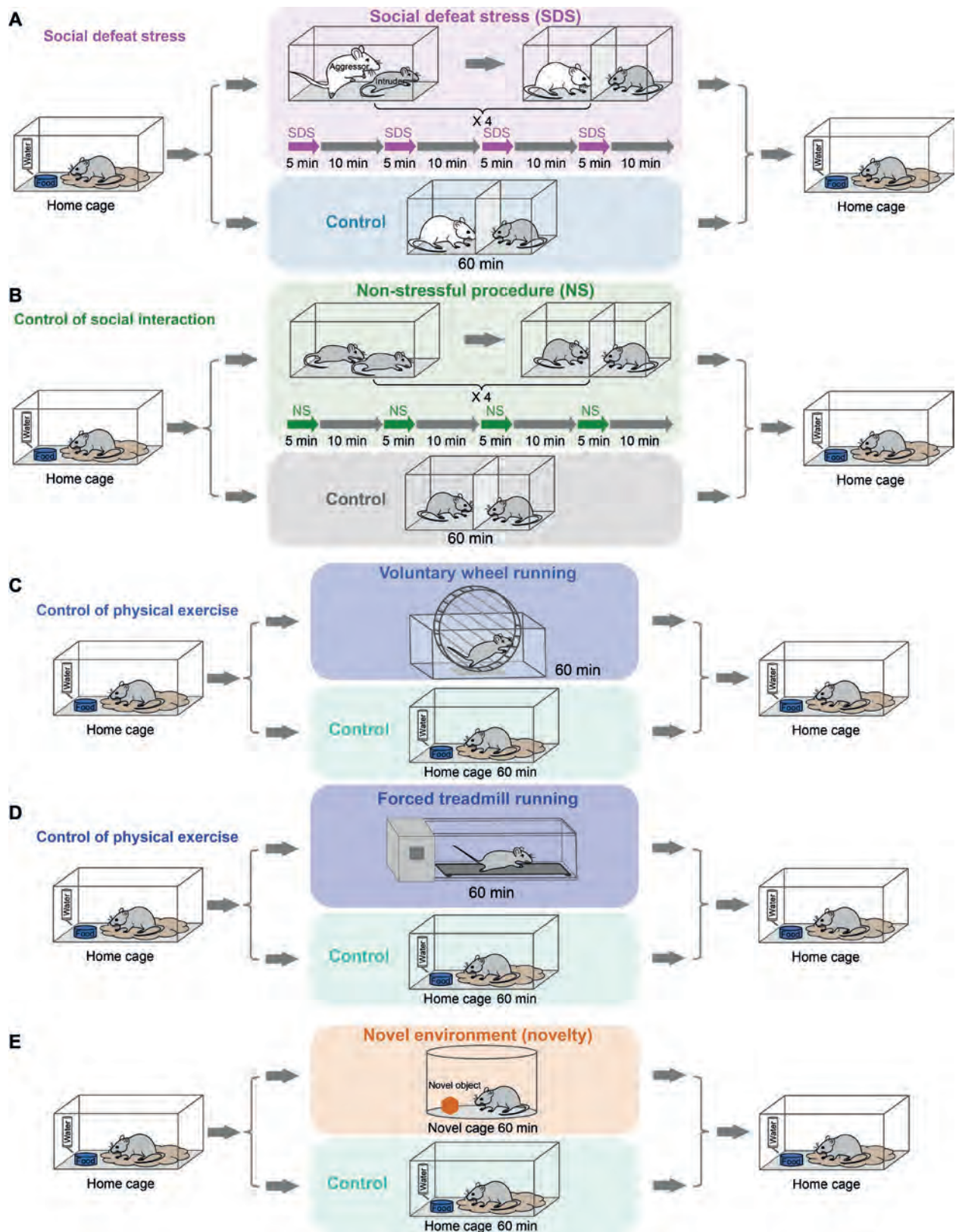


Fig. S1. Behavioral procedures of SDS, non-stressful procedure, voluntary wheel running, forced treadmill running and novel environment (Related to Fig. 1)

Plan of the SDS / control **(A)**, non-stressful procedure / control **(B)**, voluntary wheel running / control **(C)**, forced treadmill running / control **(D)** and novel environment / control **(E)** experimental procedures. See the 'Behavioral protocols' section in Materials and Methods.

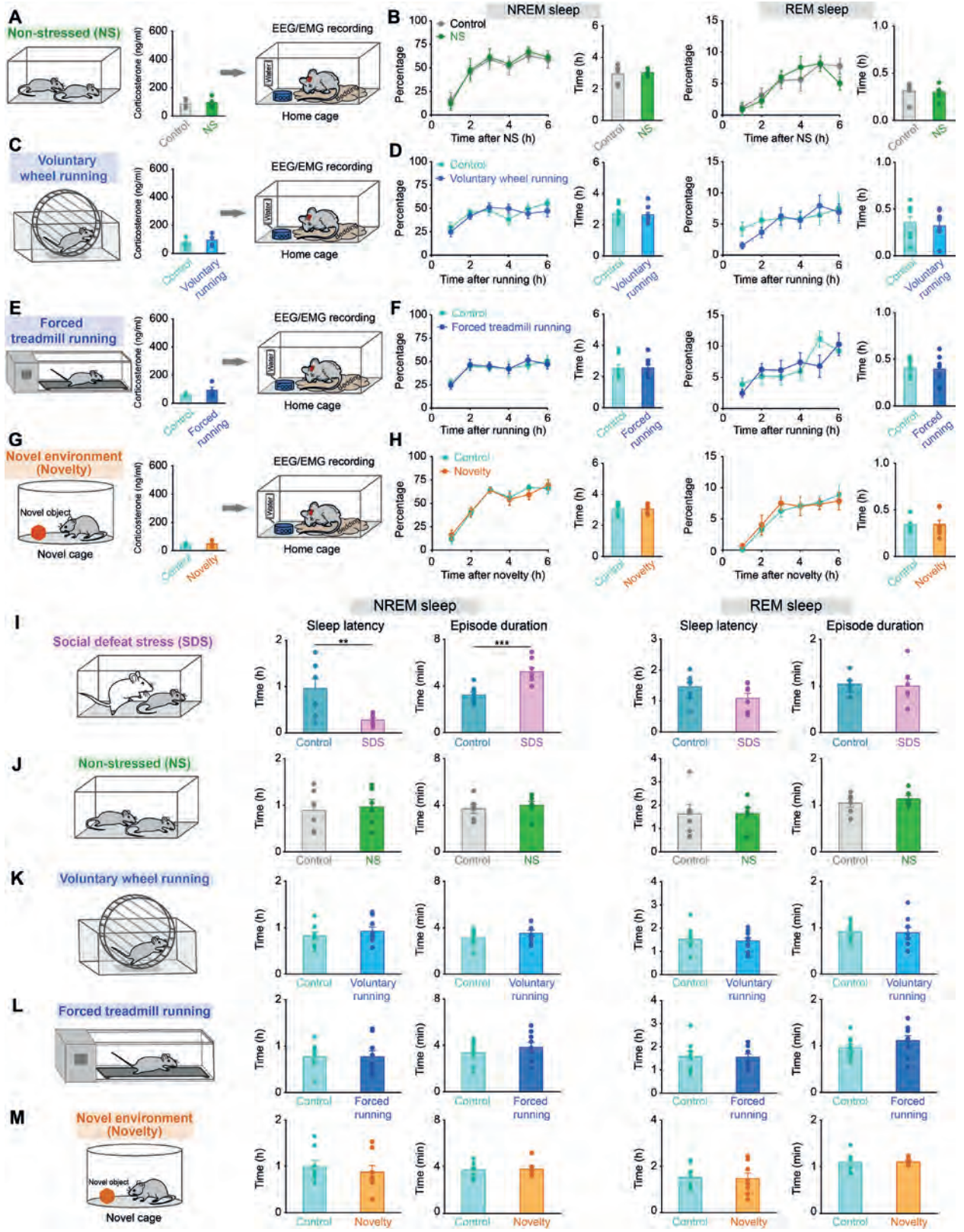


Fig. S2. NREM and REM sleep parameters after SDS, non-stressful procedure, voluntary wheel running, forced treadmill running and novel environments (Related to Fig. 1)

(A) The experimental procedure and corticosterone levels after control or non-stressful procedure (NS) (n = 5 mice per group). Unpaired *t*-test, $p > 0.05$.

(B) Percentage and time of NREM and REM sleep after control or non-stressful procedure (NS) (n = 6 mice per group). Unpaired *t*-test, $p > 0.05$.

(C) The experimental procedure and corticosterone levels after control or voluntary wheel running (n = 4 mice per group). Unpaired *t*-test, $p > 0.05$.

(D) Percentage and time of NREM and REM sleep after control or voluntary wheel running (n = 9 mice per group). Unpaired *t*-test, $p > 0.05$.

(E) The experimental procedure and corticosterone levels after control or forced treadmill running (n = 4 mice per group). Unpaired *t*-test, $p > 0.05$.

(F) Percentage and time of NREM and REM sleep after control or forced treadmill running (n = 9 mice per group). Unpaired *t*-test, $p > 0.05$.

(G) The experimental procedure and corticosterone levels after control or novel environment (novelty) (n = 6 mice per group). Unpaired *t*-test, $p > 0.05$.

(H) Percentage and time of NREM and REM sleep after control or novel environment (novelty) (n = 8 mice per group). Unpaired *t*-test, $p > 0.05$.

(I-M) Sleep latency and episode duration of NREM and REM sleep after SDS / control (n = 8 mice per group) (I), non-stressful procedure (NS) / control (n = 6 mice per group) (J), voluntary wheel running / control (n = 9 mice per group) (K), forced treadmill running / control (n = 9 mice per group) (L) and novel environment (novelty) / control (n = 8 mice per group) (M). Unpaired *t*-test, ** $p < 0.01$, *** $p < 0.0001$.

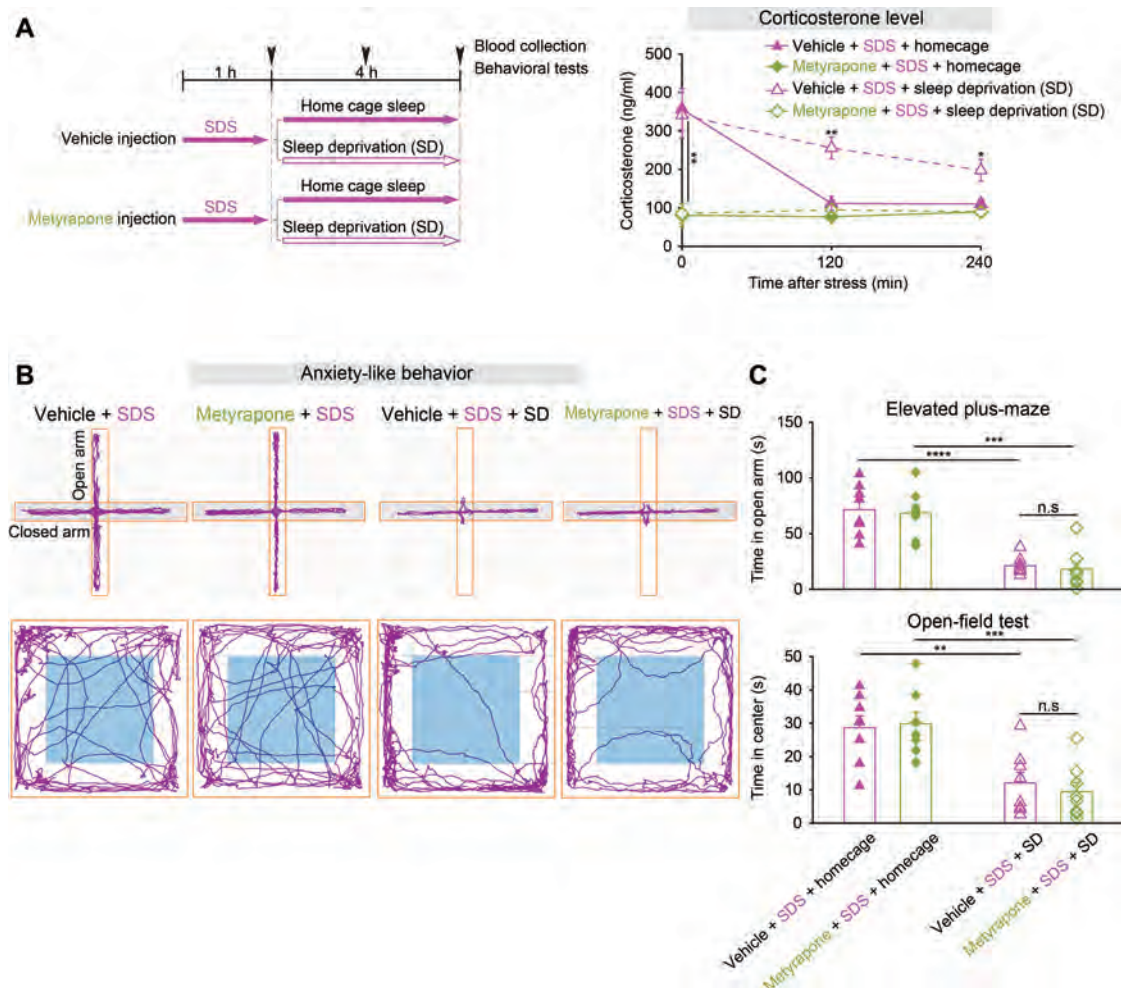


Fig. S3. Pharmacologically decreasing corticosterone levels induced by SDS during sleep deprivation does not reduce anxiety

(A) Plan of the experimental procedure and corticosterone levels during home cage sleep or sleep deprivation following SDS after vehicle or metyrapone injection ($n = 4$ mice per group). Two-way ANOVA with bonferroni *post hoc* test, $*p < 0.05$, $**p < 0.01$.

(B, C) Tracing of locomotion for representative animals (B), and time spent in the open arms of the elevated plus-maze and in the center zone during the open-field test (C) ($n = 8$ mice per group). Two-way ANOVA with bonferroni *post hoc* test, $**p < 0.01$, $***p < 0.001$, $****p < 0.001$.

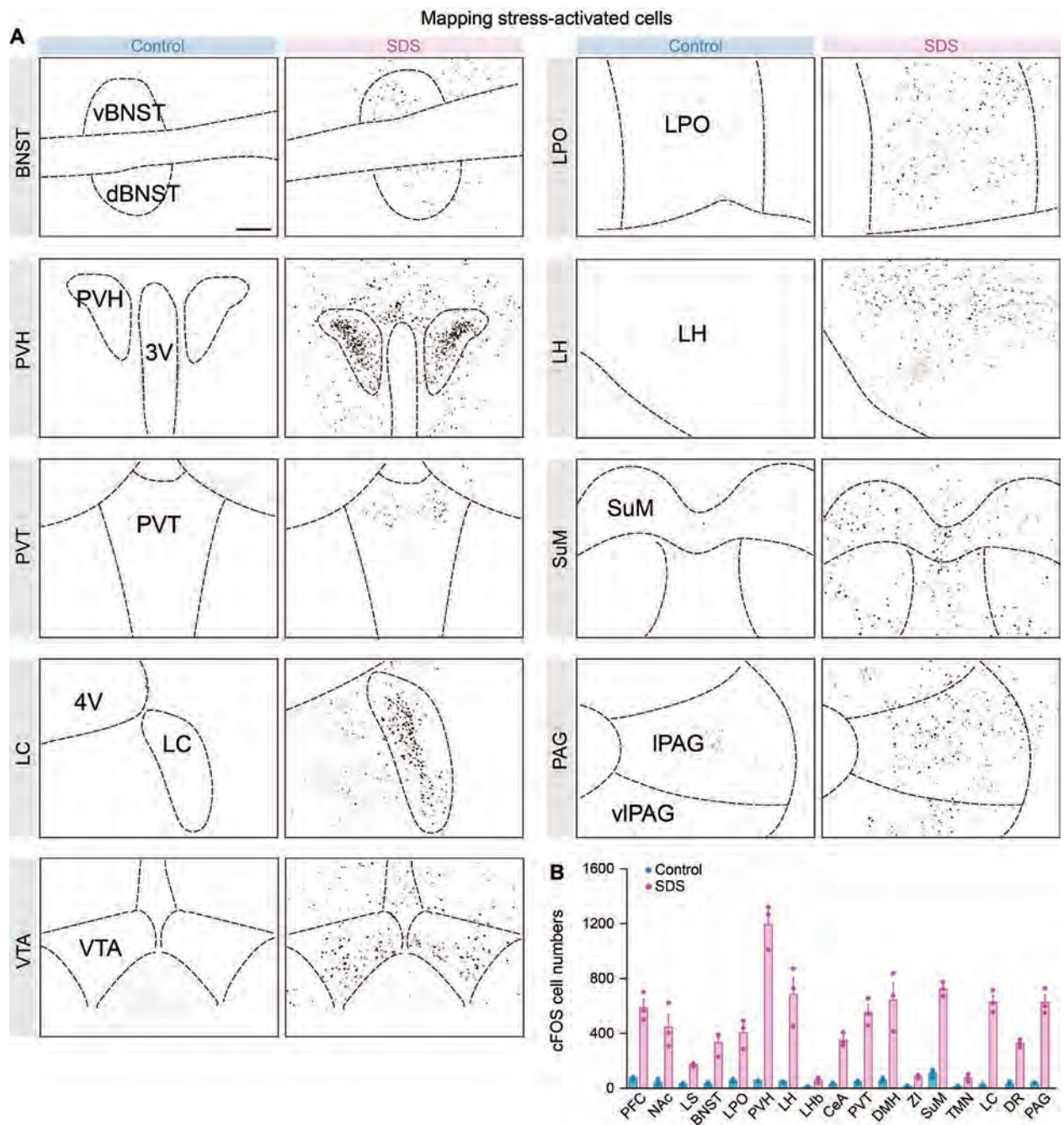


Fig. S4. Brain-wide mapping of SDS-activated regions (Related to Fig. 1)

(A) Immunostaining images showing cFOS-positive cells after control or SDS in diverse brain areas (n = 3 mice per group). Scale bar, 150 μ m.

(B) Summary of numbers of cFOS-positive cells after control or SDS in diverse brain areas (n = 3 mice per group). PFC, prefrontal cortex; NAc, nucleus acumbens; LS, lateral septum; BNST, bed nucleus stria terminalis; LPO, lateral preoptic area; PVH, paraventricular hypothalamus; LH, lateral hypothalamus; LH, lateral habenula; CeA, central amygdala; PVT, paraventricular thalamus; DMH, dorsal medial hypothalamus; ZI, zona incerta; SuM, supramammillary

nucleus; TMN, tuberomamillary nucleus; LC, locus ceruleus; DR, dorsal raphe; PAG, periaquiductal grey.

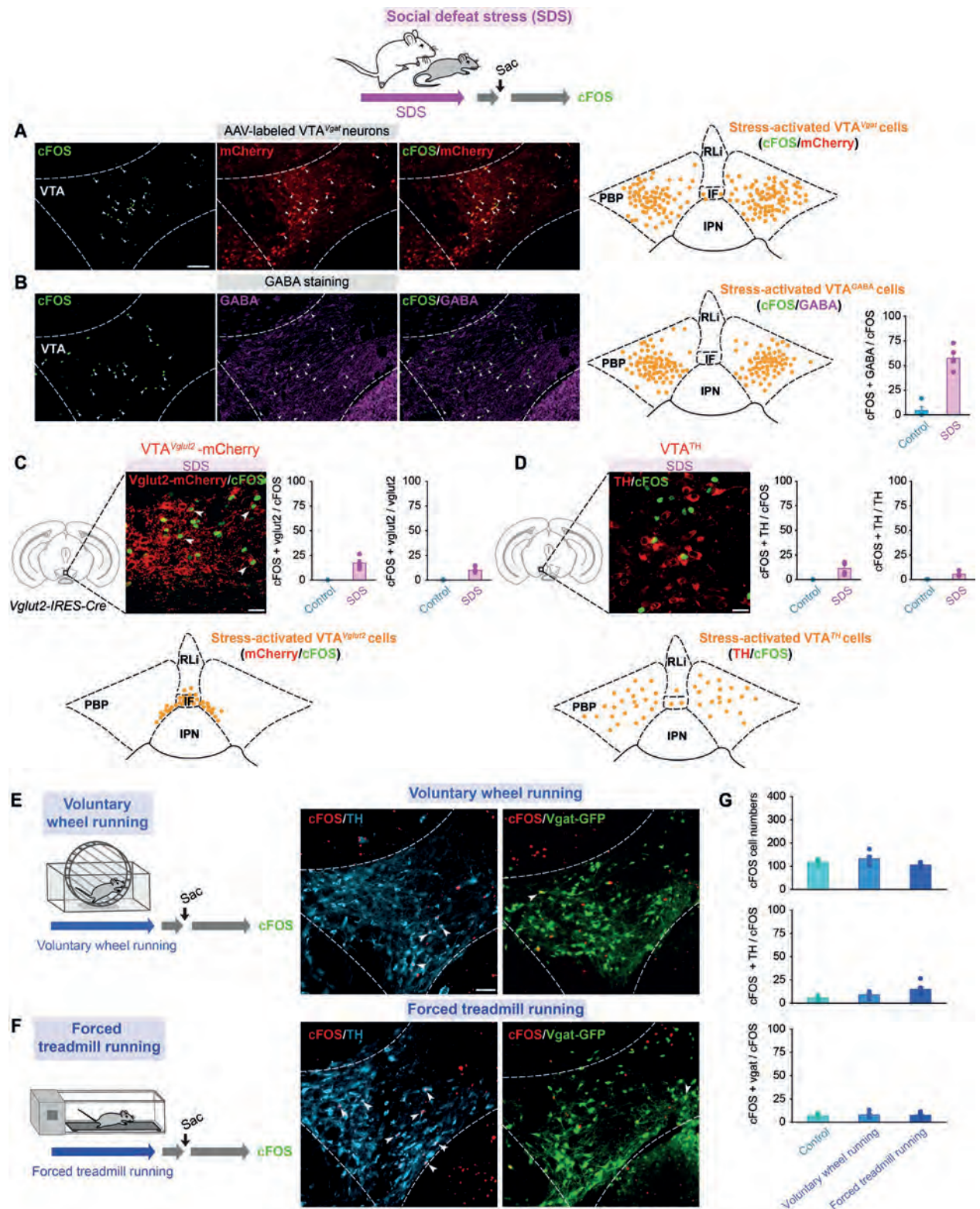


Fig. S5. Characterization of SDS-activated cells in the VTA (Related to Fig. 1)

(A) cFOS expression by immunohistochemistry (green) after control or SDS in genetically labeled VTA^{Vgat} neurons (mCherry expression – AAV-DIO-mCherry injected into the VTA of

Vgat-IRES-Cre mice). Arrowheads indicate double-labeled cells. Scale bar, 100 μm . Schematic diagram summarizing SDS-activated VTA^{Vgat} neurons (mCherry / cFOS) (n = 4 mice).

(B) cFOS expression by immunohistochemistry (green) after control or SDS in VTA^{GABA} neurons. Arrowheads indicate double-labeled cells. Schematic diagram summarizing SDS-activated VTA^{GABA} neurons (GABA / cFOS) (n = 4 mice). Quantification represents cFOS and GABA double-labeled cells / total cFOS-positive cells (n = 4 mice for control group; n = 6 mice for SDS group).

(C) cFOS expression by immunohistochemistry (green) and quantification after control or SDS in genetically labeled $\text{VTA}^{\text{Vglut2}}$ neurons (mCherry expression – AAV-DIO-mCherry injected into the VTA of *Vglut2-IRES-Cre* mice). Arrowheads indicate double-labeled cells. Scale bar, 50 μm . Diagram summarizing SDS-activated $\text{VTA}^{\text{Vglut2}}$ neurons (mCherry / cFOS) (n = 4 mice). Quantification represents cFOS and *vglut2* double-labeled cells / total cFOS-positive cells, and cFOS and *vglut2* double-labeled cells / total *vglut2*-positive cells (n = 4 mice per group).

(D) cFOS expression and quantification after control or SDS in VTA^{TH} neurons (wild-type mice, immunohistochemistry with tyrosine hydroxylase, TH). Scale bar, 50 μm . Diagram summarizing SDS-activated VTA^{TH} neurons (TH / cFOS) (n = 4 mice). Quantification represents cFOS and TH double-labeled cells / total cFOS-positive cells, and cFOS and TH double-labeled cells / total TH-positive cells (n = 4 mice per group). IF, interfascicular nucleus; RLi, rostral linear nucleus; PBP, parabrachial pigmented nucleus; IPN, interpeduncular nucleus.

(E, F) cFOS expression by immunohistochemistry (red) after control / voluntary wheel running **(E)** or control / forced treadmill running **(F)** in VTA^{TH} neurons (immunohistochemistry with tyrosine hydroxylase, TH) or genetically labeled VTA^{Vgat} neurons (GFP expression – AAV-DIO-GFP injected into the VTA of *Vgat-IRES-Cre* mice).

(G) Quantification of total cFOS-positive cells in the VTA, cFOS and TH double-labeled cells / total cFOS-positive cells or cFOS and *vgat* double-labeled cells / total cFOS-positive cells in control, voluntary wheel running and forced treadmill running group (n = 6 mice per group). Scale bar, 100 μm .

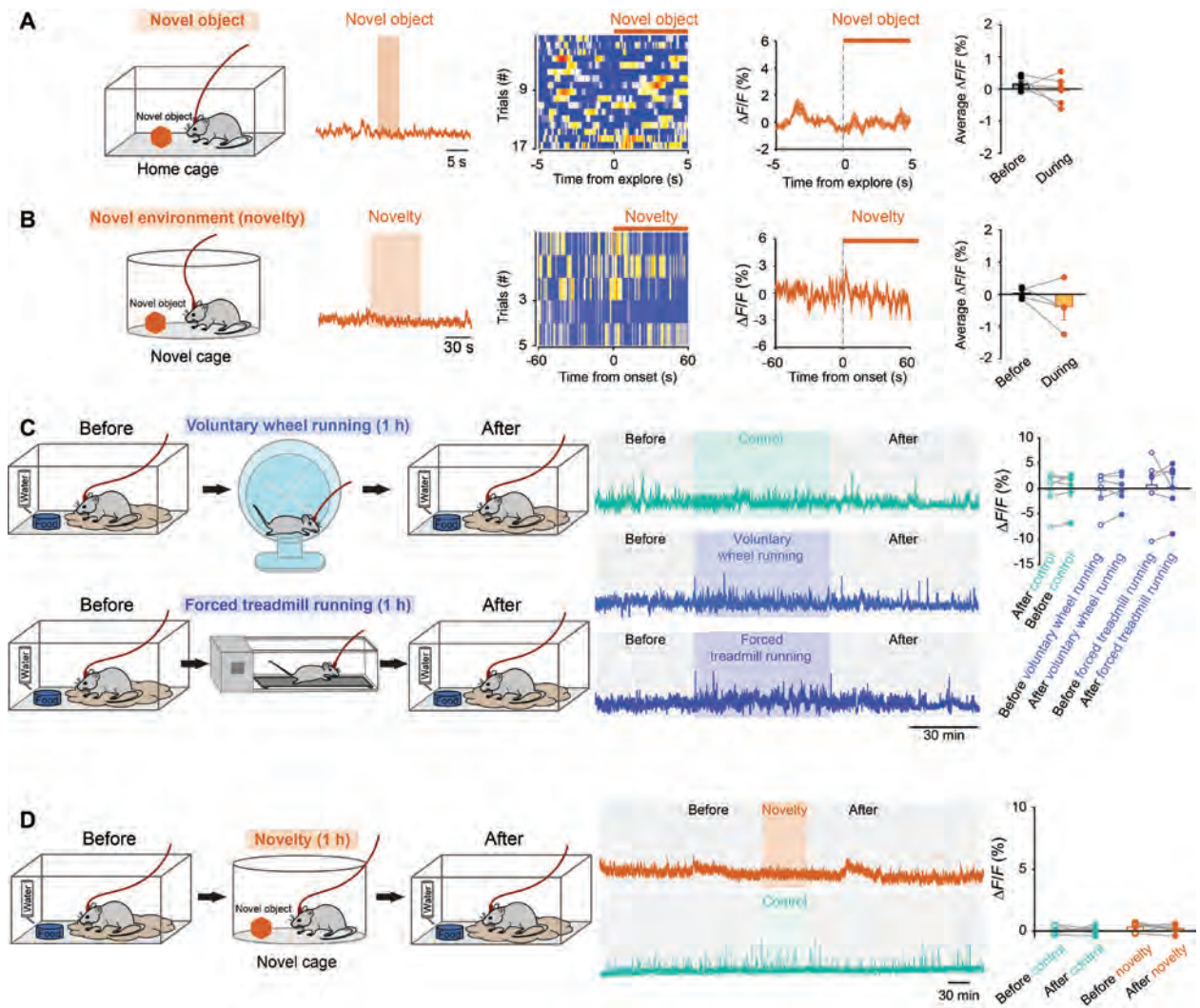


Fig. S6. VTA^{Vgat} neurons do not respond to novel objects, voluntary wheel running, forced treadmill running or novel environments (Related to Fig. 1)

(A, B) Fiber photometry experiments measuring calcium signals in VTA^{Vgat} neurons when mice were presented with a novel object (A) or placed in a novel environment (novelty) (B). Raw calcium signal traces, color matrix of GCaMP6 signals for all trials, $\Delta F/F$ ratios across the experimental period and average $\Delta F/F$ ratios before and during the novel object presentation (n = 6 mice, 17 trials) or novel environment (novelty) (n = 4 mice, 5 trials). Paired two-tailed *t*-test, $p > 0.05$.

(C, D) Fiber photometry measuring long-term calcium signals in VTA^{Vgat} neurons. Traces across the experimental procedure and average $\Delta F/F$ ratios before and after 1-h voluntary wheel running or 1-h forced treadmill running (C), or in a novel environment (novelty) (D) for an hour (n = 6 mice per group). Paired two-tailed *t*-test, $p > 0.05$.

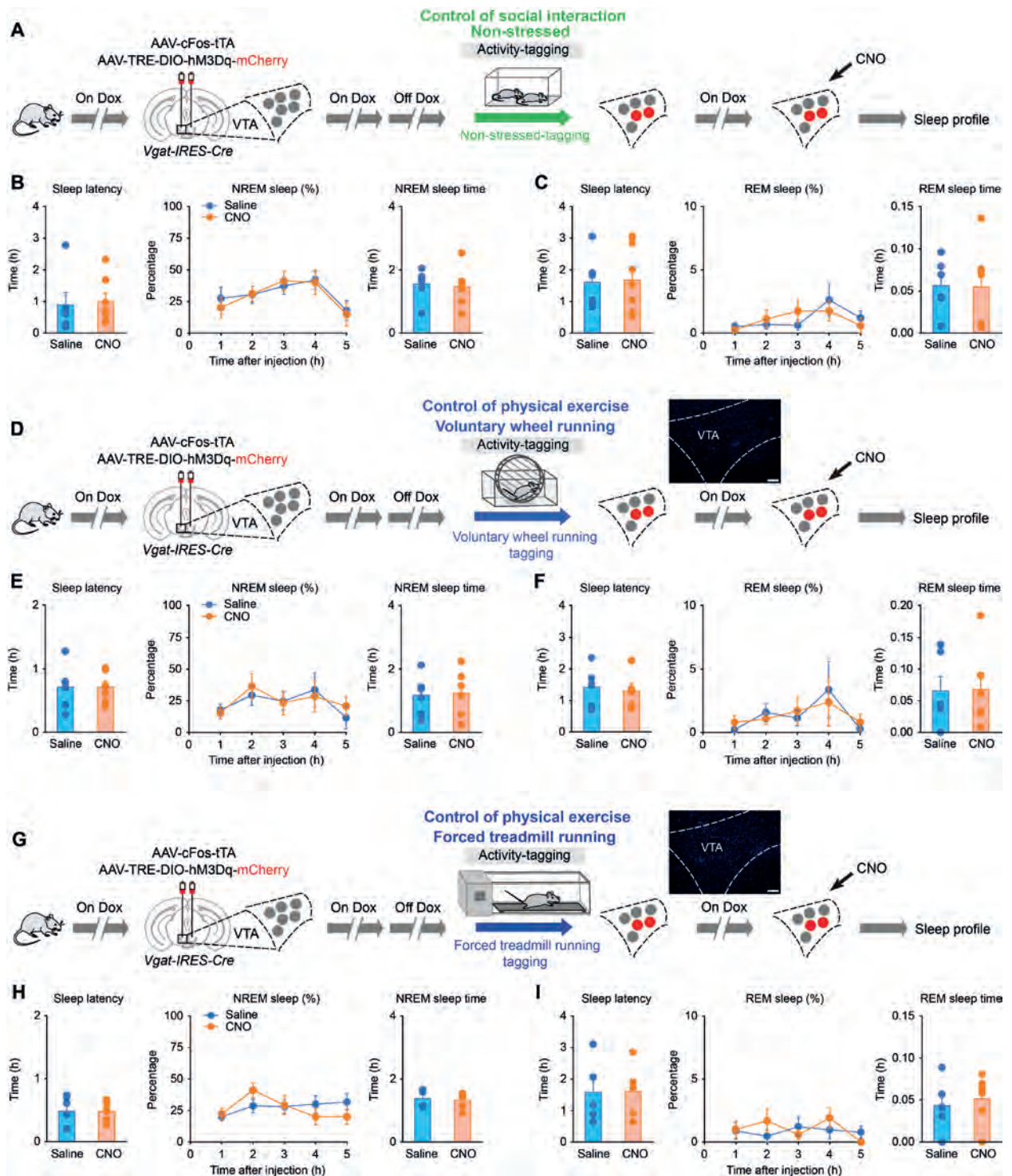


Fig. S7. No sleep is induced after chemogenetic reactivation of non-stressful procedure, voluntary wheel running or forced treadmill running tagged VTA^{Vgat} neurons (activity-tagging control of social interaction or physical activity) (Related to Fig. 2)

(A) The activity-tagging protocol for testing non-stressful procedure activated VTA^{Vgat} cells for sleep.

(B, C) Sleep latency, percentage and time of NREM **(B)** or REM **(C)** sleep after chemogenetic reactivation of non-stressful procedure tagged VTA^{Vgat} neurons (n = 6 mice per group). Unpaired *t*-test, $p > 0.05$.

(D) The activity-tagging protocol for testing voluntary wheel running activated VTA^{Vgat} cells for sleep and activity-tagged hM3Dq-mCherry transgene in VTA^{Vgat} neurons. Scale bar, 100 μm .

(E, F) Sleep latency, percentage and time of NREM **(E)** or REM **(F)** sleep after chemogenetic reactivation of voluntary wheel running tagged VTA^{Vgat} neurons (n = 6 mice per group). Unpaired *t*-test, $p > 0.05$.

(G) The activity-tagging protocol for testing forced treadmill running activated VTA^{Vgat} cells for sleep and activity-tagged hM3Dq-mCherry transgene in VTA^{Vgat} neurons. Scale bar, 100 μm .

(H, I) Sleep latency, percentage and time of NREM **(E)** or REM **(F)** sleep after chemogenetic reactivation of forced treadmill running tagged VTA^{Vgat} neurons (n = 6 mice per group). Unpaired *t*-test, $p > 0.05$.

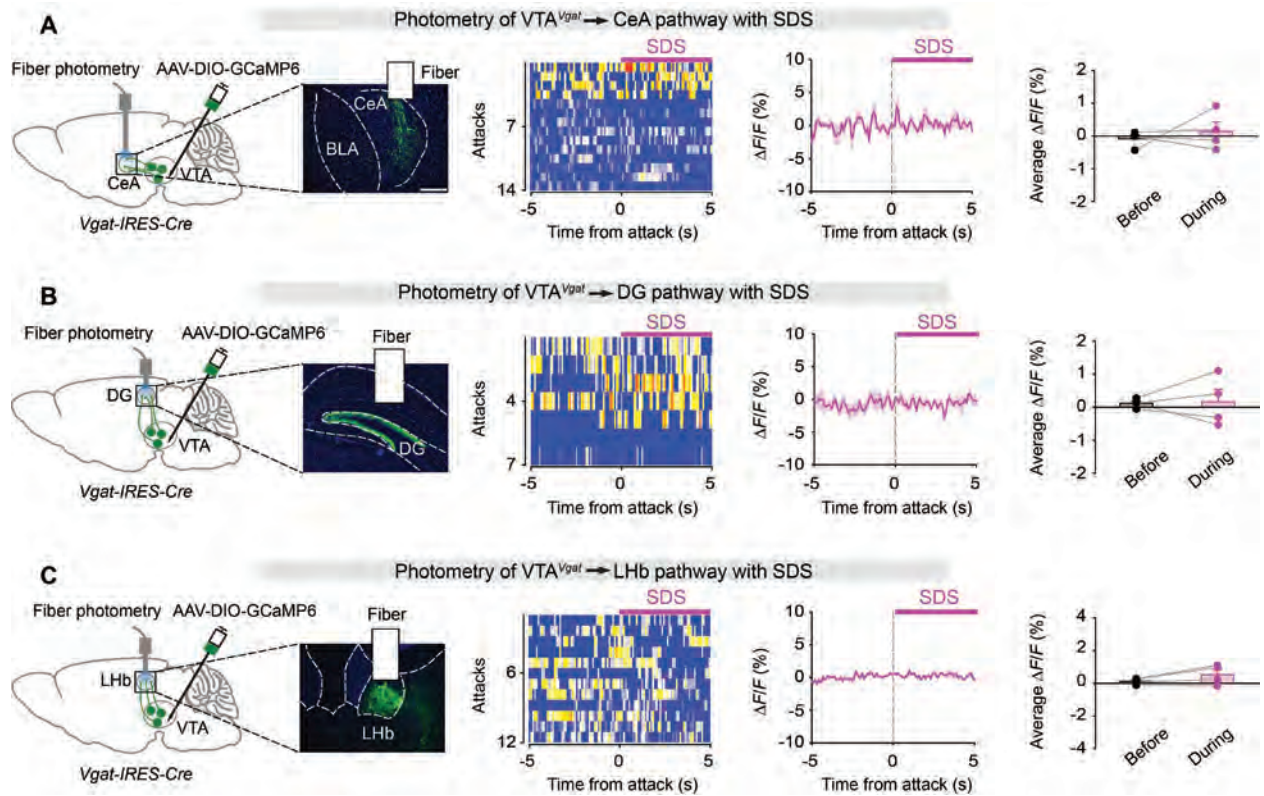


Fig. S8. Fiber photometry shows no changes in calcium signals in VTA^{Vgat} terminals in the CeA, DG or Lhb during SDS (Related to Fig. 3)

(A-C) Fiber photometry measuring terminal activity of VTA^{Vgat} neurons in CeA (A), DG (B) or Lhb (C) during SDS. Color matrix of GCaMP6 signals in CeA (A), DG (B) or Lhb (C) for all trials, $\Delta F/F$ ratios across the experimental period and average $\Delta F/F$ ratios before and during the SDS ($n = 4$ mice per group). Paired t -test, $p > 0.05$. Scale bar, 200 μm .

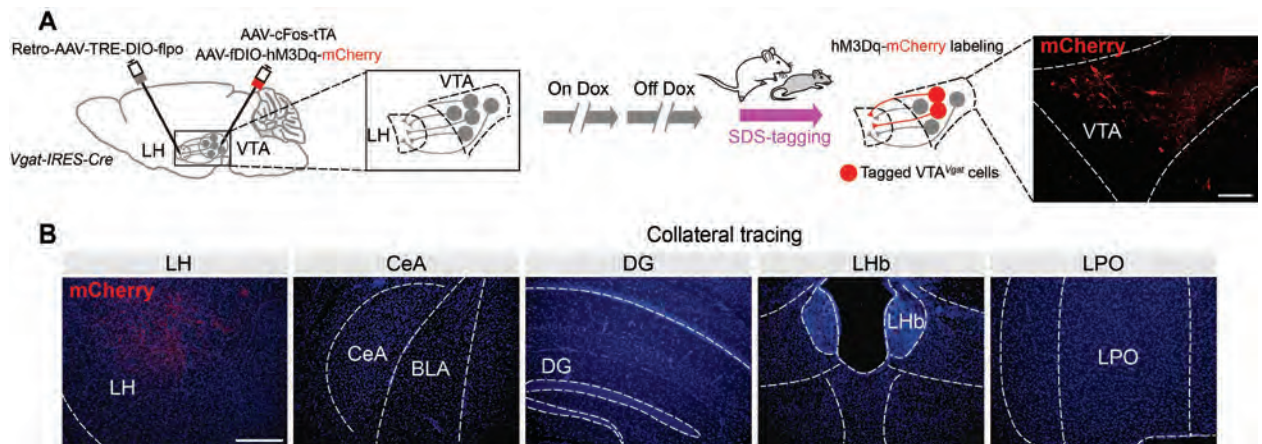


Fig. S9. Collateral tracing of SDS-tagged LH-projecting VTA^{Vgat} cells shows that the LH is their main projection site (Related to Fig. 3)

(A) The activity-tagging protocol and expression of the hM3Dq-mCherry transgene in SDS-tagged LH-projecting VTA^{Vgat} cells. Scale bar, 100 μ m.

(B) Tracing of SDS-tagged LH-projecting VTA^{Vgat} cells in the LH and collateral tracing in other brain regions. Scale bar, 200 μ m. LPO, lateral preoptic area; LH, lateral hypothalamus; LHb, lateral habenula; CeA, central amygdala; BLA, basolateral amygdala; DG, dentate gyrus of the hippocampus.

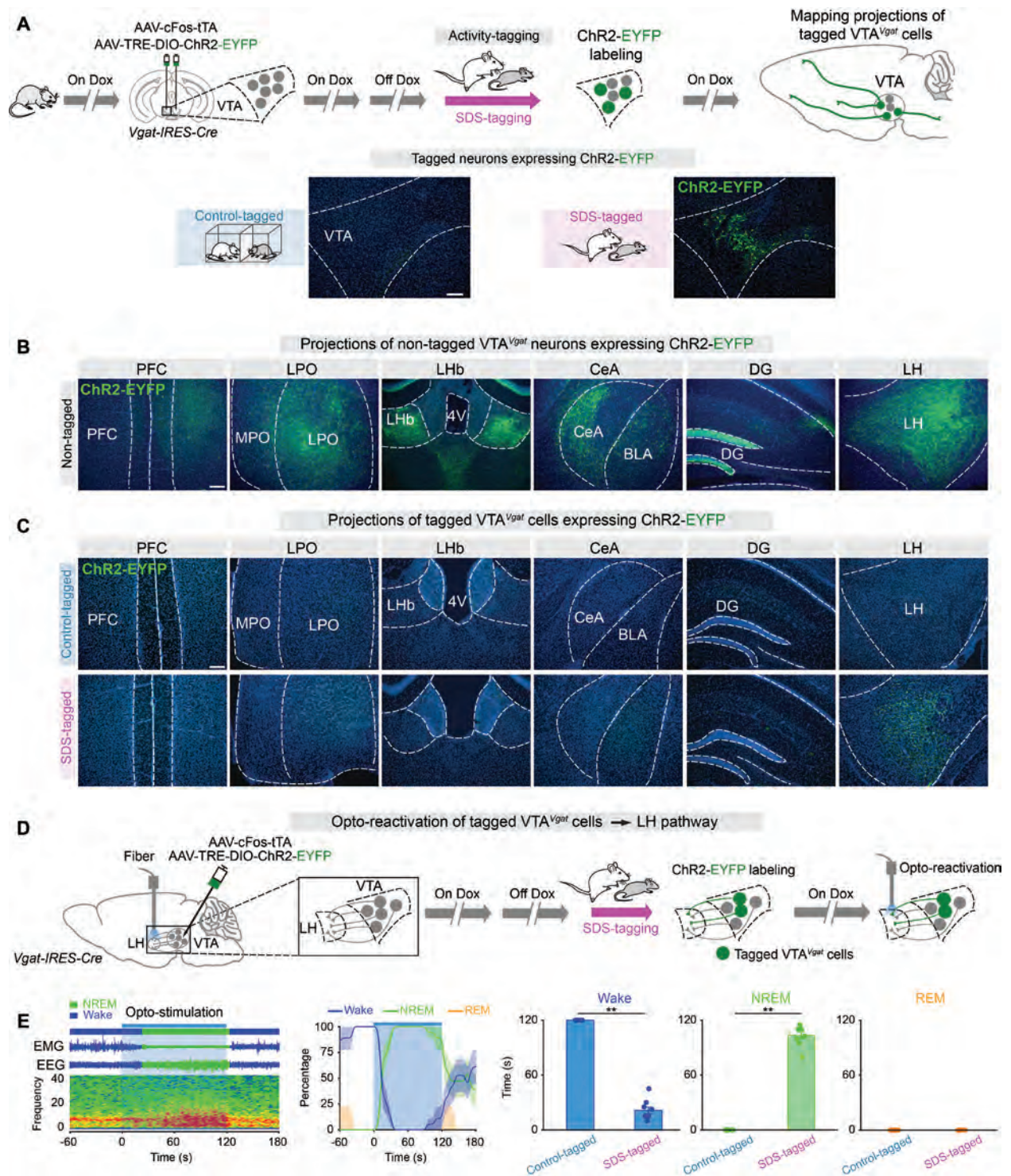


Fig. S10. Optogenetic manipulation of SDS-tagged VTA^{Vgat} neurons (Related to Fig. 3)

(A) The activity-tagging protocol for anterograde tracing of activity-tagged VTA^{Vgat} neurons using ChR2-EYFP and the expression of control- or SDS-tagged ChR2-EYFP in VTA^{Vgat} neurons. Scale bar, 200 μ m.

(B) Projections of non-tagged VTA^{Vgat} neurons (pan expression) in diverse brain areas (AAV-DIO-ChR2-EYFP injected into the VTA of Vgat-IRES-Cre mice). Scale bar, 100 μ m.

(C) Projections of control- or SDS-tagged VTA^{Vgat} neurons in diverse brain areas. PFC, prefrontal cortex; MPO, medial preoptic area; LPO, lateral preoptic area; LH, lateral hypothalamus; LHb, lateral habenula; CeA, central amygdala; BLA, basolateral amygdala; DG, dentate gyrus of the hippocampus; 4V, 4th ventricle of the brain. Scale bar, 100 μ m.

(D) The activity-tagging protocol for opto-reactivation of the tagged $VTA^{Vgat} \rightarrow$ LH pathway.

(E) Opto-reactivation of SDS-tagged $VTA^{Vgat} \rightarrow$ LH pathway from waking. EMG, EEG, spectra, percentage and time of wakefulness, NREM or REM sleep (n = 6 control-tagged mice; n = 9 SDS-tagged mice). Mann-Whitney test, **p < 0.01.

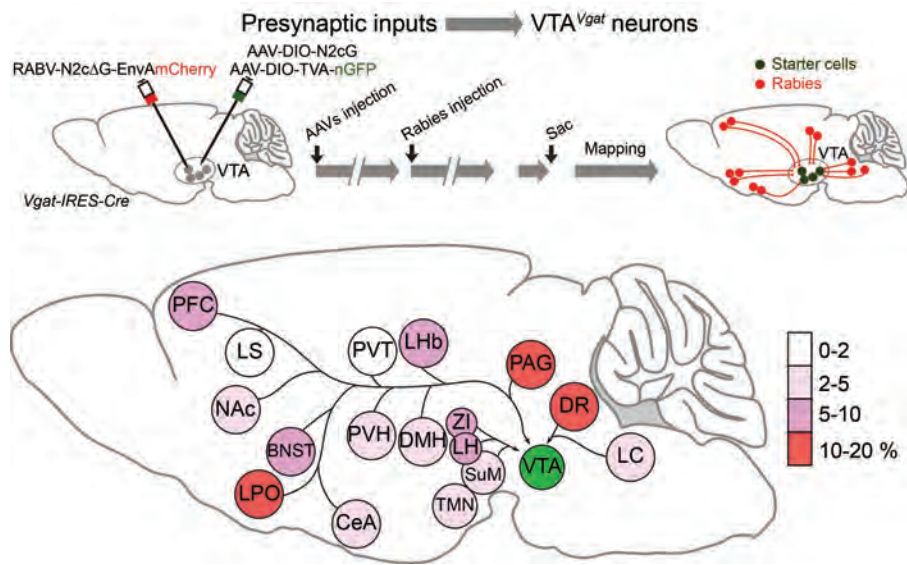


Fig. S11. Presynaptic inputs to VTA^{Vgat} neurons (Related to Fig. 3)

The protocol using rabies virus-based retrograde tracing for identification of presynaptic inputs to VTA^{Vgat} neurons and a schematic color matrix showing the percentage of total inputs from the whole brain to the VTA^{Vgat} neurons as determined by N2CΔG rabies retrograde tracing. The heat code indicates the percentage of total inputs as determined by counting the numbers of rabies-labeled presynaptic cells.

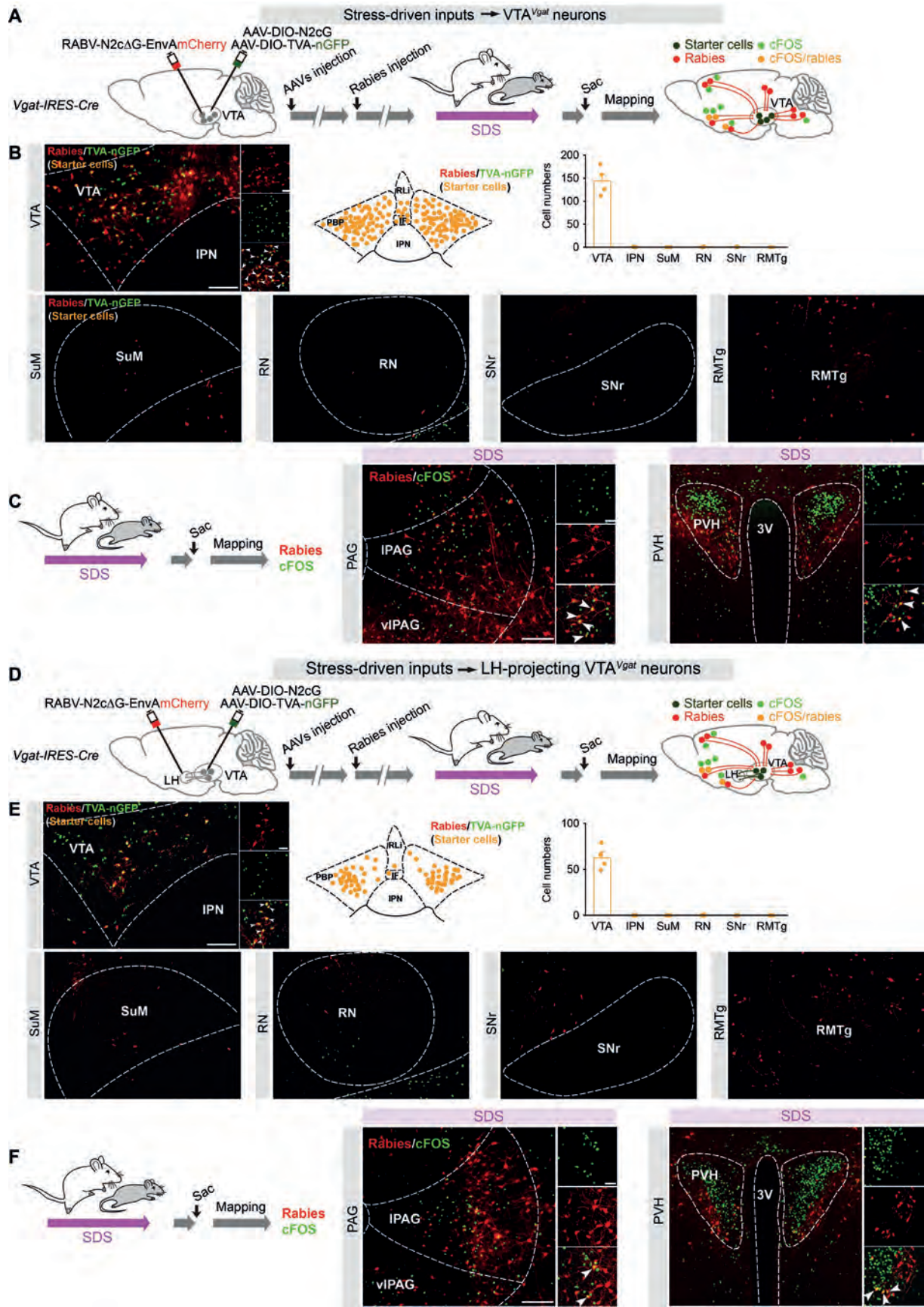


Fig. S12. Stress-driven inputs to VTA^{Vgat} neurons from PAG and PVH (Related to Fig. 3)

(A) Rabies virus-mediated tracing protocol for identification of stress-driven inputs to VTA^{Vgat} neurons.

(B) Immunostaining images, diagram and the number of VTA^{Vgat} starter cells (n = 4 mice) in the VTA and surrounding areas. Scale bar, 200 μm and 50 μm (inset).

(C) Immunostaining images showing presynaptic inputs to VTA^{Vgat} neurons from PAG or PVH and cFOS-positive cells activated by SDS. cFOS (green) and mCherry (rabies, red) were stained by immunocytochemistry. Scale bar, 200 μm and 50 μm (inset).

(D) Rabies virus-mediated tracing protocol for identification of stress-driven inputs to LH-projecting VTA^{Vgat} neurons.

(E) Immunostaining images, diagram and the number of LH-projecting VTA^{Vgat} starter cells in the VTA and surrounding areas (n = 4 mice). Scale bar, 200 μm and 50 μm (inset).

(F) Immunostaining images showing presynaptic inputs to LH-projecting VTA^{Vgat} neurons from PAG or PVH and cFOS-positive cells activated by SDS. Scale bar, 200 μm and 50 μm (inset). PVH, paraventricular hypothalamus; PAG, periaquiductal grey; 3V, 3rd ventricle.

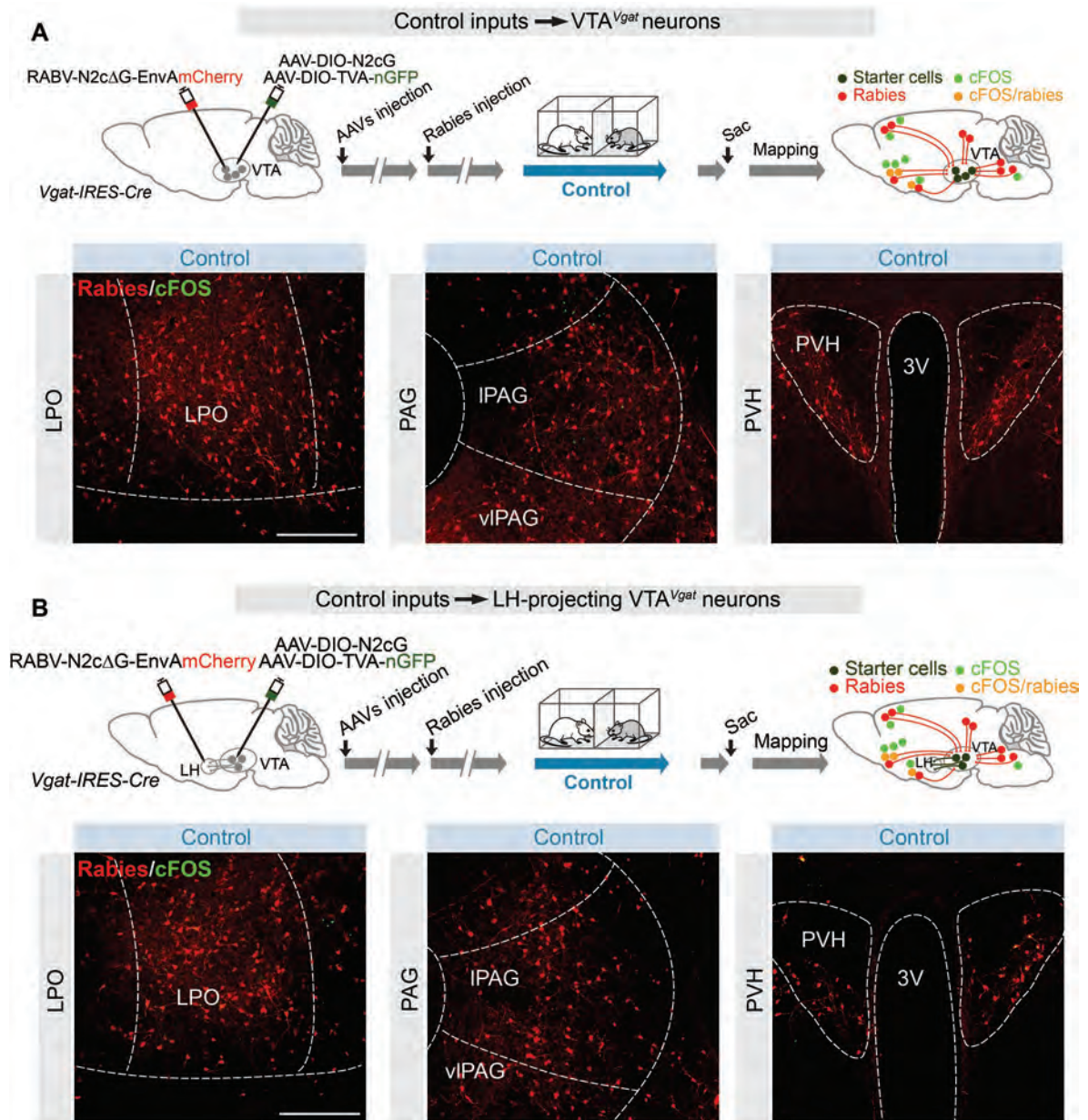


Fig. S13. Control inputs to VTA^{Vgat} neurons from LPO, PAG and PVH (Related to Fig. 3)

(A) Tracing protocol and immunostaining images showing presynaptic inputs to VTA^{Vgat} neurons from LPO, PAG or PVH and cFOS-positive cells of control. cFOS (green) and mCherry (rabies, red) were stained by immunocytochemistry. Scale bar, 200 μ m.

(B) Tracing protocol and immunostaining images showing presynaptic inputs to LH-projecting VTA^{Vgat} neurons from LPO, PAG or PVH and cFOS-positive cells of control. Scale bar, 100 μ m. LPO, lateral preoptic area; PVH, paraventricular hypothalamus; PAG, periaquiductal grey; 3V, 3rd ventricle of the brain.

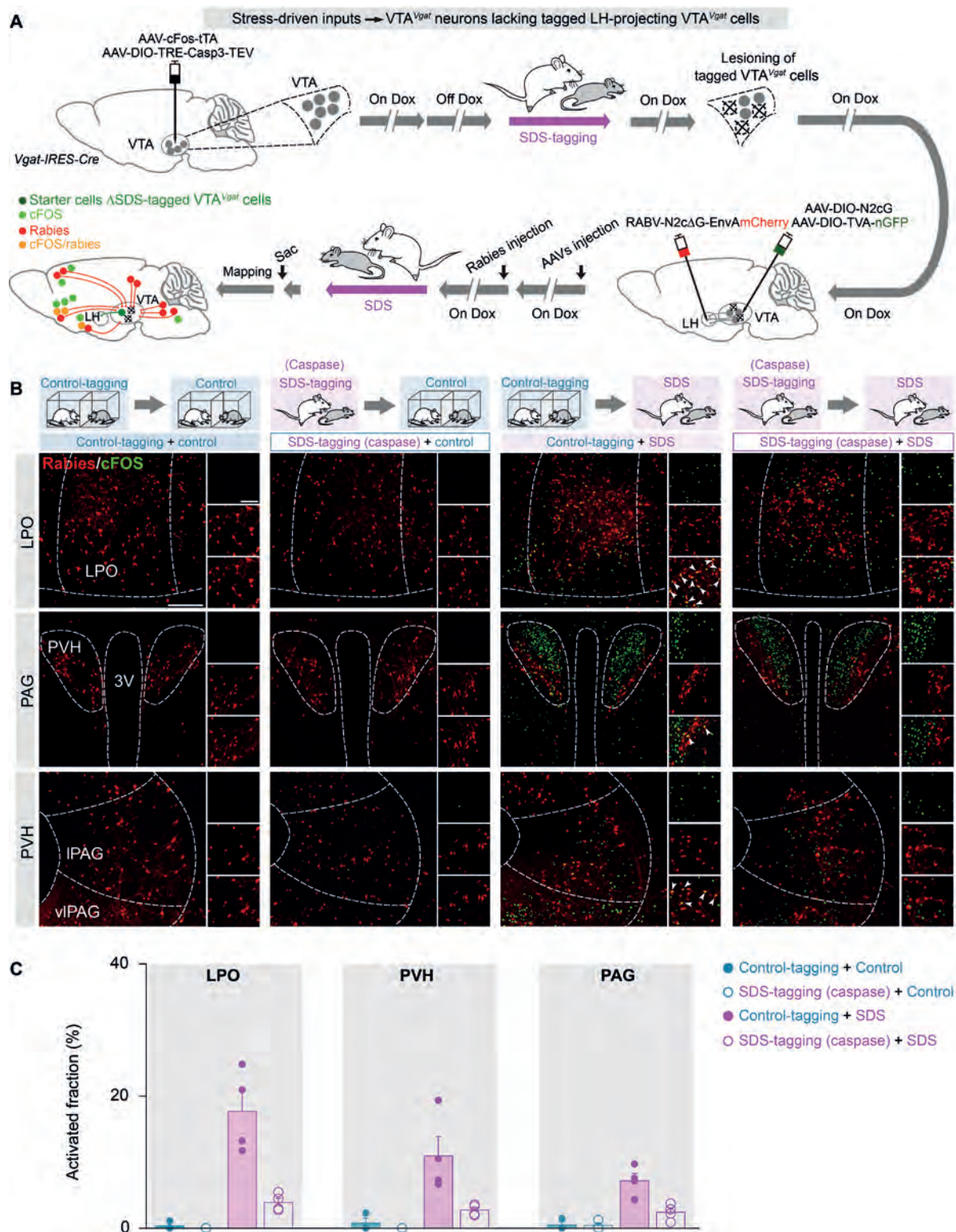


Fig. S14. Specificity of stress-driven inputs to SDS-activated VTA^{Vgat} cells (Related to Fig. 3)

(A) The work-flow protocol for identifying SDS-driven inputs to VTA^{Vgat} neurons lacking SDS-tagged VTA^{Vgat} cells (activity-tagging-induced expression of caspase).

(B) Immunostaining images showing that stress-driven inputs to LH-projecting VTA^{Vgat} neurons identified by rabies labeling (mCherry) disappeared when SDS-tagged VTA^{Vgat} cells have been specifically ablated by caspase (SDS-tagging-induced expression of Caspase, thereby ablation of SDS-activated VTA^{Vgat} cells). In control, images where VTA^{Vgat} neurons were control-experience-tagged with caspase (control experience did not induce caspase expression). Scale bar, 150 μ m and 100 μ m (inset).

(C) Summary of activated fractions in diverse brain areas for all groups shown in B (n = 3 mice per group for control-tagged; n = 4 mice per group for SDS-tagged).

PFC, prefrontal cortex; NAc, nucleus acumbens; LS, lateral septum; BNST, bed nucleus of the stria terminalis; LPO, lateral preoptic area; PVH, paraventricular hypothalamus; LH, lateral hypothalamus; LH, lateral habenula; CeA, central amygdala; PVT, paraventricular thalamus; DMH, dorsal medial hypothalamus; ZI, zona incerta; SuM, supramammillary nucleus; TMN, tuberomammillary nucleus; LC, locus ceruleus; DR, dorsal raphe; PAG, periaquiductal grey. 3V, 3rd ventricle.

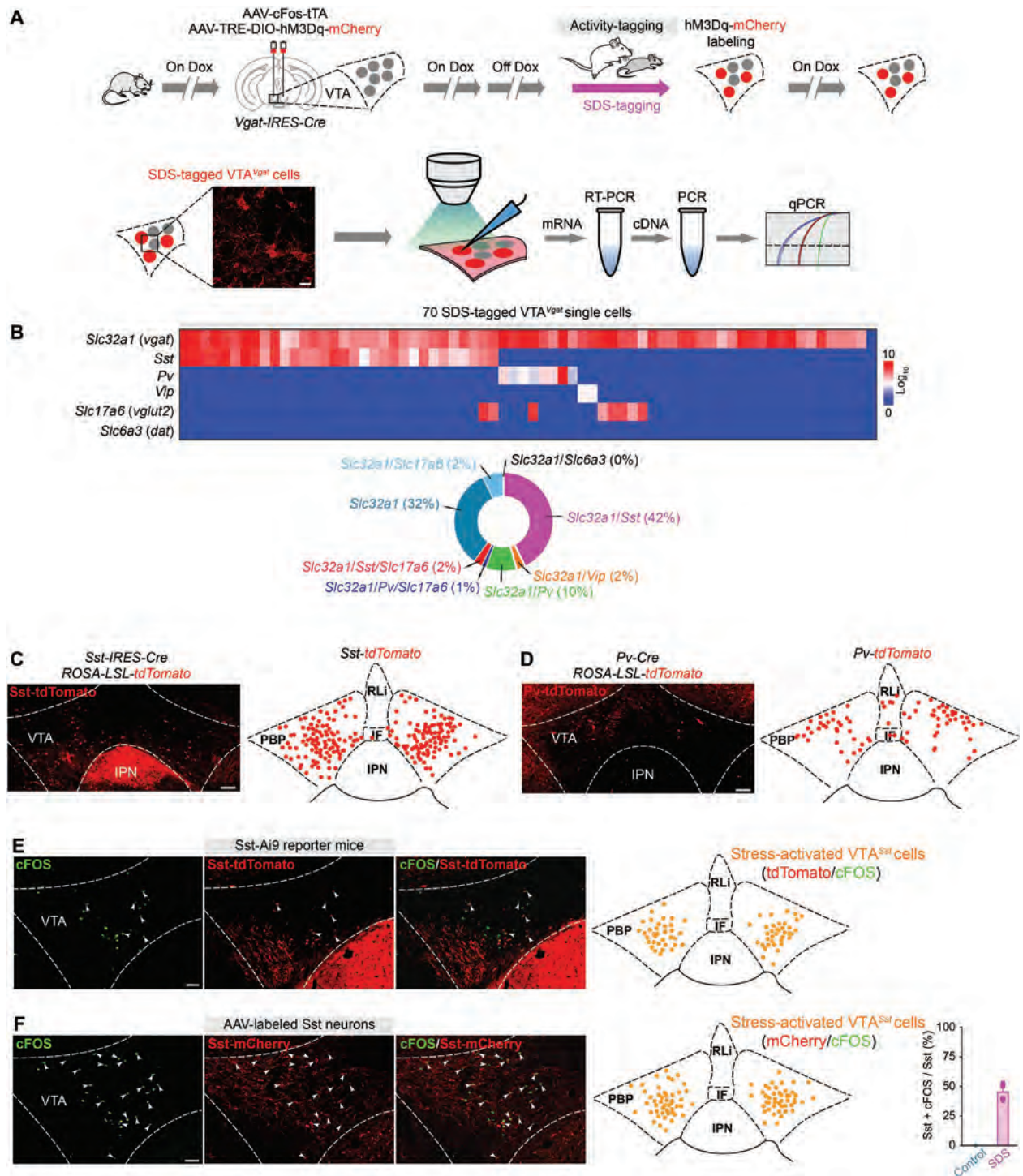


Fig. S15. Molecular identities of SDS-tagged VTA^{Vgat} neurons and topology of VTA^{Sst} and VTA^{Pv} neurons (Related to Fig. 4)

(A) The activity-tagging and single-cell RT-qPCR protocol to profile SDS-tagged VTA^{Vgat} neurons. Scale bar, 25 μ m.

(B) Heat map and doughnut chart for the single-cell qPCR of patched SDS-tagged VTA^{Vgat} cells (n = 70 cells from 9 mice). The genes tested were: *Slc32a1* (*vgat*); *Sst*; *Pv*; *Vip*; *Slc17a6* (*vglut2*); *Slc6a3* (*dat*).

(C) Immunostaining image showing *Sst-Ai9-tdTomato* cells (*Sst-IRES-Cre* X Ai9 reporter mice) in the VTA and diagram summarizing *Sst-Ai9-tdTomato* cells in the VTA (n = 3 mice). Scale bar, 100 μ m.

(D) Immunostaining image showing *Pv-Ai9-tdTomato* cells (*Pv-Cre* X Ai9 reporter mice) in the VTA and diagram summarizing *Pv-Ai9-tdTomato* cells in the VTA (n = 3 mice). Scale bar, 100 μ m.

(E) cFOS expression by immunohistochemistry (green) after SDS in VTA^{*Sst-tdTomato*} neurons (*Sst-Ai9-tdTomato*). Arrowheads indicate double-labeled cells. Scale bar, 100 μ m. Schematic diagram summarizing SDS-activated VTA^{*Sst-tdTomato*} neurons (*Sst-tdTomato* / cFOS) (n = 4 mice). Scale bar, 100 μ m.

(F) cFOS expression by immunohistochemistry (green) after SDS in VTA^{*Sst-mCherry*} neurons (AAV-*DIO-hM3Dq-mCherry* injected into the VTA of *Sst-IRES-Cre* mice). Arrowheads indicate double-labeled cells. Diagram summarizing SDS-activated VTA^{*Sst-mCherry*} neurons (*Sst-mCherry* / cFOS) (n = 4 mice). Quantification represents cFOS and *Sst-mCherry* double-labeled cells / total *Sst-mCherry* cells (n = 4 mice per group). Scale bar, 100 μ m.

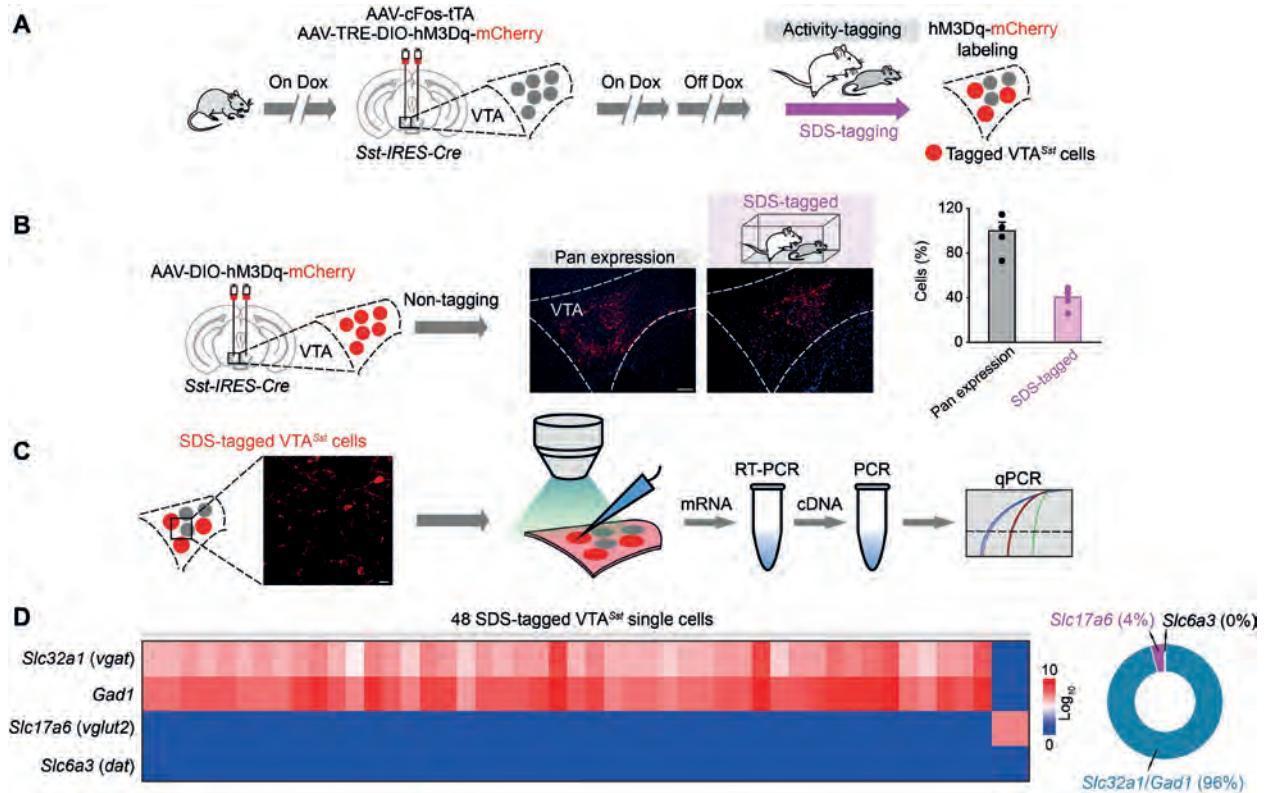


Fig. S16. Molecular identities of SDS-tagged *VTA*^{*Sst*} neurons (Related to Fig. 4)

(A, B) The activity-tagging protocol (A), expression of the hM3Dq-mCherry transgene in pan (AAV-DIO-mCherry injected into the VTA of *Sst-IRES-Cre* mice) or SDS-tagged *VTA*^{*Sst*} neurons (n = 5 mice per group) (B). Scale bar, 100 μ m.

(C) Single-cell RT-qPCR protocol to profile SDS-tagged *VTA*^{*Sst*} neurons. Scale bar, 25 μ m.

(D) Heat map and doughnut chart for the single-cell qPCR of patched SDS-tagged *VTA*^{*Sst*} cells (n = 48 cells from 6 mice). The genes tested were: *Slc32a1* (*vgat*); *Gad1*; *Slc17a6* (*vglut2*); *Slc6a3* (*dat*).

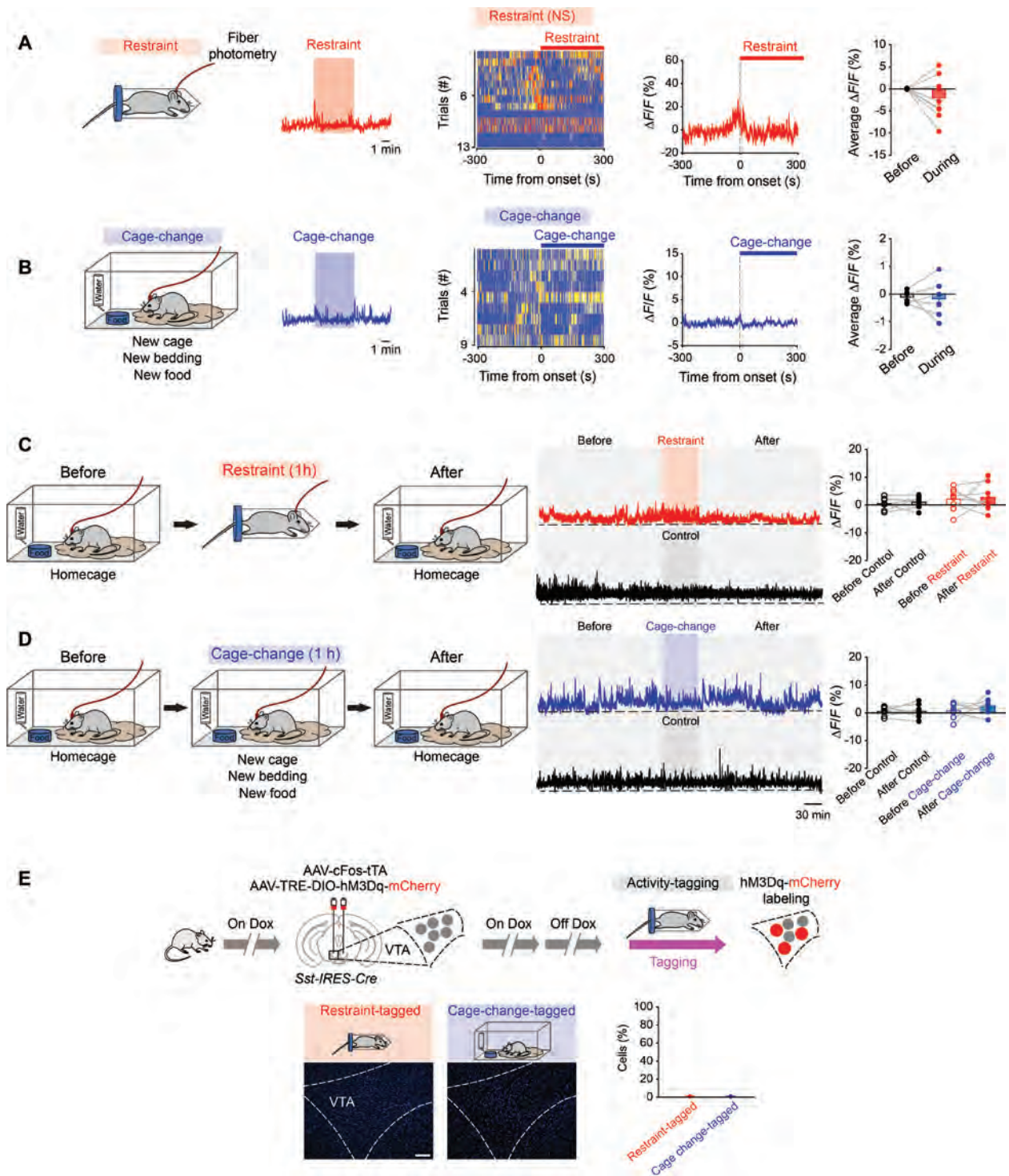


Fig. S17. VTA^{Sst} neurons do not respond to restraint or cage-change stress (Related to Fig. 4)

(A, B) Fiber photometry measuring calcium signals in VTA^{Sst} neurons responding to restraint (n = 9 mice per group, 13 trials) (A) or cage-change (n = 6 mice per group, 9 trials) (B). Raw calcium signal traces, color matrix of GCaMP6 signals for all trials, $\Delta F/F$ ratios across the

experimental period and average $\Delta F/F$ ratios before and during the procedures. Paired t -test, $p > 0.05$.

(C, D) Fiber photometry measuring long-term calcium signals in VTA^{Sst} neurons ($n = 8$ per group) in response to restraint **(C)** or cage-change stress **(D)**. Raw traces and average $\Delta F/F$ ratios before and after procedures. Paired t -test, $p > 0.05$.

(E) The activity-tagging protocol, expression and quantification of restraint- or cage-change-tagged hM3Dq-mCherry transgene expression in VTA^{Sst} neurons ($n = 4$ mice per group).

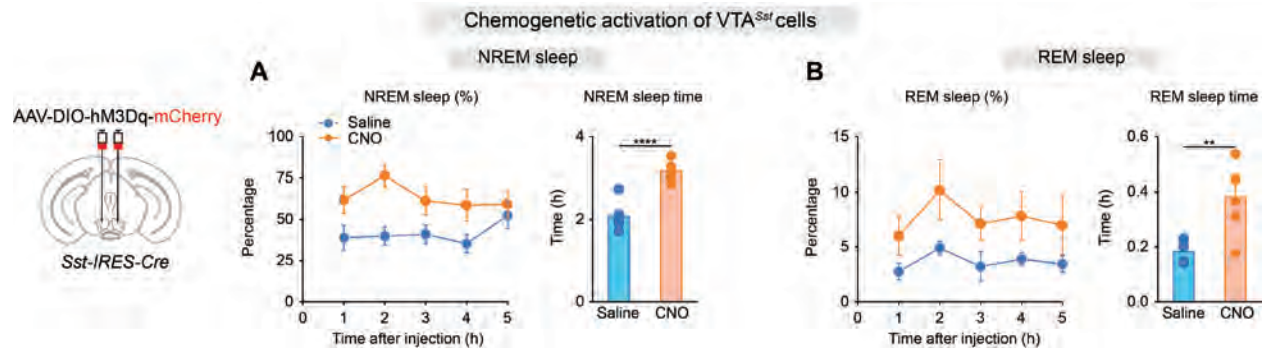


Fig. S18. Chemogenetic activation of VTA^{Sst} neurons promotes NREM and REM sleep (Related to Fig. 5)

(A, B) Percentage and time of NREM (A) or REM (B) sleep after chemogenetic activation of VTA^{Sst} neurons (n = 6 mice per group). Unpaired *t*-test, ***p* < 0.01, *****p* < 0.0001.

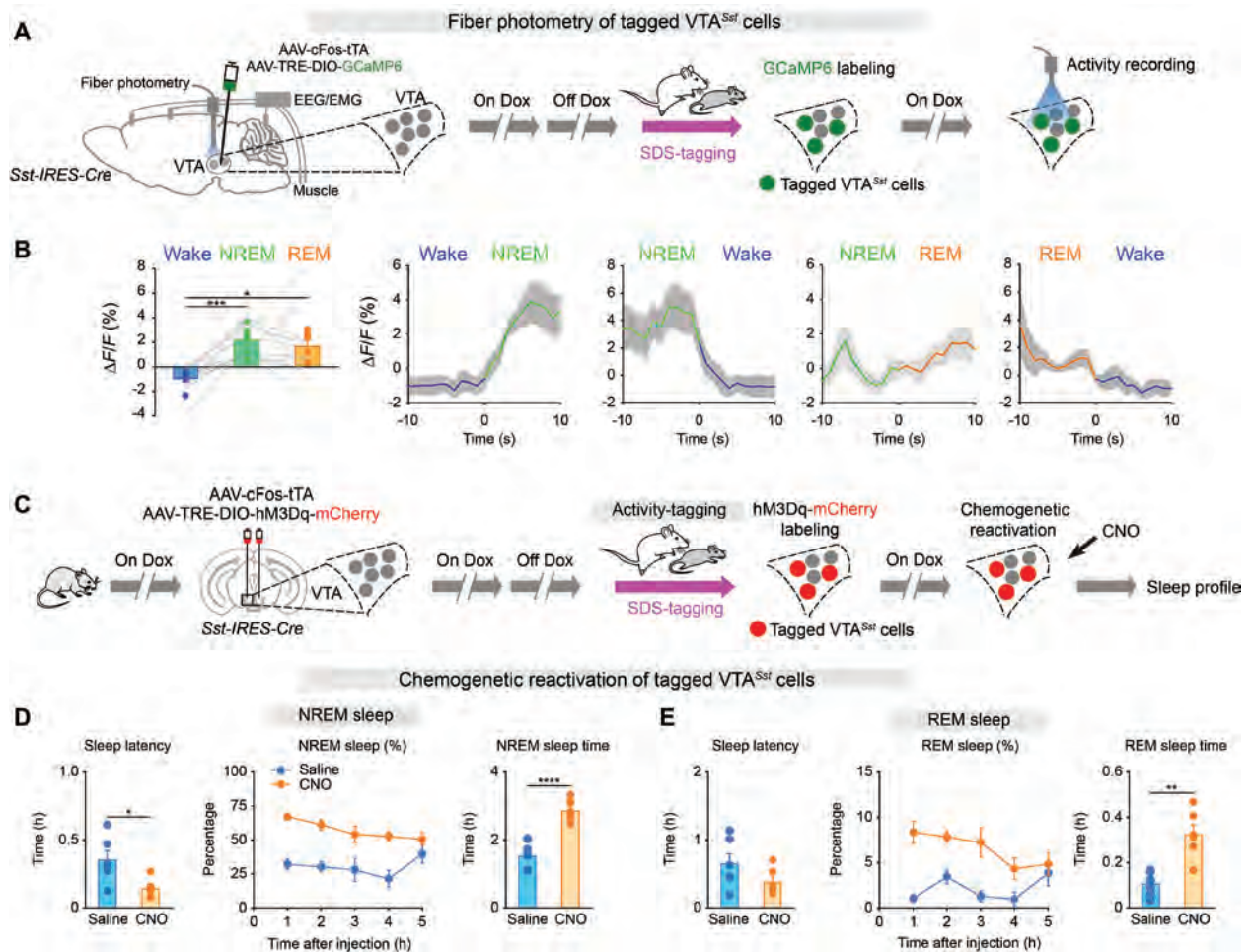


Fig. S19. SDS-tagged VTA^{Sst} neurons are NREM and REM sleep-active and activation of SDS-tagged VTA^{Sst} neurons promotes NREM and REM sleep (Related to Fig. 5)

(A) The activity-tagging protocol for fiber photometry with EEG/EMG measuring the spontaneous activity of SDS-tagged VTA^{Sst} neurons across brain states.

(B) $\Delta F/F$ ratio of the Ca²⁺ signal in SDS-tagged VTA^{Sst} neurons during wakefulness, NREM and REM sleep (n = 6 mice per group). Photometry signals in SDS-tagged VTA^{Sst} neurons at transitions of vigilance states (n = 6 mice per group). One-way repeated ANOVA, *p < 0.05, ***p < 0.001.

(C) The activity-tagging protocol for testing the sufficiency of SDS-tagged VTA^{Sst} cells for sleep.

(D, E) Sleep latency, percentage and time of NREM (D) or REM (E) sleep after chemogenetic reactivation of SDS-tagged VTA^{Sst} neurons (n = 6 mice per group). Unpaired t-test, *p < 0.05, **p < 0.01, ****p < 0.0001.

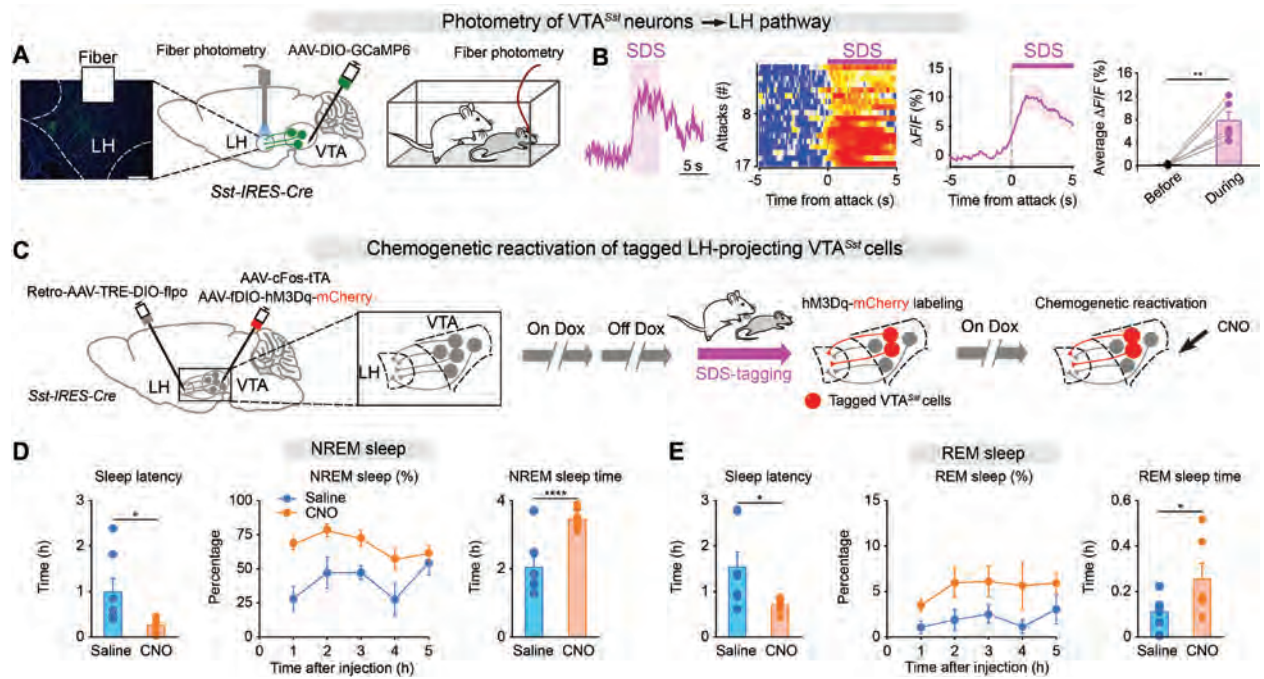


Fig. S20. VTA^{Sst} neurons mediate SDS-induced sleep via the LH (Related to Fig. 5)

(A, B) Fiber photometry measuring the terminal calcium signals of the VTA^{Sst}→LH pathway during SDS. The image shows GCaMP6 fiber in the LH (A). Raw traces, color matrix of GCaMP6 signals of VTA^{Sst}→LH pathway for all trials, $\Delta F/F$ ratios across the experimental period, and average $\Delta F/F$ before and during the SDS (B) (n = 8 mice, 17 trials). Paired *t*-test, ***p* < 0.01. Scale bar, 100 μ m.

(C) The intersectional activity-tagging protocol for chemogenetic reactivation of SDS-tagged LH-projecting VTA^{Sst} cells.

(D, E) Sleep latency, percentage and time of NREM (D) and REM (E) sleep after chemogenetic reactivation of SDS-tagged LH-projecting VTA^{Sst} cells (n = 6 mice per group). Unpaired *t*-test, **p* < 0.05, *****p* < 0.0001.

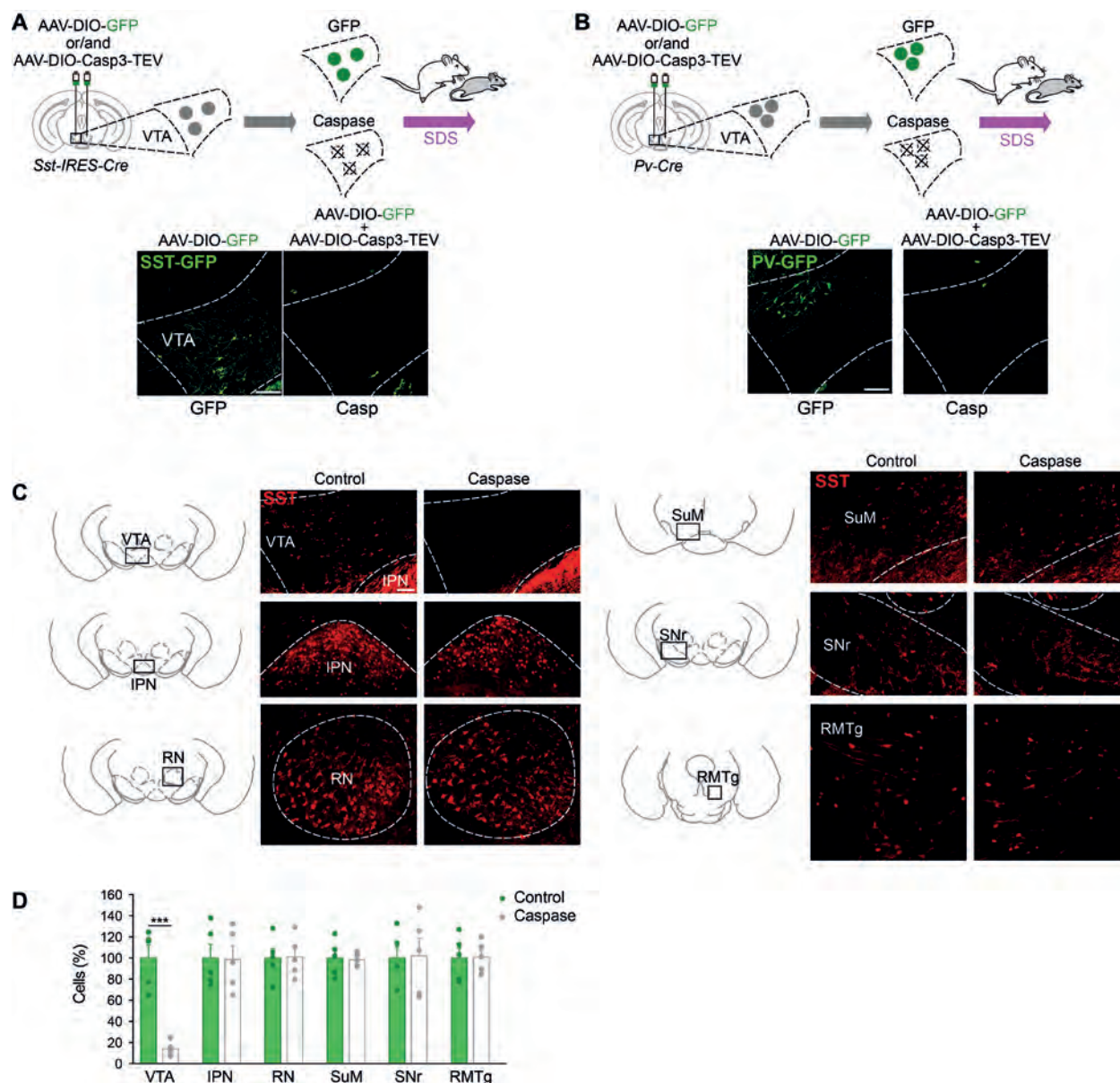


Fig. S21. Efficacy and specificity of genetic ablation (Related to Fig. 5)

(A, B) Genetic ablation of VTA^{Sst} (A) or VTA^{Pv} (B) neurons. Image showing GFP expression in AAV-DIO-GFP injected controls or AAV-DIO-GFP and AAV-DIO-Casp3-TEV injected group. Scale bar, 100 μ m.

(C, D) Immunostaining images (C) and quantifications (D) showing somatostatin (SST)-positive cells in the VTA and surrounding areas in control or caspase mice (n = 5 mice per group). Scale bar, 100 μ m. RN, red nucleus; IPN, interpeduncular nucleus; SuM, supramammillary nucleus; RMTg, rostromedial tegmental nucleus; SNr, substantia nigra. Unpaired *t*-test, ***p < 0.001.

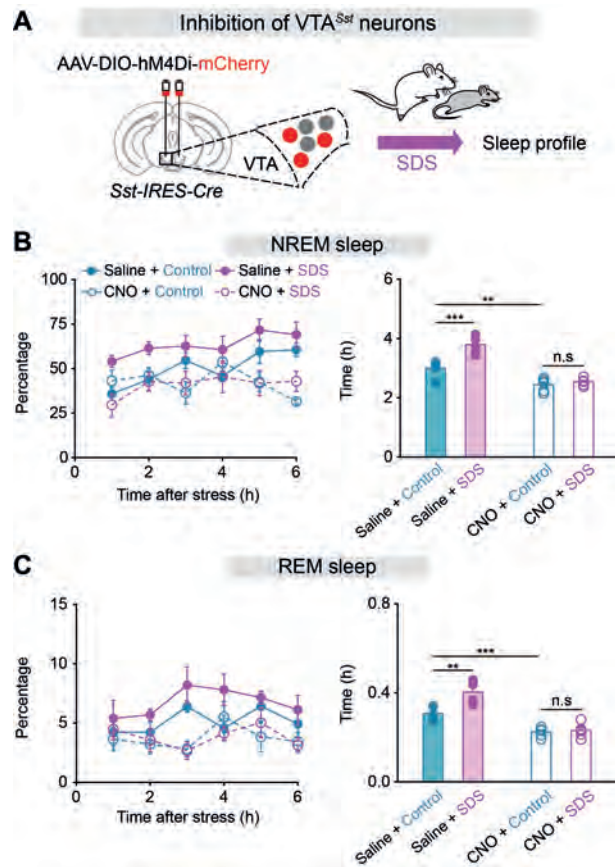


Fig. S22. VTA^{Sst} neurons are necessary for SDS-induced sleep (Related to Fig. 5)

(A) Chemogenetic inhibition for testing the necessity of VTA^{Sst} cells for SDS-induced sleep.

(B, C) Percentage and time of NREM (B) or REM sleep (C) in mice given SDS after chemogenetic inhibition of VTA^{Sst} cells (n = 6 mice per group). Two-way ANOVA with bonferroni *post hoc* test. **p<0.01, ***p<0.001, n.s: not significant.

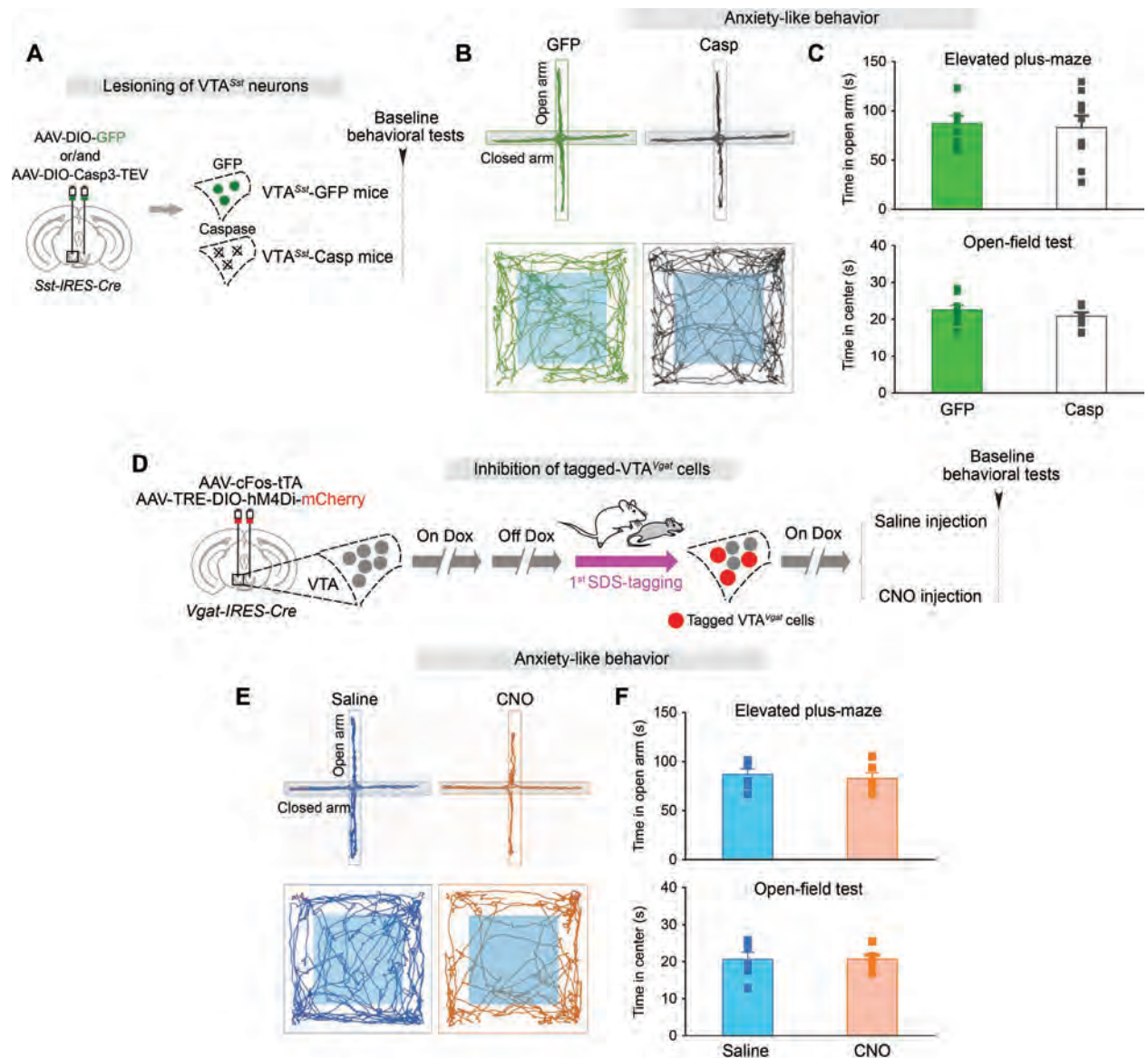


Fig. S23. Lesioning of VTA^{Sst} neurons or inhibition of SDS-tagged VTA^{Vgat} neurons does not affect baseline anxiety levels in mice (Related to Fig. 6)

(A) Plan of the experimental procedure. Behavioral tests (EPM and OFT) were performed as arrowhead indicates.

(B, C) Tracing of locomotion for representative animals (B), time spent in the open arms of the elevated plus-maze and in the center zone during the open-field test of GFP mice and caspase mice (n = 9 mice per group) (C). Unpaired *t*-test, *p* > 0.05.

(D) Plan of the experimental procedure and the activity-tagging protocol for chemogenetic manipulation of SDS-activated VTA^{Vgat} cells. Behavioral tests (EPM and OFT) were performed as arrowhead indicates.

(E, F) Tracing of locomotion for representative animals (E), time spent in the open arms of the elevated plus-maze and in the center zone during the open-field test of saline- and CNO-injected mice (n = 6 mice per group) (F). Unpaired *t*-test, $p > 0.05$.

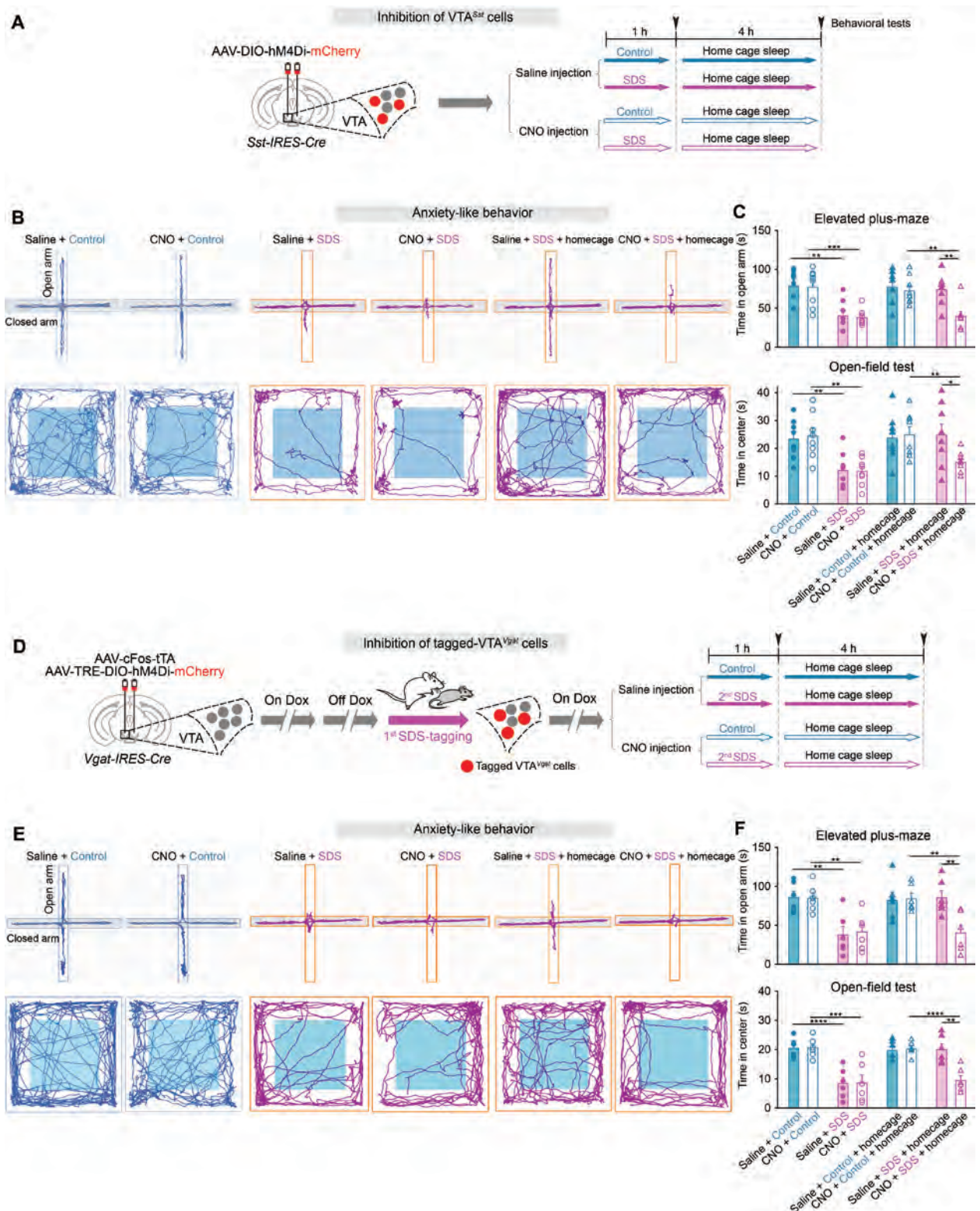


Fig. S24. SDS-induced sleep by VTA^{Sst} neurons and SDS-tagged VTA^{Vgat} neurons reduces SDS-induced anxiety (Related to Fig. 6)

(A) Plan of the experimental procedure for chemogenetic inhibition of VTA^{Sst} cells followed by control or SDS for behavioral tests, as arrowheads indicate.

(B, C) Tracing of locomotion for representative animals (B), time spent in the open arms of the elevated plus-maze and in the center zone during the open-field test of saline- or CNO-injected mice (n = 8 mice per group) (C). Two-way ANOVA with Bonferroni *post hoc* test, *p < 0.05, **p < 0.01, ***p < 0.001.

(D) Plan of the experimental procedure and the activity-tagging protocol for chemogenetic manipulation of SDS-activated VTA^{Vgat} cells (1st SDS-tagging) followed by control or SDS (2nd SDS) for behavioral tests, as arrowheads indicate.

(E, F) Tracing of locomotion for representative animals (E), time spent in the open arms of the elevated plus-maze and in the center zone during the open-field test of saline- or CNO-injected mice (F) (n = 6 mice per group). Two-way ANOVA with Bonferroni *post hoc* test, **p < 0.01, ***p < 0.001, ****p < 0.0001.

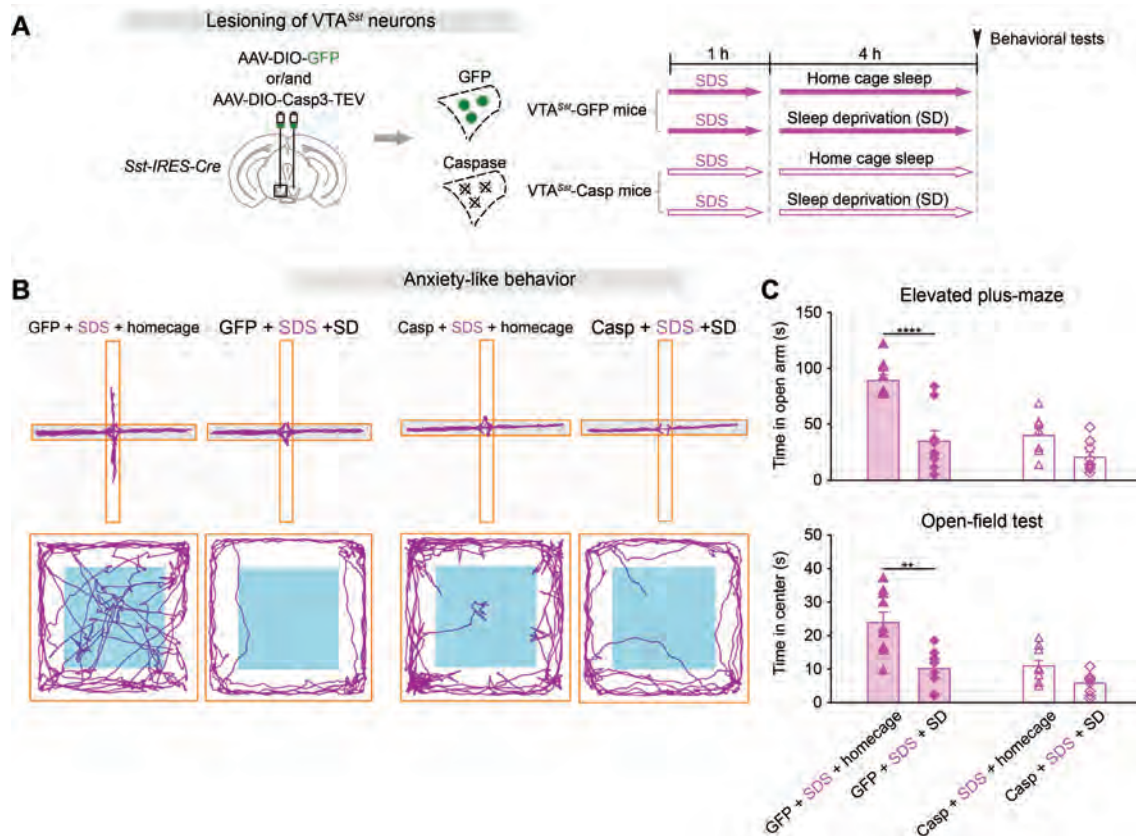


Fig. S25. Lacking SDS-induced sleep by lesioning of VTA^{Sst} neurons does not reduce SDS-induced anxiety, and is similar to the effect of sleep deprivation (Related to Fig. 6)

(A) Plan of the experimental procedure. Behavioral tests were performed as arrowhead indicates.

(B, C) Tracing of locomotion for representative animals (B), time spent in the open arms of the elevated plus-maze and in the center zone during the open-field test of GFP and caspase mice after control or SDS followed by 4-h home cage sleep or sleep deprivation (C) (n = 9 mice per group). Two-way ANOVA with Bonferroni *post hoc* test, **p < 0.01, ****p < 0.0001.

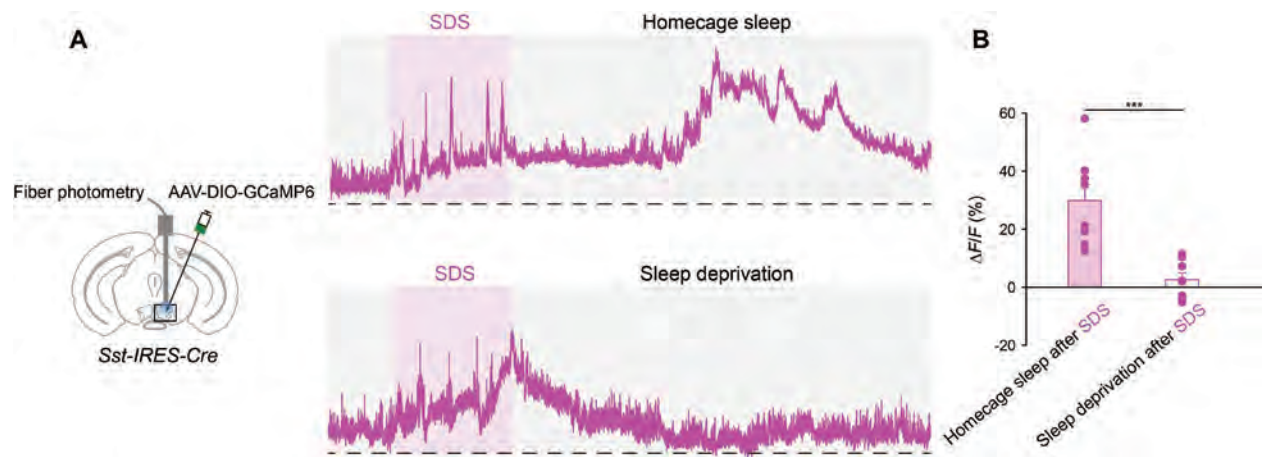


Fig. S26. Sleep deprivation suppresses the activity in VTA^{Sst} neurons induced by SDS (Related to Fig. 6)

Fiber photometry measuring long-term calcium signals in VTA^{Sst} neurons in response to SDS followed by sleep deprivation or home cage sleep. Raw traces (**A**) and average $\Delta F/F$ ratios (**B**) during sleep deprivation or home cage sleep after SDS (n = 8 mice per group). Unpaired *t*-test, ****p* < 0.001.

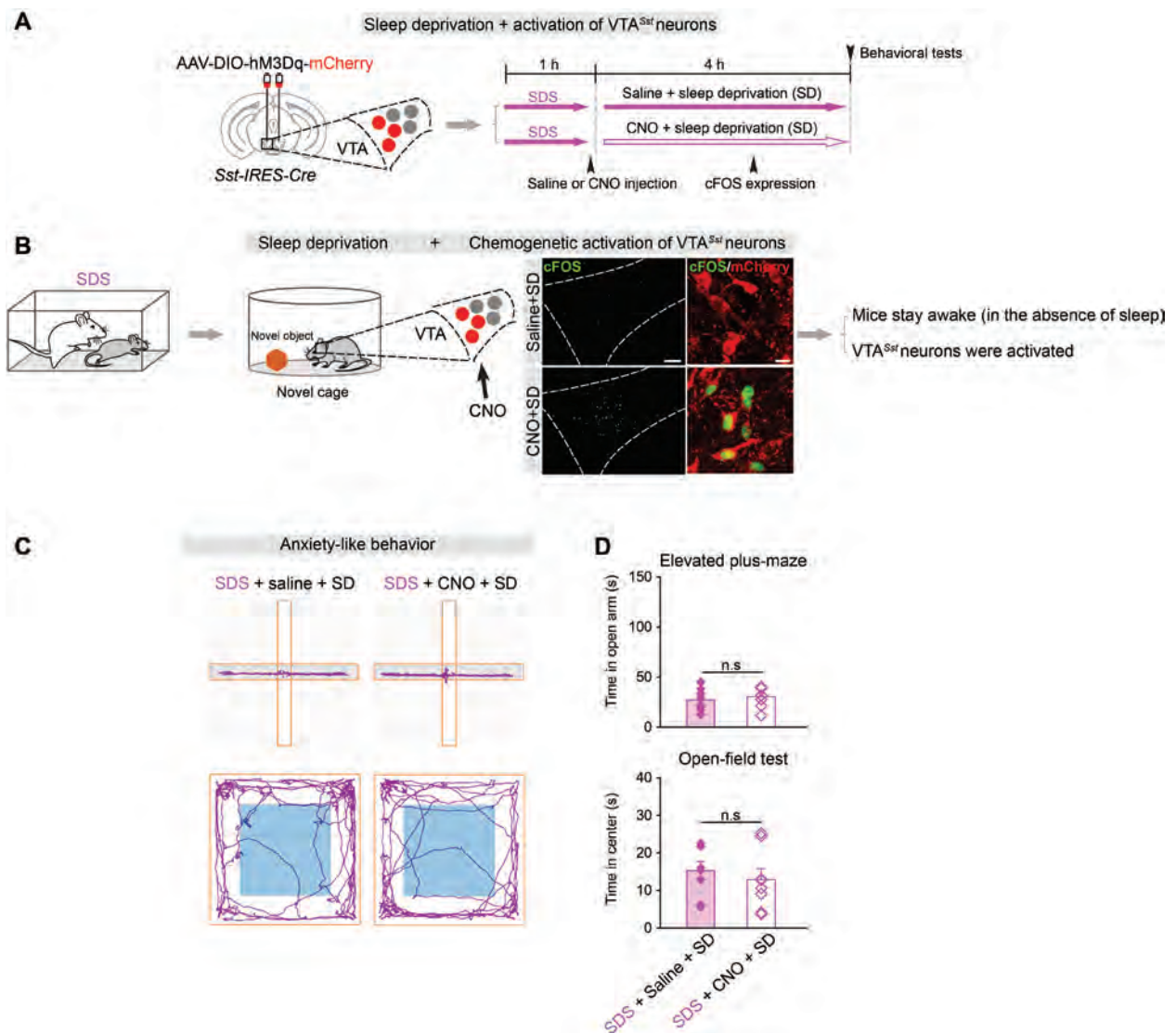


Fig. S27. Activation of VTA^{Sst} neurons during sleep deprivation (in the absence of sleep) after SDS does not reduce anxiety

(A) Plan of the experimental procedure for chemogenetic activation of VTA^{Sst} neurons during sleep deprivation after SDS for behavioral tests, as arrowhead indicate.

(B) cFOS expression and cFOS expression in VTA^{Sst} neurons (hM3Dq-mCherry) 3 hours after saline or CNO injection during sleep deprivation after SDS. Scale bar, 100 μ m (left) and 25 μ m (right).

(C, D) Tracing of locomotion for representative animals (B) and time spent in the open arms of the elevated plus-maze and in the center zone during the open-field test (C) (n = 8 mice per group). Two-way ANOVA with bonferroni *post hoc* test, p > 0.05, n.s, not significant.

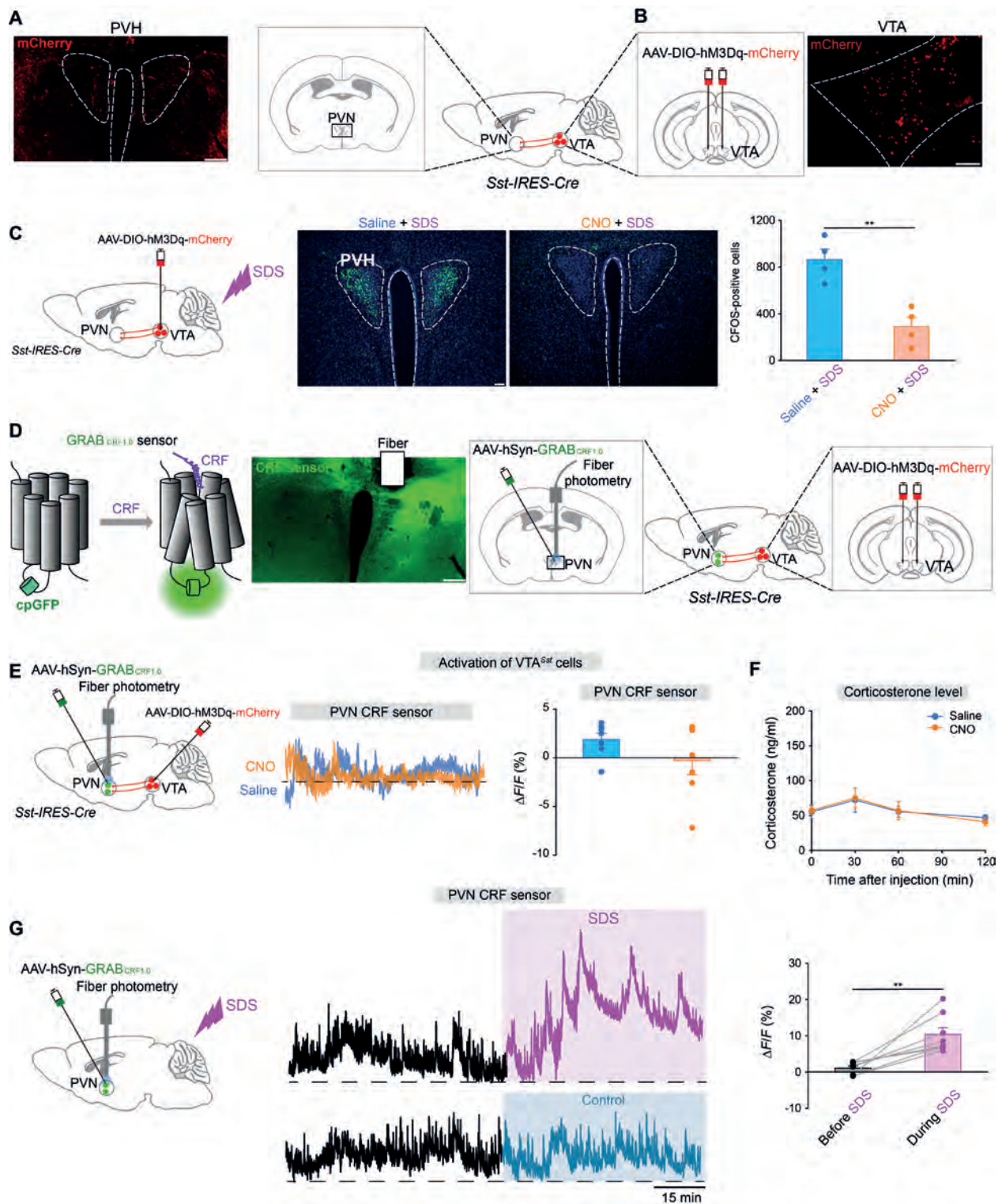


Fig. S28. Innervations of VTA^{Sst} neurons and PVN (Related to Fig. 6)

(A, B) mCherry-positive terminals in the PVN region from VTA^{Sst} neurons (A) with AAV-DIO-hM3Dq-mCherry injection into the VTA of Sst-IRES-Cre mice (B). Scale bar, 200 μ m.

(C) cFOS expression and quantification in the PVN region following SDS after chemogenetic activation of VTA^{Sst} neurons (n = 4 mice per group). Scale bar, 100 μ m.

(D) Expression of GRAB_{CRF1.0} sensor in the surrounding area of PVN after delivery of AAV-*hSyn-CRF1.0* into the PVN area of *Sst-IRES-Cre* mice. Scale bar, 200 μ m.

(E) Plan of the experimental procedure for chemogenetic activation of VTA^{Sst} neurons for measuring CRF levels in the surrounding area of PVN. Raw traces and $\Delta F/F$ ratios after saline or CNO injection (n = 8 mice per group). Unpaired *t*-test, $p > 0.05$.

(F) Corticosterone levels after chemogenetic activation of VTA^{Sst} neurons (n = 6 mice per group). Two-way ANOVA with Bonferroni *post hoc* test, $p > 0.05$.

(G) Plan of the experimental procedure for measuring CRF levels around PVN area in response to SDS. Raw traces and $\Delta F/F$ ratios before or during SDS (n = 8 mice per group). Paired *t*-test, ** $p < 0.01$.

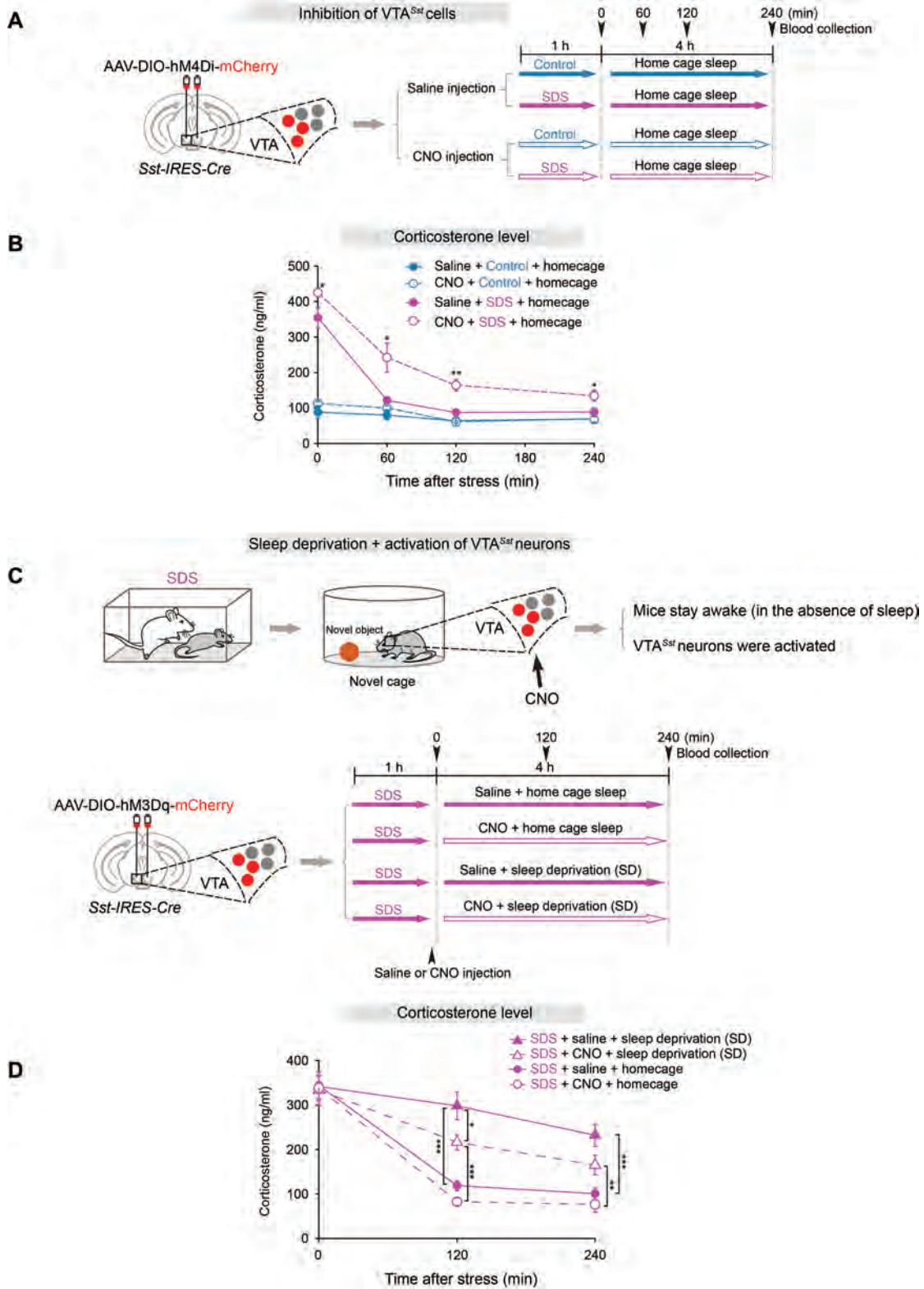


Fig. S29. SDS-induced sleep by VTA^{Sst} neurons aids alleviating corticosterone levels after SDS (Related to Fig. 6)

(A) Plan of the experimental procedure for chemogenetic inhibition of VTA^{Sst} neurons followed by control or SDS for measuring corticosterone levels.

(B) Corticosterone levels of saline- or CNO-injected mice during home cage sleep after control or SDS (n = 4-6 mice per group). Two-way ANOVA with Bonferroni *post hoc* test, *p < 0.05, **p < 0.01.

(C) Plan of the experimental procedure for chemogenetic activation of VTA^{Sst} neurons during sleep deprivation (in the absence of sleep) after SDS for measuring corticosterone levels.

(D) Corticosterone levels of saline- or CNO-injected mice during home cage sleep or sleep deprivation after SDS (n = 6 mice per group). Two-way ANOVA with Bonferroni *post hoc* test, *p < 0.05, **p < 0.01, ***p < 0.001.

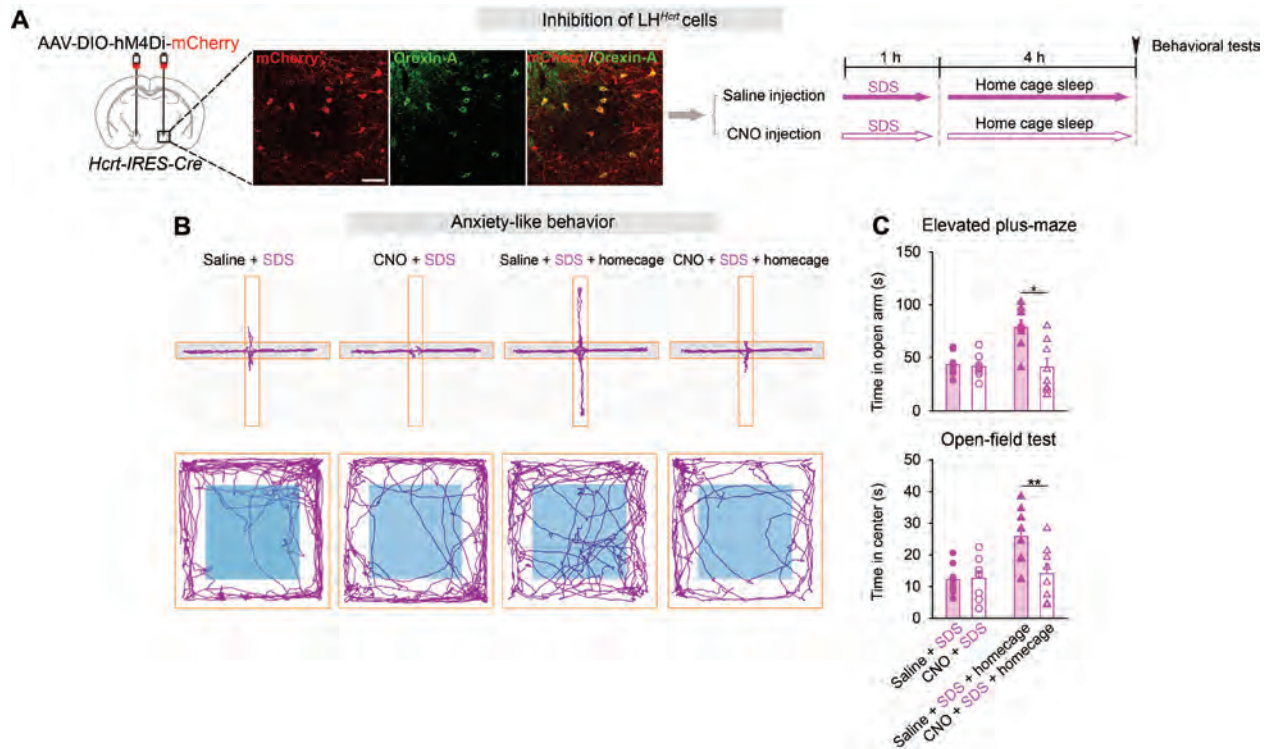


Fig. S30. Chemogenetic inhibition of LH^{Hcrt} neurons does not reduce SDS-induced anxiety (Related to Fig. 6)

(A) Immunostaining images showing mCherry expression in Orexin-A-positive cells and plan of the experimental procedure for chemogenetic inhibition of LH^{Hcrt} cells followed by control or SDS for behavioral tests, as arrowheads indicate.

(B, C) Tracing of locomotion for representative animals (B), time spent in the open arms of the elevated plus-maze and in the center zone during the open-field test of saline- or CNO-injected mice (n = 8 mice per group) (C). Two-way ANOVA with Bonferroni *post hoc* test, *p < 0.05, **p < 0.01.

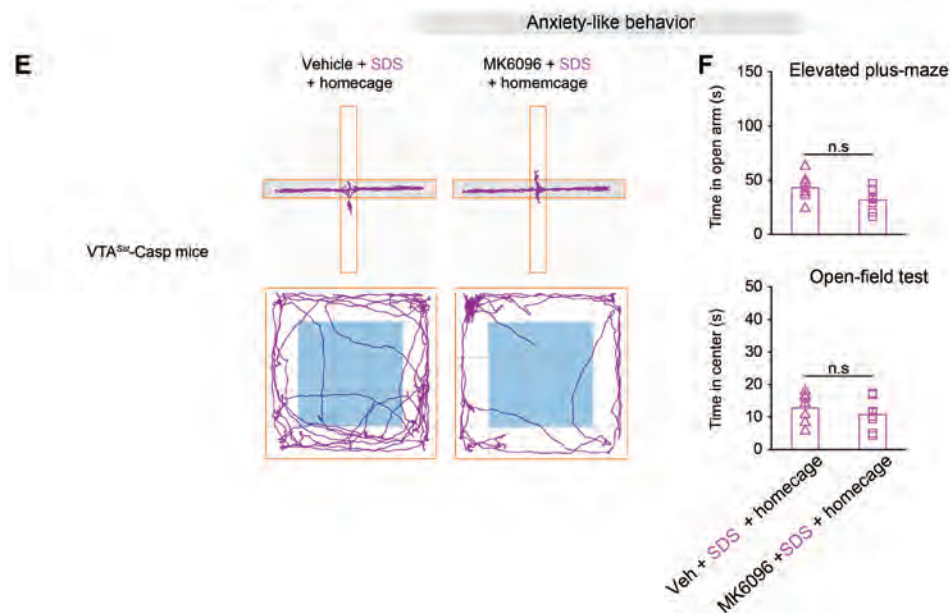
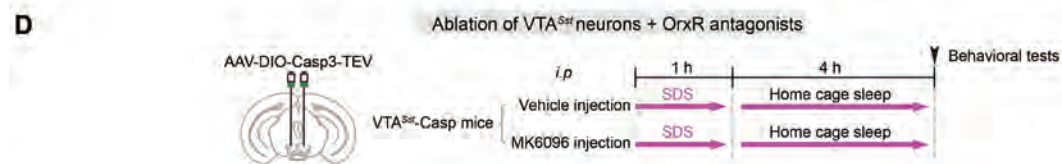
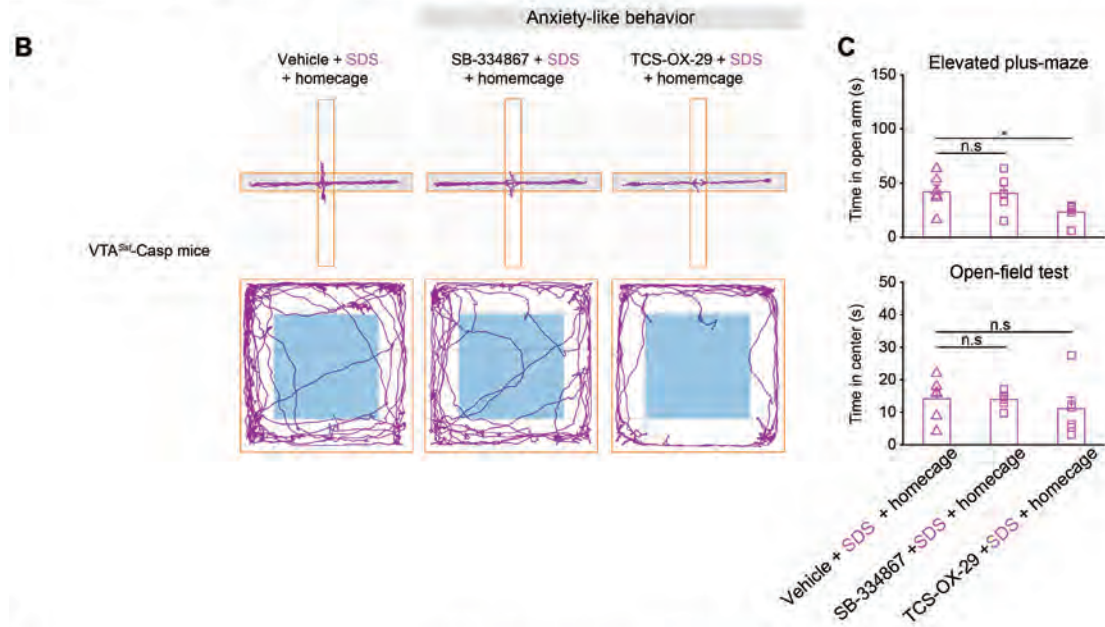
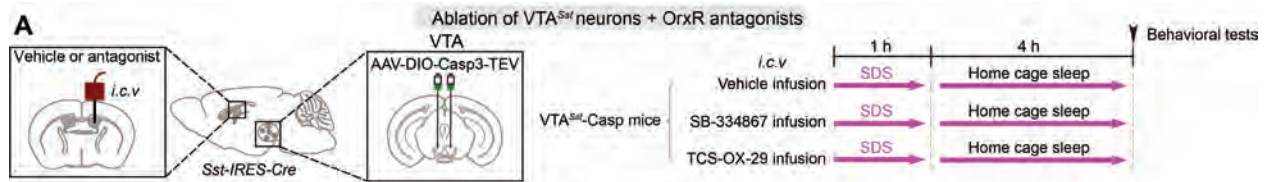


Fig. S31. Blocking orexin/hcrt receptors does not restore the anxiolytic effects on VTA^{Sst} lesioned mice (Related to Fig. 6)

(A) Plan of the experimental procedure for infusion of (*i.c.v.*) orexin receptor antagonist (SB-334867 or TCS-OX-29) into the VTA^{Sst} lesioned mice followed by SDS for behavioral tests, as arrowhead indicate.

(B, C) Tracing of locomotion for representative animals (B), time spent in the open arms of the elevated plus-maze and in the center zone during the open-field test (C) (n = 6 mice per group). Two-way ANOVA with bonferroni *post hoc* test, *p < 0.05, n.s, not significant.

(D) Plan of the experimental procedure for injection of (*i.p.*) dual orexin receptor antagonist MK6096 (filorexant) into the VTA^{Sst} lesioned mice followed by SDS for behavioral tests, as arrowhead indicate.

(E, F) Tracing of locomotion for representative animals (E), time spent in the open arms of the elevated plus-maze and in the center zone during the open-field test (F) (n = 7 mice per group). Unpaired *t*-test, p > 0.05, n.s, not significant.

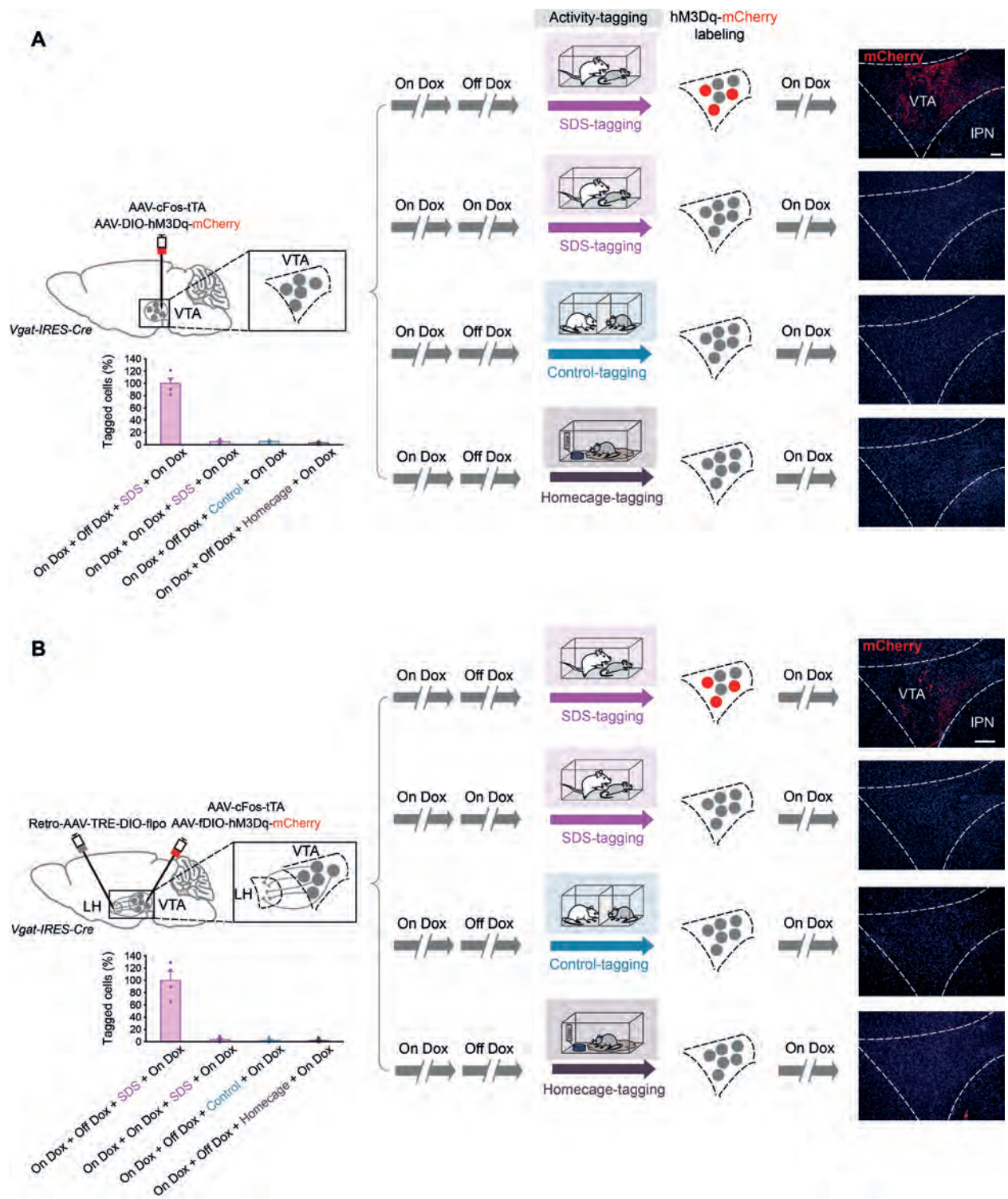


Fig. S32. Specificity of the activity-tagging system for SDS (Related to Fig. 2 and Fig. 3)

(A, B) Testing the efficacy and specificity of the activity-tagging system. The activity-tagging transgenes were delivered into the VTA (A) or intersectionally into the LH and VTA (B) of *Vgat-IRES-Cre* mice. Expression and quantification of activity-tagged hM3Dq-mCherry transgenes

in VTA^{Vgat} neurons under different activity-tagging conditions (n = 4 mice per group). Scale bar, 100 μ m.

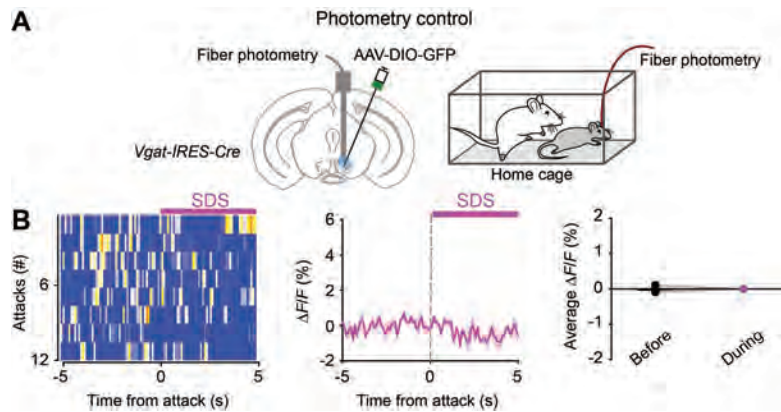


Fig. S33. Control experiments for GCaMP6 photometry of VTA^{Vgat} neurons (Related to Fig. 1, Fig. 2 and Fig. 3)

(A) Fiber photometry set up and control experiments measuring baseline fluorescence and controlling for movement artifacts in VTA^{Vgat}-GFP (AAV-DIO-GFP injected into the VTA of *Vgat-IRES-Cre* mouse) neurons when the mouse underwent SDS.

(B) Raw calcium signal traces, a color matrix of GCaMP6 signals for all trials, the $\Delta F/F$ ratios across the experimental period and average $\Delta F/F$ ratios before and during the SDS ($n = 4$ mice). Paired t -test, $p > 0.05$.

33. L. Vong *et al.*, Leptin action on GABAergic neurons prevents obesity and reduces inhibitory tone to POMC neurons. *Neuron* **71**, 142-154 (2011).
34. H. Taniguchi *et al.*, A resource of Cre driver lines for genetic targeting of GABAergic neurons in cerebral cortex. *Neuron* **71**, 995-1013 (2011).
35. S. Hippenmeyer *et al.*, A developmental switch in the response of DRG neurons to ETS transcription factor signaling. *PLoS Biol* **3**, e159 (2005).
36. L. Madisen *et al.*, A robust and high-throughput Cre reporting and characterization system for the whole mouse brain. *Nat Neurosci* **13**, 133-140 (2010).
37. W. J. Giardino *et al.*, Parallel circuits from the bed nuclei of stria terminalis to the lateral hypothalamus drive opposing emotional states. *Nature Neuroscience* **21**, 1084-1095 (2018).
38. S. Ren *et al.*, The paraventricular thalamus is a critical thalamic area for wakefulness. *Science* **362**, 429-434 (2018).
39. Z. Zhang *et al.*, Neuronal ensembles sufficient for recovery sleep and the sedative actions of $\alpha 2$ adrenergic agonists. *Nature Neuroscience* **18**, 553-561 (2015).
40. E. C. Harding *et al.*, A Neuronal Hub Binding Sleep Initiation and Body Cooling in Response to a Warm External Stimulus. *Current Biology* **28**, 2263-2273.e2264 (2018).
41. M. J. Krashes *et al.*, Rapid, reversible activation of AgRP neurons drives feeding behavior in mice. *J Clin Invest* **121**, 1424-1428 (2011).
42. T. W. Chen *et al.*, Ultrasensitive fluorescent proteins for imaging neuronal activity. *Nature* **499**, 295-300 (2013).

43. K. T. Beier *et al.*, Rabies screen reveals GPe control of cocaine-triggered plasticity. *Nature* **549**, 345-350 (2017).
44. C. F. Yang *et al.*, Sexually dimorphic neurons in the ventromedial hypothalamus govern mating in both sexes and aggression in males. *Cell* **153**, 896-909 (2013).
45. A. J. Murray *et al.*, Parvalbumin-positive CA1 interneurons are required for spatial working but not for reference memory. *Nat Neurosci* **14**, 297-299 (2011).
46. D. G. Tervo *et al.*, A Designer AAV Variant Permits Efficient Retrograde Access to Projection Neurons. *Neuron* **92**, 372-382 (2016).
47. R. Lin *et al.*, Cell-type-specific and projection-specific brain-wide reconstruction of single neurons. *Nat Methods* **15**, 1033-1036 (2018).
48. T. R. Reardon *et al.*, Rabies Virus CVS-N2cΔG Strain Enhances Retrograde Synaptic Transfer and Neuronal Viability. *Neuron* **89**, 711-724 (2016).
49. S. A. Golden, H. E. Covington, 3rd, O. Berton, S. J. Russo, A standardized protocol for repeated social defeat stress in mice. *Nat Protoc* **6**, 1183-1191 (2011).
50. N. Charoenphandhu *et al.*, Mild-intensity physical activity prevents cardiac and osseous iron deposition without affecting bone mechanical property or porosity in thalassemic mice. *Scientific Reports* **12**, 5959 (2022).
51. G.-W. Zhang *et al.*, Medial preoptic area antagonistically mediates stress-induced anxiety and parental behavior. *Nature Neuroscience* **24**, 516-528 (2021).
52. X. Yu *et al.*, Dysfunction of ventral tegmental area GABA neurons causes mania-like behavior. *Molecular Psychiatry* **26**, 5213-5228 (2021).
53. K. Tossell *et al.*, Sleep deprivation triggers somatostatin neurons in prefrontal cortex to initiate nesting and sleep via the preoptic and lateral hypothalamus. *bioRxiv*, 2020.2007.2001.179671 (2020).
54. G. M. Alexander *et al.*, Remote control of neuronal activity in transgenic mice expressing evolved G protein-coupled receptors. *Neuron* **63**, 27-39 (2009).
55. E. S. Boyden, F. Zhang, E. Bamberg, G. Nagel, K. Deisseroth, Millisecond-timescale, genetically targeted optical control of neural activity. *Nat Neurosci* **8**, 1263-1268 (2005).
56. V. N. Anisimov *et al.*, Reconstruction of vocal interactions in a group of small songbirds. *Nature Methods* **11**, 1135-1137 (2014).
57. P. Mitra, H. Bokil, *Observed Brain Dynamics*, Oxford Univ. Press, (2008).
58. C. Tronche *et al.*, Increased stress-induced intra-hippocampus corticosterone rise associated with memory impairments in middle-aged mice. *Neurobiology of Learning and Memory* **93**, 343-351 (2010).
59. R. M. Sears *et al.*, Orexin/hypocretin system modulates amygdala-dependent threat learning through the locus coeruleus. *Proc Natl Acad Sci U S A* **110**, 20260-20265 (2013).